Ana Marques Pereira da Silva

Graduate in Mechanical Engineering Sciences

Topology optimization considering geometrical nonlinear behavior

Dissertation to obtain a master's degree in Mechanical Engineering

Thesis supervisor: Prof. Ph.D João Mário Burguete Botelho Cardoso, Assistant Professor in Faculty of Science and Technology, Universidade Nova de Lisboa

Committee:

President: Tiago Alexandre Narciso da Silva, Assistant Professor, Faculty of Science and Technology, Universidade NOVA de Lisboa

Members: Pedro Samuel Gonçalves Coelho, Assistant Professor, Faculty of Science and Technology, Universidade NOVA de Lisboa

João Mário Burguete Botelho Cardoso, Assistant
Professor, Faculty of Science and Technology, Universidade NOVA de Lisboa

FACULDADE DE CIÊNCIAS E TECNOLOGIA
UNIVERSIDADE NOVA DE LISBOA

September 2019

Topology optimization considering geometrical nonlinear behavior

To my brothers,

Maria and Tiago

ACKNOWLEDGMENTS

The author wishes to express her profound gratitude to her thesis supervisor, Professor João Cardoso, for his advice and guidance during the development of this project which played a crucial role in the understanding of concepts and the surpassing of hardships.

The author would also like to thank all the professors that have been part of this journey for all the knowledge that was shared and the dedication they demonstrated.

To all the friends that have walked beside me during this path, a special thanks is due for all the support, hope, and cheer for they have brought light and happiness to every moment.

To my family, thank you for giving me the opportunity to pursue my studies and the trust, encouragement and support to reach higher in every step of my life. What they have taught me will always guide me and forever serve as a reminder of the preciousness of life.

ABSTRACT

The validation of an already developed nonlinear finite element analysis program, PROAES_NL, was made. To this end, four examples found in the literature were solved using the program and the results were compared with the values presented in published papers and also with the results obtained using the finite element software *ANSYS*. The relative error between results obtained using PROAES_NL and the two other sources were found to be relatively small and the program was considered validated.

The theory for sizing design sensitivity for geometrically nonlinear analysis developed by Santos [1] was studied, interpreted and translated into the physical domain. The resulting equations were then numerically implemented in Octave within PROAES_NL using only finite element post-processing data. To validate the sizing design sensitivity analysis expressions applied five examples were solved. The results obtained were compared with the values obtained using finite difference method and with results presented by Santos [1]. The relative error between PROAES_NL and the previously mentioned sources was small, and the sensitivity expressions were considered validated. Also, it is demonstrated that a difference between calculating linear and nonlinear design sensitivity analysis exists.

Design sensitivities were then used to perform nonlinear topology optimizations. The goal was to verify if any difference would arise between performing a linear and nonlinear topology optimization. Although some of the articles studied showed a difference between optimum designs considering linear and nonlinear optimization, using PROAES_NL the difference only appeared in one of the two examples. During the final phase of this work, limitations in the convergence of the nonlinear analysis resulted in restrictions in the selection of the optimization parameters.

RESUMO

Foi realizada a validação de um programa de análise de elementos finitos não lineares já desenvolvido, PROAES_NL. Para tal, quatro exemplos encontrados na literatura foram resolvidos utilizando o programa e os resultados foram comparados com os valores apresentados em artigos publicados e também com os resultados obtidos com o software de elementos finitos *ANSYS*. O erro relativo entre os resultados obtidos utilizando o PROAES_NL e as duas outras fontes mencionadas anteriormente foi relativamente pequeno e o programa foi considerado validado.

A teoria de cálculo de sensibilidades em estruturas com comportamento não linear desenvolvida por Santos [1] foi estudada, interpretada e traduzida para o domínio físico. As equações resultantes foram implementadas numericamente em linguagem *Octave* completando o código PROAES_NL usando apenas dados de pós-processamento de elementos finitos. Para validar as expressões de análise de sensibilidade utilizadas foram resolvidos cinco exemplos. Os resultados obtidos foram comparados com os valores obtidos pelo método das diferenças finitas e com os resultados apresentados por Santos [1]. O erro relativo entre o programa PROAES_NL e as fontes mencionadas anteriormente foi pequeno e as expressões de sensibilidade foram consideradas validadas. Além disso, é demonstrado que existe uma diferença entre o cálculo da análise de sensibilidades numa análise linear e numa análise não linear.

As expressões de sensibilidades implementadas foram depois usadas para executar otimizações de topologia. O objetivo era verificar se haveria alguma diferença entre executar uma otimização de topologia utilizando análises lineares e não lineares. Embora alguns dos artigos estudados mostrem diferenças entre a configuração ótima obtida com análise linear e análise não linear, usando o programa PROAES_NL, a diferença foi visível em apenas um dos dois exemplos estudados. Durante a fase final deste trabalho, limitações na convergência da análise não linear resultaram em restrições na seleção dos parâmetros de otimização.

CONTENT

FIGURE INDEX

TABLE INDEX

CHAPTER 1

INTRODUCTION

1.1 LITERATURE REVIEW

Structural optimization has become an integrant part of the design process since it delivers efficient designs promptly when compared with the traditional method of trial and error. Two types of structural optimization exist: size/shape optimization where, for a given topology, geometry and material properties are optimized and topology optimization where the distribution of the material in a pre-determined space is optimized. The focus of this thesis remains within the last type of structural optimization.

Topology optimization had as its pioneer Maxwell (1880) [2], and it's a structural optimization technique that within an admissible region with boundary conditions and applied loads allows one to obtain the most structurally efficient design. Given the high complexity of the structures that are generally obtained through this type of technique, topology optimization was, for many years, left in the research and development field. The development of additive manufacturing, commonly known as 3D printing, continuously evolving to bigger production sizes and new materials, is disrupting the limitations in size and complexity of the components that are producible [3]. This technology breakthrough has shed new light and interest in topology optimization, making its applicability a reality.

Similarly to structural optimization, topology optimization can be divided into two types: continuum density-based optimization wherein for a specific region the distribution of material is varied from solid to void and optimization based on an initial ground structure where the area of the elements is modified. For this thesis, the last type of topology optimization mentioned above is used.

Topology optimization using initial *ground structures* was first proposed by Dorn et al. in 1964 [4]. The quality of the obtained solution using the ground structure method is highly dependent on the location of the nodes, and the element connectivity's that are considered at the beginning of the optimization process. Thus, the ground structure must be sufficiently dense to allow the obtention of the optimum configuration since the initial formulation for this method considered only the possibility of removal of elements. To move past this limitation, many alternative ways have arisen throughout the years. Hajela and Lee (1994) [5] proposed the incorporation of the genetic algorithm to allow for the addition or removal of elements throughout the optimization process. Similarly, Hagishita and Ohsaki (2008) [6] proposed a growing ground structure method based on five growing strategies developed, taking into consideration the mechanical properties of the structure. It's stated [6] that these strategies deliver satisfactory results for small dimension problems but that for more complex structures, further developments need to be made.

The final solutions obtained using the ground structure method have frequently a high number of elements with minimal cross-sectional areas which increases the artificial stiffness of the structure and that leads to an invalid structural system[7]. To avoid this problem, Zhang, Ramos, and Paulino (2017) [7] proposed a filter that removes the elements with a reduced area and the nodes associated with them. This way, in each iteration, the calculations are made considering only the essential elements. The results obtained have shown a significant improvement regarding computational time, and the usage of this filter also eliminates the need to post-process the solution.

Since its introduction, topology optimization has been highly developed considering the analysis of structures with a linear elastic response. Few papers have emerged considering the study of structures with a geometrical nonlinear behavior. It is of the author's knowledge of an early article dealing with geometrical nonlinearities by Bruns and Tortorelli (1998) [8]. Since then, some papers have emerged, showing that a slight difference may exist in design when geometrically nonlinear structural behavior is taken into consideration. It is the example of Gea and Luo (2000) [9], Buhl, Pedersen, and Sigmund (2000) [10] and Kang and Luo (2009) [11]. In the articles mentioned before the optimization problem is studied considering density-based optimization methods. To the author's knowledge, an even smaller amount of papers exist taking on the nonlinear optimization problem using the ground structure method. An example is a paper by Changizi and Jalalpour (2018) [12] were the authors present methodologies to incorporate overall and individual member buckling prevention in the structural topology optimization of steel structures using minimum compliance and stress-based design.

An extensive literature focusing on linear structural response exists because structures have been designed considering that throughout their work-life, their structural response will remain within the elastic and small-displacement limit. This assumption is valid for a large class of problems [9]. However, the increasing attention for structures to survive extreme conditions [13], the demand for more economical structural systems resulting in increasingly slender and thin structural components [14], the design of space antennas, the design of compliant mechanisms and MicroElectroMechanical systems make the usage of nonlinear finite element analysis methods essential. Otherwise, the occurrence of nonlinearities, such as buckling could lead to the loss of the structural integrity of the structure.

When undergoing large displacements and rotations, a linear structural response can no longer be considered since the point of application of the external forces varies during the deformation when comparing to their initial position.

This nonlinearity between the applied force and the resulting displacement is known as nonlinear geometrical behavior [15]. It is highlighted the fact that in this type of nonlinear analysis, only small deformations with large rotations and displacements are considered. Therefore, the material is always within its elastic behavior zone limits.

To obtain an optimal design process considering nonlinear behavior, the development of design sensitivity analysis methods for nonlinear response is necessary [13]. These

formulations allow for the determination of the response variation of a system concerning perturbations of the design variables [16]. Several authors have studied the development of design sensitivity analysis methods for nonlinear problems. Ryu et all (1985) [13] address the issue, analyzing different analytical and numerical methods. The Newton-Raphson, a modified Newton-Raphson method, and the BFGS method are studied for nonlinear structural analysis. It is mentioned that the Newton-Raphson method shows excellent convergence properties allied with a higher computational cost when compared with the modified Newton-Raphson method. For the analysis of design sensitivities, both secant and tangent stiffness approaches are studied. It is concluded that the tangent stiffness approach is more suitable for design sensitivity analysis since the matrix at the final load step can be directly used. Park and Choi (1989) [14] present a continuum approach for analytical expressions of design sensitivity of the critical load factor. Santos and Choi (1988) [17] present a thorough analytical formulation for the adjoint variable method of design sensitivity analysis and provide the analytical integral equations for the variations of the energy and load forms. In addition, they present the design sensitivity expressions for displacement and stress functionals for truss and beam components. The results presented for the beam component in this paper have served as a starting point for the development of this thesis.

1.2 OBJECTIVES

The main objective of this work is to implement a structural design sensitivity analysis theory for sizing design variables using an already existing nonlinear finite element code for bidimensional beam components, PROAES_NL. Geometric nonlinearities are considered. GNU Octave is used for numerical implementation. The accuracy of the design sensitivity analysis code developed is proved using examples from published papers and through comparison of results.

The nonlinear finite element code, PROAES_NL, was developed by Professor João Cardoso from the Faculty of Science and Technology of Universidade Nova de Lisboa. Because the accuracy of PROAEN_NL hadn't been yet proved the first part of this thesis corresponds to the test of the program with numerical examples from published papers to compare the results obtained. Results are also compared with *ANSYS*.

In the final part of this work, the nonlinear design sensitivity analysis is used to perform topological optimization using the ground structure method. The results obtained are once again compared with published papers and with linear topology optimization optimum designs.

1.3 SCOPE

In Chapter 2, the methodology implemented in PROAES_NL is explained. The finite element method for bidimensional Euler-Bernoulli beam elements uses an interative-incremental Newton-Rapshon method combined with load control using the cylindrical arc-length technique to follow the evolution of the structure even in case of snap-through instability phenomenon. For the cinematic analysis of elements, a corotational formulation was used. Numerical examples are shown to prove the accuracy of the method.

In Chapter 3, the theoretical formulation used for sizing design sensitivity is described. The adjoint variable method is used to obtain first variations of performance functionals explicitly in terms of changes of design variables and the design sensitivity expressions for beam components. The formulation explained and applied to numerically implement design sensitivity analysis was, as mentioned before, developed by Santos [1]. Numerical examples are shown to prove the accuracy of the method and the *Octave* code created.

In Chapter 4, the nonlinear design sensitivity analysis implemented and tested in Chapter 3 is used to perform topological optimizations using the ground structure method. Topology optimization for a minimum compliance with a volume constraint is carried. Two structures are studied, the results obtained for optimum designs are compared with the results presented in published papers and with linear topological optimization.

Finally, conclusions drawn from this work and recommendations for future research are presented in Chapter 5.

CHAPTER 2

NONLINEAR ANALYSIS

2.1 THEORY DESCRIPTION

A key aspect in the development of a nonlinear finite element analysis program is the proper selection of the algorithm used to find the solution of the problem [18]. The nonlinear analysis of structures encompasses the resolution of problems where the stiffness matrix has a dependence on the displacement [15]. In the situation of an external static load the problem can be formulated as:

$$[K(u)]\{u\} = \{f\} \tag{2.1}$$

Where $K(u)$ expresses the existing dependence of the stiffness matrix is respect to the displacement vector u.

In the scope of this thesis, only geometrical nonlinear problems are to be considered. A geometrical nonlinearity exists when the structure is subjected to finite displacements and rotations, in which case, the point of application of the external loads varies with respect to their initial position. A consequence of this situation is that the effect that a certain external load has upon the structure changes throughout the deformation of the given structure making it necessary to write the equilibrium equations in the deformed configuration [15].

To analyze the cinematic of the elements, the corotational method was employed.

COROTATIONAL METHOD

The corotational method relies on the separation of the displacements to which a finite element is subjected into three different categories: rigid body translation, rigid body rotation and deformation [15]. Both an element local coordinate system and a global coordinate system are used. The large displacements and rotations effects are treated through the transformations of displacement and force components between the global and local coordinate system while the deformations, assumed infinitesimal, can be treated in the local coordinate system using the formulations commonly used within the elastic behavior domain.

The corotational or convective approach into finite element analysis has been studied throughout the years for different applications. The works of Wempner (1969) [19], Belytschko and Hsieh (1973) [20] and Rankin and Brogan (1986) [21] are highlighted having contributed to the extension of existing formulations for linearly elastic finite elements to problems involving finite rotations and buckling by using corotational formulations, also known as Element Independent Corotational (EICR) formulation.

When using linear finite element formulations, if the element only has rigid body translation, the stresses and deformations will not be affected. However, if rigid body rotation exists, there will be deformations and internal energy related to it [15]. Corotational formulation solves this problem since it separates the displacement field into a rigid body translation and rotation component, u^r, and a component that causes strain, u^d:

$$u = u^r + u^d \tag{2.2}$$

The calculations of the internal energy for each element are made using only the strain component of the displacement, u^d, making its calculation a critical step.

Consider a body undergoing a motion from its initial configuration to the current one, see Figure 2.1. Three coordinate systems are used: a global coordinate system (X, Y) a local coordinate system (x_0, y_0) and a nodal coordinate system attached to node 1 and to the last node i of the element. The global coordinate system (X, Y) and the local coordinate system (x_0, y_0) can be seen in Figure 2.1.

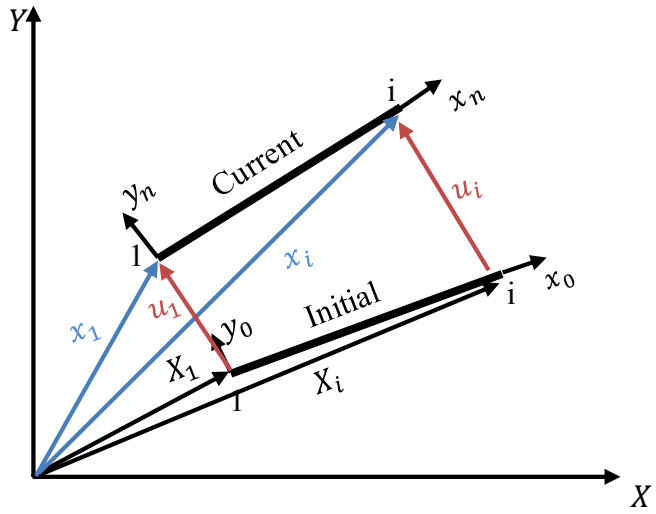

FIGURE 2.1. SCHEMATICS OF THE BODY MOVEMENT FROM THE INITIAL CONFIGURATION TO THE LAST CONFIGURATION

The current position of the i node in global coordinates is given by:

$$x_i = X_i + u_i \tag{2.3}$$

The translational component of the deformational displacement in global coordinates can be computed from the displacement field through the following expression [22]:

$$u_t^d = R_n(X + u) - X \tag{2.4}$$

Where X denotes the vector with the position of the nodes in global coordinates in the initial configuration and u the vector with the nodal displacements in global coordinates. R_n is the orthogonal rotation matrix of the local coordinate system with respect to the initial local coordinate system.

Additionally, at iteration n, the rotational components of the deformational displacement, α^d, must be computed. This can be done by eliminating from the total nodal rotation, α, the element rotation, β, see Figure 2.2 [22].

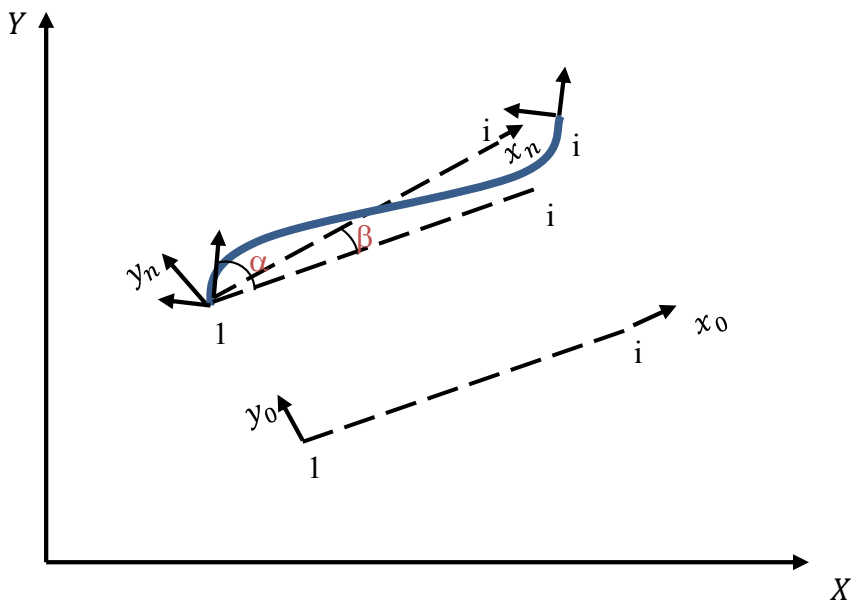

FIGURE 2.2. NODE ROTATION AND ELEMENT ROTATION

The rotational components of the deformational displacement, α^d, can then be computed with the following expression [15]:

$$\alpha^d = \alpha - \beta \tag{2.5}$$

It's now possible to write the complete vector for the deformational displacements, u^d:

$$\{u^d\}^T = \{u_{1x}^d \; u_{1y}^d \; \alpha_1^d \; u_{2x}^d \; u_{2y}^d \; \alpha_2^d\} \tag{2.6}$$

The axial and shear force and bending moment in each element are calculated in accordance with the equations presented by Menin [23] with the nodal rotations presented in Figure 2.3.

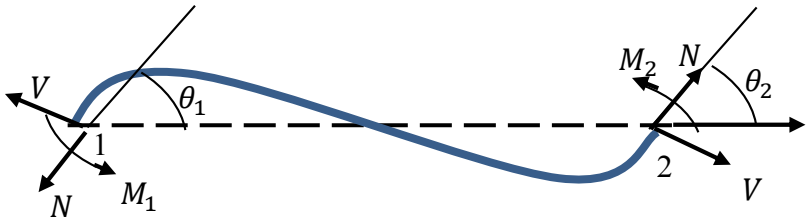

FIGURE 2.3. CONVENTION FOR AXIAL, SHEAR FORCE AND BENDING MOMENT

$$N = \frac{EA_0}{L_0} d \tag{2.7}$$

$$V = \frac{6EI}{LL_0}(\theta_1 + \theta_2) \tag{2.8}$$

$$M_1 = \frac{2EI}{L_0}(2\theta_1 + \theta_2) \tag{2.9}$$

$$M_2 = \frac{2EI}{L_0}(\theta_1 + 2\theta_2) \tag{2.10}$$

NEWTON-RAPSHON METHOD WITH CYLINDRICAL ARC LENGTH LOAD CONTROL

The study of the elastic stability of a structure is influenced by singularities that may occur along the path of its deformation. These singularities are also known as critical points which are connected to the physical phenomena of snapping and buckling [24], see Figure 2.4. Snap-through and buckling phenomena are some of the most challenging problems in the nonlinear structural analysis [25].

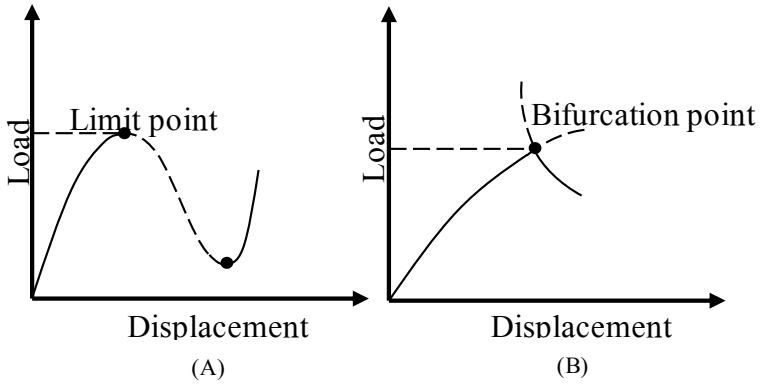

FIGURE 2.4. EXAMPLE OF SNAP-THROUGH (A) AND BUCKLING CRITICAL POINTS (B)

The geometric nonlinearity implies that both the effect of the external load and the stiffness matrix must be recalculated for each deformed configuration. Therefore, the solution of equation 2.1 can only be found through the usage of iterative techniques. In the development of PROAES_NL the incremental-iterative Newton-Raphson method was used in order to be able to trace the complete load/deflection response of the structure. However, the Newton-Raphson method can only solve problems where the load increases monotonously (positive derivative). Meaning that the derivative of the equilibrium load/deflection path must be positive. If nonlinear phenomena occur and the displacement increases with the decrease of the load, such as the case of snap-through, the derivative of the equilibrium path will be negative, and the algorithm will not be able to follow it.

To solve this problem, a load control method was employed, the cylindrical arc-length method.

The equilibrium equation is now written as:

$$[K(u)]\{u\} = \lambda\{f\} \tag{2.11}$$

The load control variable, λ, varies between zero and one and can decrease or increase throughout the computation process. This will enable the algorithm to follow the equilibrium path even if the derivative is negative. The load control parameter is dependent on another variable called the arc length, ΔL [15]. The arc length also determines the amplitude of the incremental displacement, see Figure 2.5.

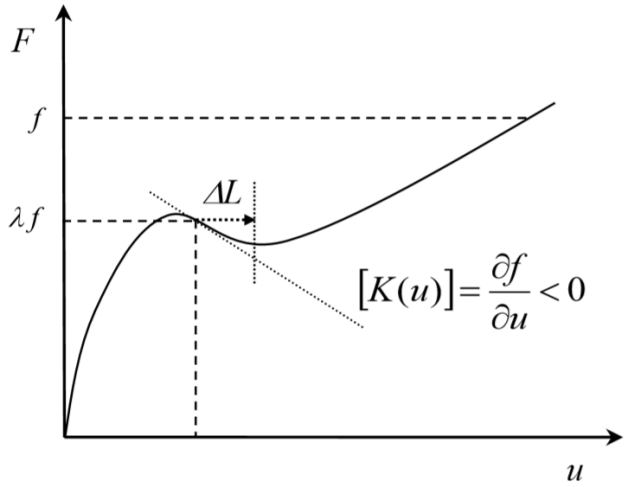

FIGURE 2.5. AMPLITUDE OF THE INCREMENTAL DISPLACEMENT GIVEN THROUGH THE ARC LENGTH. SOURCE: [14]

The system of nonlinear equations that describes static problems with geometric nonlinearities in a general i iteration can be written as [15]:

$$[K(u_i)]\{\Delta u_{i+1}\} = \lambda_{i+1}\{f\} - \{f_i\} \tag{2.12}$$

Where both Δu_{i+1} and λ_{i+1} are unknown, see Figure 2.6

.

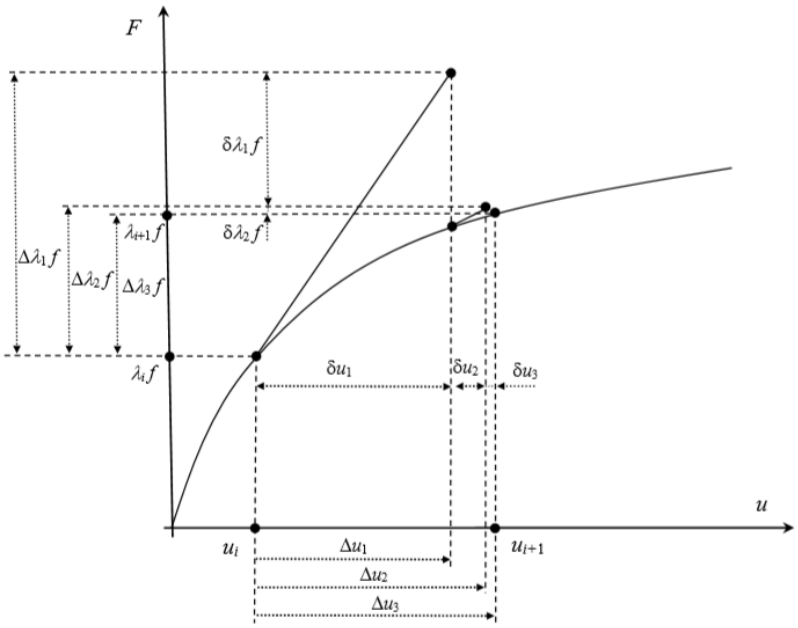

FIGURE 2.6. ITERATIVE PROCESS. SOURCE: [14]

The purpose of the iterative process is to converge to λ_{i+1} and u_{i+1}. Which can be calculated by the following expressions:

$$\{u_{i+1}\} = \{u_i\} + \{\Delta u_{i+1}\} \tag{2.13}$$

$$\{\Delta u_{i+1}\} = \{\Delta u_i\} + \{\delta u_{i+1}\} \tag{2.14}$$

$$\lambda_{i+1} = \lambda_i + \delta\lambda_i \tag{2.15}$$

If expression 2.15 is inserted in equation 2.12, the resulting equation that has to be computed for each iteration is:

$$[K(u_i)]\{\delta u_{i+1}\} = \lambda_{i+1}\{f\} + \delta\lambda\{f\} - \{f_i\} \tag{2.16}$$

Which can be divided into two equations. A first with the displacements corresponding to the load control method, δu_{i+1}^R, a second with the displacements corresponding with the totality of the externally applied forces, δu_{i+1}^T.

$$[K(u_i)]\{\delta u_{i+1}^R\} = \lambda_i\{f\} + \{f_i\} \tag{2.17}$$

$$[K(u_i)]\{\delta u_{i+1}^T\} = \{f\} \tag{2.18}$$

The increment Δu_{i+1} can be calculated by adding the contributions of both previously calculated displacements.

$$\{\delta u_{i+1}\} = \{\delta u_{i+1}^R\} + \delta\lambda\{\delta u_{i+1}^T\} \tag{2.19}$$

The supplementary equation that is necessary to calculate the value of $\delta\lambda$ is called the Arc Length Equation:

$$\{\Delta u_{i+1}\}^T\{\Delta u_{i+1}\} = \Delta L^2 \tag{2.20}$$

By replacing equation 2.19 in 2.14 and the result in the Arc Length Equation, a quadratic equation appears. This equation allows for the determination of $\delta\lambda$:

$$a_1(\delta\lambda)^2 + a_2(\delta\lambda) + a_3 = 0 \tag{2.21}$$

Where,

$$a_1 = \{\delta u_{i+1}^T\}^T.\{\delta u_{i+1}^T\} \tag{2.22}$$

$$a_2 = 2\{\delta u_{i+1}^T\}.(\{\Delta u_i\} + \{\delta u_{i+1}^R\}) \tag{2.23}$$

$$a_3 = (\{\Delta u_i\} + \{\delta u_{i+1}^R\})^T.(\{\Delta u_i\} + \{\delta u_{i+1}^R\}) - \Delta L^2 \tag{2.24}$$

Having calculated δu_{i+1}^{T}, δu_{i+1}^{R} and $\delta\lambda$ it's now possible to determine λ_{i+1} and u_{i+1}.

ARC LENGTH

For the first iteration of the first step Cardoso [15] proposed the following expression for the determination of the arc length, ΔL.

$$\Delta L_1 = \lambda_1 \sqrt{\{\Delta u_1\}^T \{\Delta u_1\}} \tag{2.25}$$

In the remaining load increments, the following expression proposed by Crisfield [26] was used.

$$\Delta L_i = \Delta L_{i-1} \sqrt{\frac{N_{op}}{N_{i-1}}} \tag{2.26}$$

Where N_{op} is the optimum number of iterations considered for each step, ΔL_{i-1} is the value of the arc length from the previous iteration and N_{i-1} is the number of iterations that took to reach convergence in the previous increment.

SIGNAL OF THE LOAD FACTOR INCREMENT

For the first iteration of each step, the signal of the load factor increment is estimated through the result of the following expression:

$$\Delta u'_{i-1} * (+1) u^T > \Delta u'_{i-1} * (-1) u^T \tag{2.27}$$

Being the signal positive if the expression is validated and negative if the expression is violated.

The flow chart for the computational implementation is presented on the next page as Figure 2.7. The following space is left intentionally empty.

COMPUTATIONAL IMPLEMENTATION

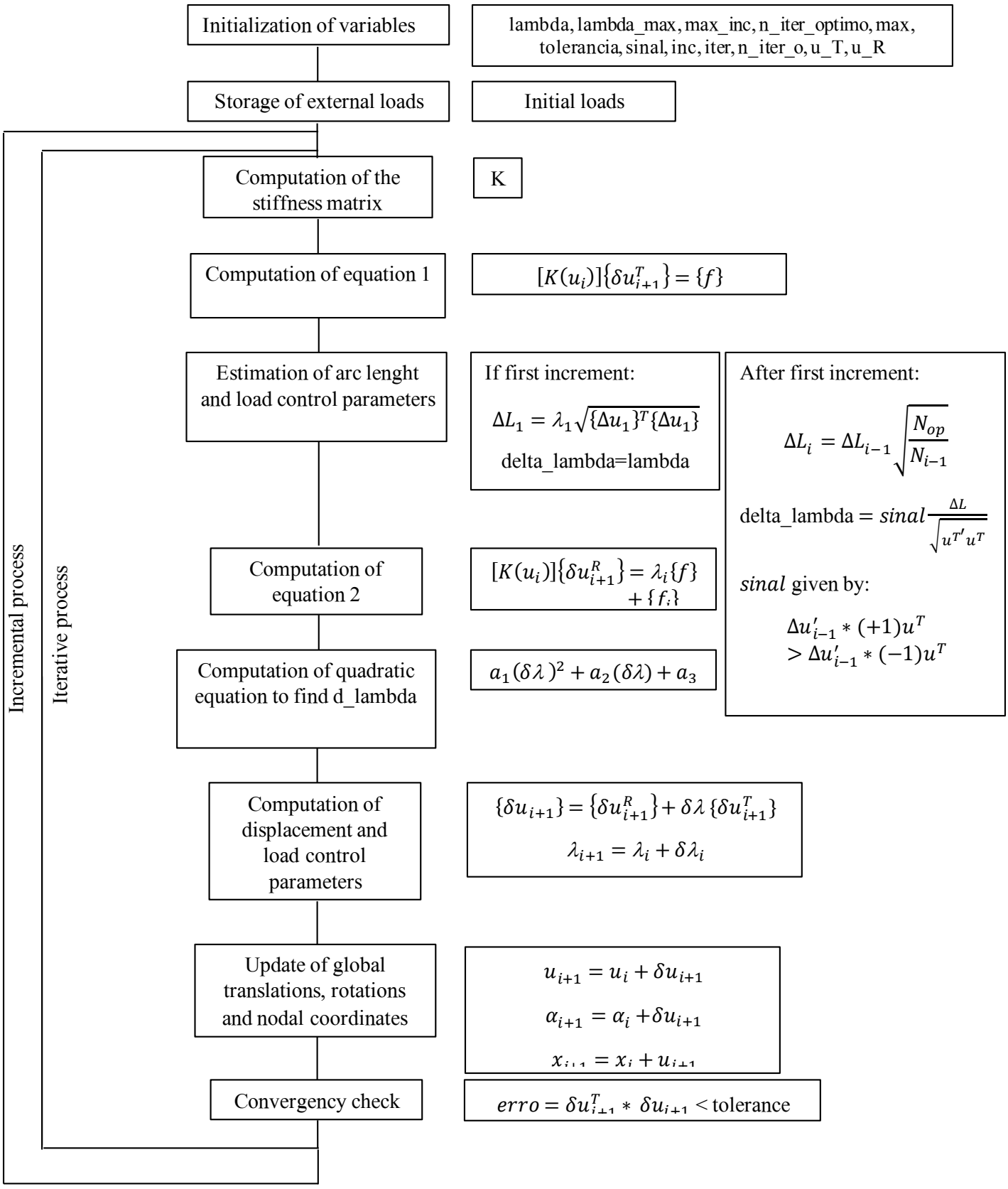

FIGURE 2.7. COMPUTATIONAL IMPLEMENTATION OF ARC-LENGTH NEWTON RAPHSON METHOD

2.2 VALIDATION OF PROAES_NL

The relative error between the values obtained using PROAES_NL and the values presented in published articles or the results obtained using *ANSYS* will always be calculated using the following formulae, 2.28.

$$E = \left| \frac{PROAES.NL - Ref.Value}{Ref.Value} \right| * 100 \tag{2.28}$$

2.2.1 EXAMPLE 1

The first numerical example considers the deformation of the frame shown in Fig.2.8 (a). Accordingly to Cichon [27] the analytical solution for this problem was presented by Lee et all in 1968 [28] and the solution using finite elements was provided by Cescotto in 1978 [29]. Cichon provided the solution for this frame supplying tables with the values obtained for the horizontal, *U*, and vertical displacement, *W*, of the structure for several values of the load factor, λ. For this reason, to test the accuracy of the results, a comparison was made with the article by Cichon [27].

The frame is made of an *L* shaped beam with a quadrangular cross-section of area *A*, moment of inertia *I* and Young's modulus *E*. In each of its extremities a fixed support in constrained the horizontal and vertical translations of both nodes. The structure is subjected to a concentrated vertical force *P* that acts along the negative direction of the y-axis considered, and that has a value of 1000 kgf. The point of application of the load is at 24 centimeters from the left extremity of the horizontal section of the beam. For better understanding, the reader is asked to observe Fig.2.8 (a).

For the finite element analysis, 21 nodes and 20 beam elements with 3 degrees of freedom, vertical and horizontal translation and rotation per node were defined as one can observe in Fig.2.8 (b).

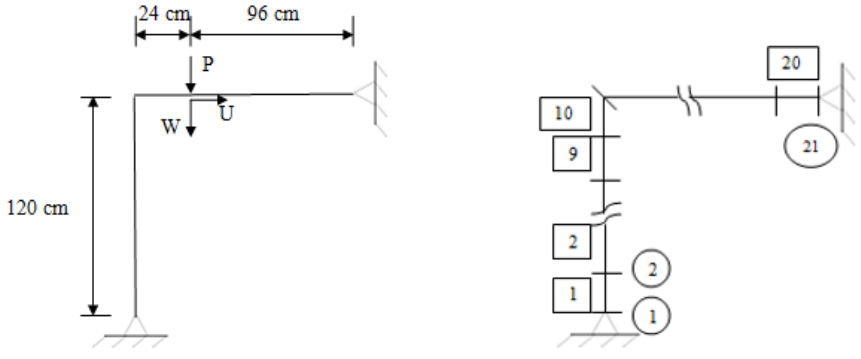

FIGURE 2.8. LEE'S FRAME (A) SCHEMATIC (B) FINITE ELEMENT MODEL

The geometric and material properties used are given in the Table 2.1.

TABLE 2.1. GEOMETRIC AND MATERIAL PROPERTIES

Property	A (cm^2)	I (cm^2)	E (Kgf/cm^2)
Value	6.0	2.0	720000

2.2.1.1 NUMERICAL SOLUTION AND COMPARISON OF RESULTS

The response for the horizontal and vertical displacement was measured in the node where the load *P* is applied.

In the article [27] 9 values for the displacement vs. load factor are supplied.

The final configuration of the structure with the full magnitude of the force *P* applied is represented in Figure 2.9.

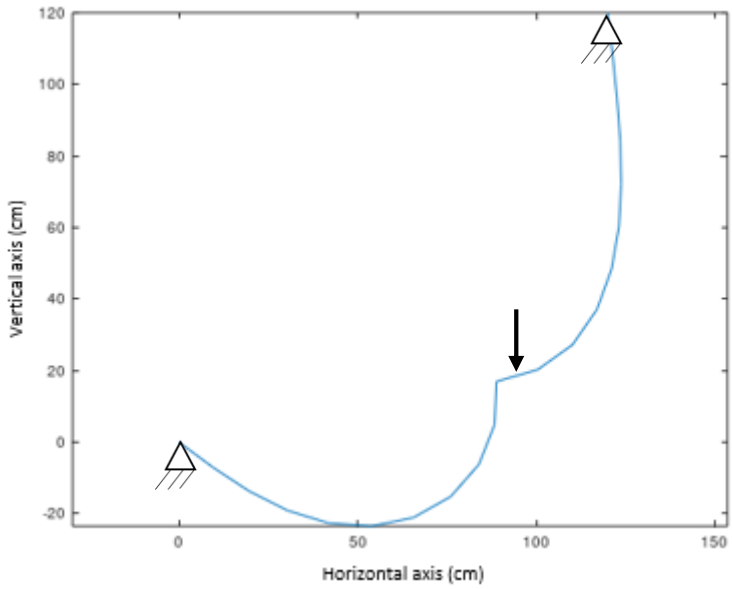

FIGURE 2.9. DEFORMED CONFIGURATION OF THE STRUCTURE

Tables 2.2 and 2.3 contain the results for the horizontal, *U*, and vertical, *V*, displacement, respectively, obtained using PROAES_NL and the comparison with the published results [26] with the relative error calculated with (2.28).

The applied load is obtained multiplying the vertical load P by the load factor. However, because a snap-through critical point occurs, it was not possible to match the exact same values for load factor used in [27] since there are symmetric values and negative load factor values.

TABLE 2.2. COMPARISON OF RESULTS FOR THE HORIZONTAL DISPLACEMENT

Load factor (Cichon)	U (cm) (Cichon)	Load factor (PROAES_NL)	U (cm) (PROAES_NL)	Relative error U (%)
0.5	0.3102	0.5	0.30402	1.9923
1.2989	4.5534	1.2989	4.48705	1.4572
1.7355	14.537	1.7355	14.735	1.3620
1.8744	25.449	1.8658	27.118	6.5582
1.3490	57.359	1.3368	57.534	0.3051
-0.07214	79.612	-0.0911	79.678	0.0829
-0.98781	90.314	-0.9618	90.225	0.0985
0.27050	88.974	0.2408	88.932	0.0472
1.4496	86.199	1.5716	86.226	0.0313

TABLE 2.3. COMPARISON OF THE RESULTS FOR THE VERTICAL DISPLACEMENT

Load factor (Cichon)	W (cm) (Cichon)	Load factor (PROAES_NL)	W (cm) (PROAES_NL)	Relative error W (%)
0.5	3.7514	0.5	3.7816	0.8050
1.2989	18.212	1.2989	18.235	0.1263
1.7355	35.924	1.7355	36.657	2.0404
1.8744	47.073	1.8658	47.309	0.5013
1.3490	60.347	1.3368	60.901	0.9180
-0.07214	52.850	-0.0911	52.333	0.9782
-0.98781	58.257	-0.9618	58.122	0.2317
0.27050	87.607	0.2408	87.589	0.0205
1.4496	91.867	1.5716	92.219	0.3832

The graphic comparison of the results is shown in Figure 2.10 and Figure 2.11.

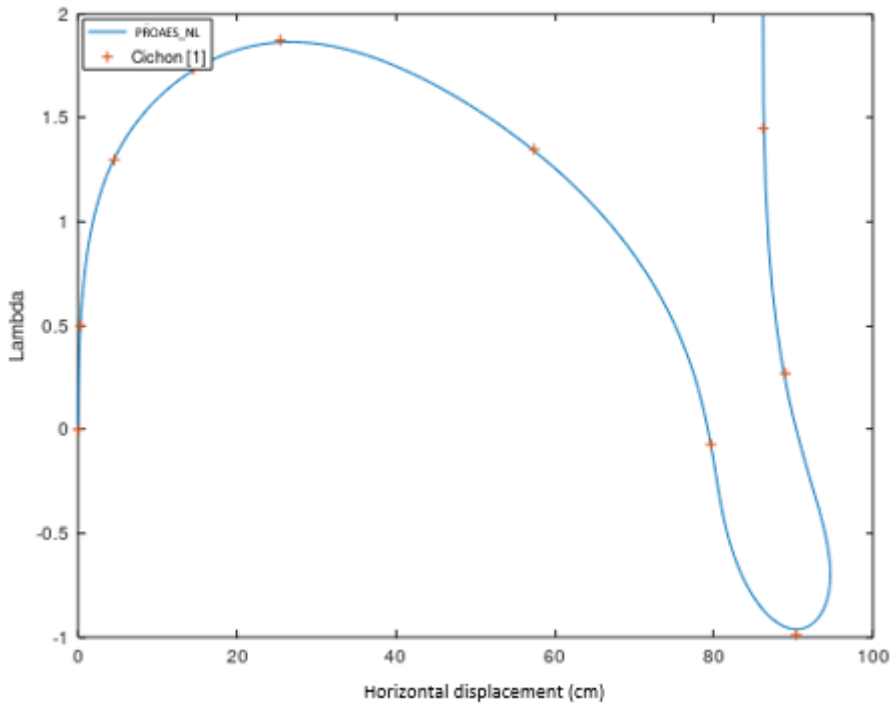

FIGURE 2.10. GRAPHICAL COMPARISON LAMBDA VS VERTICAL DISPLACEMENT FOR THE POINT OF APPLICATION OF P

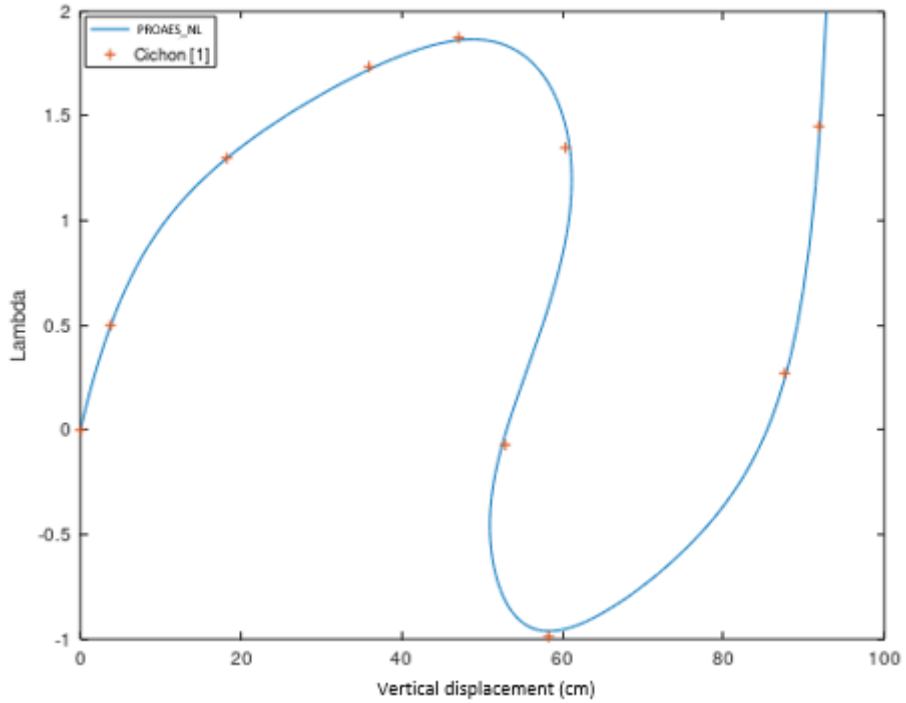

FIGURE 2.11. GRAPHICAL COMPARISON LAMBDA VS HORIZONTAL DISPLACEMENT FOR THE POINT OF APPLICATION OF P

The results obtained for this example are in close accordance with the values presented in [27] with a relative error below 6%.

2.2.1.2 COMPARISON OF THE RESULTS WITH *ANSYS*

The comparison of the results obtained for the horizontal and vertical displacement of node 13 for the full value of the applied load using PROAES_NL and *ANSYS* are presented in Table 2.4 using formulae 2.28.

TABLE 2.4. COMPARISON BETWEEN PROAES_NL AND ANSYS

	PROAES_NL	ANSYS	Relative error (%)
U (cm)	86.170	86.241	0.082
W (cm)	92.797	92.813	0.017

A minimal discrepancy exists between both results with a relative error below 0.1%.

2.2.2 EXAMPLE 2

The second example is a cantilever beam with an applied moment in its free end. This configuration was studied analytically by Lewis and Monasa [30] and numerically studied by Hsiao and Hou [31] and Urthaler and Reddy [32]. In both [31] and [32], the numerical results were compared with the analytical results. Therefore, this example is of extreme usefulness, given the fact that it's possible to compare the results obtained using PROAES_NL with analytical results. The analytical equations that provide the values of the horizontal and vertical displacement of the free end of the beam can be obtained through a geometric analysis of the situation of curvature of the beam and with the usage of the equations for the stress in a beam subjected to bending.

For the numerical solution, 11 nodes and 10 finite beam elements with 3 DOF were defined. The reader is referred to the Figure 2.12 (b) for better understanding.

For the applied moment, *M*, a value of 6280.672 Nm was used to obtain a full rotation of the beam.

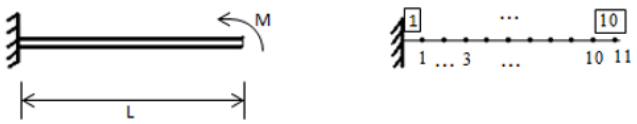

(A) (B)

FIGURE 2.12. CANTILEVER BEAM WITH APPLIED MOMENT (A) SCHEMATICS (B) FINITE ELEMENT MODEL

The cantilever beam has a rectangular section of area *A*, a moment of inertia *I*, length *L* and Young's modulus *E*. The values for the properties mentioned before are presented in Table 2.5.

TABLE 2.5. GEOMETRIC AND MATERIAL PROPERTIES

Property	L (m)	A(m^2)	I (m^4)	E (N/m^2)
Value	10	0.1	$8.3(3)*10^{-5}$	$1.2*10^8$

2.2.2.1 ANALYTICAL SOLUTION

Using as a starting point the equations for the stress in a Euler-Bernoulli beam subjected to bending:

$$\sigma_{xx} = -\frac{yE}{\rho} \tag{2.29}$$

$$\sigma_{xx} = -\frac{M}{I}y \tag{2.30}$$

Equalizing both equations the formulae for the curvature radius of the beam is obtained.

$$\rho = \frac{EI}{M} = \frac{M_0 L}{M} \tag{2.31}$$

Where,

$$M_0 = \frac{EI}{L} \tag{2.32}$$

For the deduction of the formulae for the horizontal, *U*, and vertical, *W*, displacement of the free end of the beam, a geometric analysis of the beam bent in a generic position is necessary.

The deduction for the vertical displacement, *W*, is presented below, see Figure 2.13.

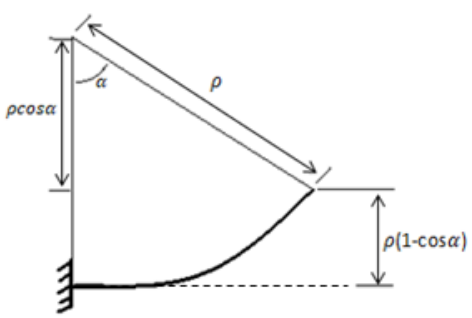

FIGURE 2.13. SCHEMATIC FOR THE DEDUCTION OF THE FORMULAE FOR THE VERTICAL DISPLACEMENT

It's necessary to define a relation between α and the applied moment similar to the one found for the curvature radius.

$$\rho\alpha = L \tag{2.33}$$

$$\Leftrightarrow \alpha = \frac{L}{\rho}$$

$$\Leftrightarrow \alpha = \frac{LM}{EI}$$

$$\Leftrightarrow \alpha = \frac{M}{M_0}$$

The vertical displacement, *W*, is given by the following expression:

$$W = \rho(1 - cos\alpha) \tag{2.34}$$

Adding the expressions 2.33 and 2.34 in equation 2.31 the following formulae for the normalized vertical displacement is found.

$$\frac{W}{L} = \frac{M_0}{M}\left(1 - cos\frac{M}{M_0}\right) \tag{2.35}$$

The horizontal displacement is given by the following expression, see Figure 2.14:

$$U = L - \rho sen\alpha \tag{2.36}$$

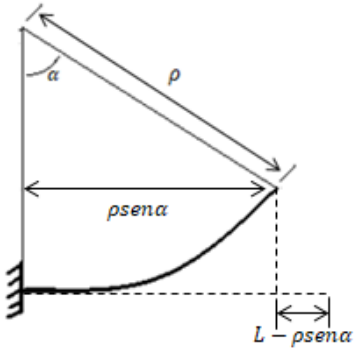

FIGURE 2.14. SCHEMATIC FOR THE DEDUCTION OF THE FORMULAE FOR THE HORIZONTAL DISPLACEMENT

Adding the relations 2.33 and 2.36 in equation 2.31 the following formulae, 2.37, for the normalized horizontal displacement is found.

$$\frac{U}{L} = 1 - \frac{M_0}{M} sen \frac{M}{M_0} \tag{2.37}$$

2.2.2.2 NUMERICAL SOLUTION AND COMPARISON OF RESULTS

The calculations were made for a full rotation of the beam. To achieve that the curvature radius, ρ, must be equal to the entire length of the beam, L, divided by $2\,\pi$.

A comparison was made for the normalized displacements obtained for various load factors obtained using PROAES_NL and obtained through the analytical method.

The final configuration of the beam is presented in Figure 2.15.

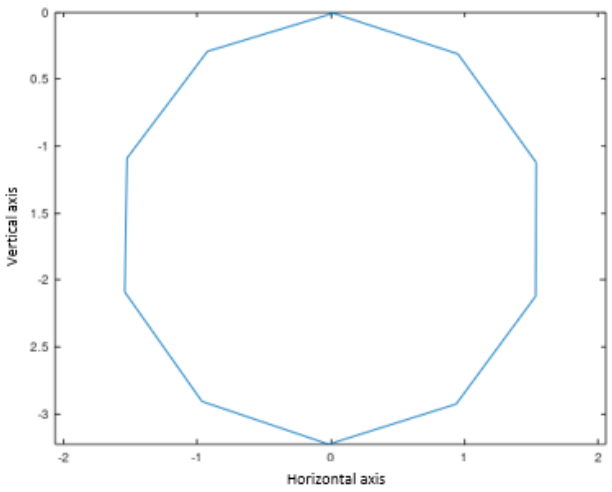

FIGURE 2.15. DEFORMED CONFIGURATION OF THE STRUCTURE

In Table 2.6 a comparison of the results for the modulus of the normalized horizontal displacement, *U/L* is shown.

TABLE 2.6. COMPARISON OF THE RESULTS OBTAINED FOR THE NORMALIZED HORIZONTAL DISPLACEMENT

Load (Nm)	U/L (PROAES_NL)	U/L (Analytical)	Relative error U/L (%)
314.66	0.01651	0,01642	0,54477

607.06	0.06063	0,06030	0,55005
879.61	0.12473	0,12405	0,55143
1134.3	0.20214	0,20106	0.53720
1899.9	0.50445	0,50191	0.50607
2651.2	0.82610	0,82237	0.45357
3158.7	1.00944	1,00542	0.40000
3903.1	1.18011	1,17679	0.28212
5155.7	1.17470	1,17521	0.04334
6280.7	0.99663	1.00040	0.37685

In Table 2.7 a comparison of the results for the modulus of the normalized vertical displacement, *W/L* is shown.

TABLE 2.7. COMPARISON OF THE RESULTS OBTAINED FOR THE NORMALIZED VERTICAL DISPLACEMENT

Load factor	W/L (PROAES_NL)	W/L (Analytical)	Relative error W/L (%)
314.66	0.15666	0,15604	0,39912
607.06	0.29548	0,29432	0,39344
879.61	0.41374	0,41217	0.38100
1134.3	0.51075	0,50889	0.36550
1899.9	0.69851	0,69646	0.29435
2651.2	0.71104	0,70992	0.15776
3158.7	0.63315	0,63312	0.00474
3903.1	0.43990	0,44164	0.39399
5155.7	0.10793	0,11077	2.56387
6280.7	0	0	0

The graphical comparison of the results obtained is shown in Figure 2.16.

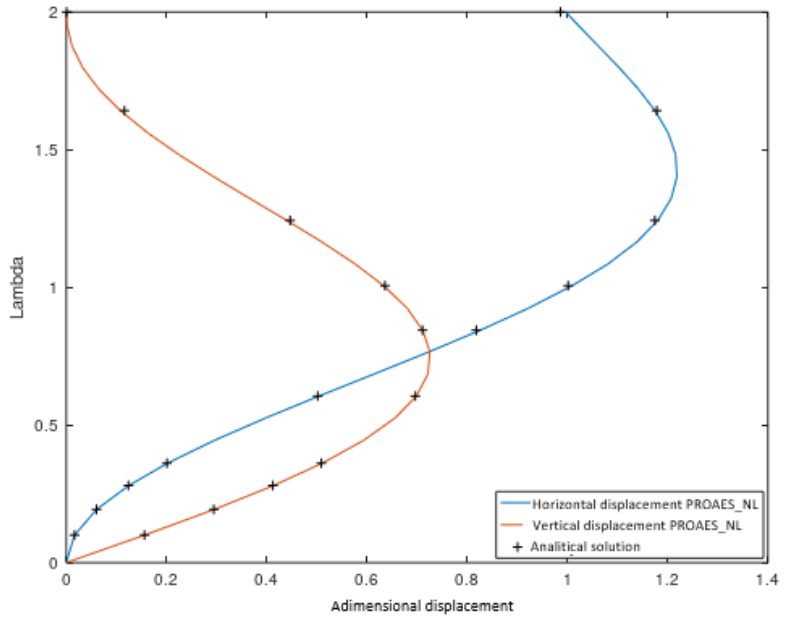

FIGURE 2.16. GRAPHIC REPRESENTATION OF THE RESULTS OBTAINED AND COMPARISON WITH ANALYTICAL SOLUTION

The results obtained for this example are entirely satisfactory since there's close accordance with the analytical values with a relative error below 3%.

2.2.2.3 COMPARISON OF THE RESULTS WITH *ANSYS*

In addition, the results obtained using PROAES_NL were compared with the results obtained using the non-linear option available in *ANSYS*. The comparison of results was made for nodes 2, 6 and 11. The results obtained are presented in Table 2.8 and Table 2.9.

The comparison of the results for the modulus of the normalized horizontal displacement, *U/L*, is presented in Table 2.8.

TABLE 2.8. COMPARISON OF THE RESULTS FOR THE NORMALIZED HORIZONTAL DISPLACEMENT PROAES_NL VS. ANSYS

	U/L (PROAES_NL)	U/L (ANSYS)	Relative error(%)
Node 2	0.00493	0.00489	0.81800
Node 6	0.50168	0.49980	0.37615
Node 11	0.99663	1.00040	0.37685

The comparison of the results for the modulus of the normalized vertical displacement, *W/L*, is presented in Table 2.9.

TABLE 2.9. COMPARISON OF THE RESULTS FOR THE NORMALIZED VERTICAL DISPLACEMENT PROAES_NL VS. ANSYS

	W/L (PROAES_NL)	W/L (ANSYS)	Relative error (%)
Node 2	0.03100	0.03089	0.35610
Node 6	0.32257	0.32373	0.35832
Node 11	0	0	0

The results obtained using PROAES_NL are in close accordance with the results obtained using *ANSYS* with a relative error below 1%.

2.2.3 EXAMPLE 3

The third example studied is a cantilever beam with two concentrated loads of value 0.85P and 1.35P, where *P* has a value of 4.45N. The beam has a uniform rectangular cross-section of area *A*. This problem was studied in its analytical form through two different methods by Frisch-Fay [33] and F.S.Manuel and S.Lee [34]. After that, it was numerically studied using finite elements by Backlund [35] where the results obtained are compared with the results presented in [33] and [34]. For this reason, for comparison of the results obtained using PROAES_NL, the article [35] was used, allowing for the comparison with three already existing studies.

For the numerical solution, 11 nodes and 10 finite beam elements with 3 DOF per node were defined. The reader is referred to the Figure 2.17 (b) for better understanding.

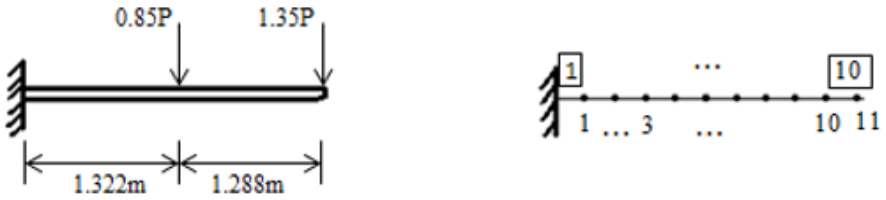

(A) (B)

FIGURE 2.17. CANTILEVER BEAM WITH TWO CONCENTRATED LOADS (A) SCHEMATICS (B) FINITE ELEMENT MODEL

The values for the geometric and material properties of the beam are presented in Table 2.10.

TABLE 2.10. GEOMETRIC AND MATERIAL PROPERTIES

Property	L (m)	A(m^2)	I (m^4)	E (N/m^2)

Value	2.61	0.000125	$6.5*10^{-11}$	$207*10^{9}$

2.2.3.1 NUMERICAL SOLUTION AND COMPARISON OF THE RESULTS WITH OTHER AUTHORS

The values for the response of the vertical and horizontal displacement of the structure were measured in node 11. These displacements can be compared with the analytical results mentioned at the beginning of this section.

The final configuration obtained for the structure is represented in Figure 2.18.

In Table 2.11 are shown the results obtained for the horizontal displacement, *U*.

TABLE 2.11. OBTAINED RESULTS FOR THE HORIZONTAL DISPLACEMENT IN LITERATURE AND PROAES_NL

Node	U (Frisch-Fay) (m)	U (Manuel and Lee) (m)	U (Backlund) (m)	U (PROAES_NL) (m)
11	0.788	0.781	0.787	0.827

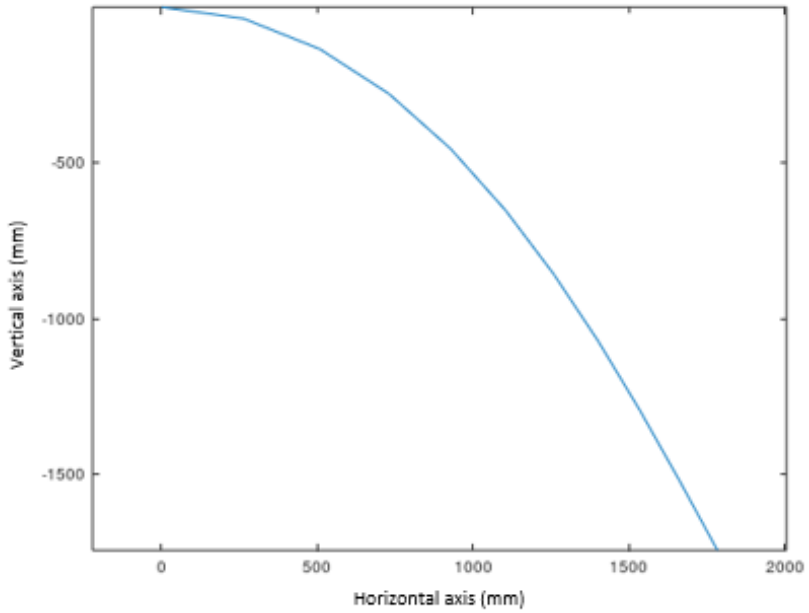

FIGURE 2.18. DEFORMED CONFIGURATION OF THE STRUCTURE

In Table 2.12 are shown the comparison of results for the horizontal displacement, *U*.

TABLE 2.12. COMPARISON OF RESULTS IN LITERATURE AND PROAES_NL

Node	Error U PROAES_NL vs [33] %	Error U PROAES_NL vs [34] %	Error U PROAES_NL vs [35] %
11	4.950	5.890	5.083

In Table 2.13 are shown the results obtained for the vertical displacement, W.

TABLE 2.13. OBTAINED RESULTS FOR VERTICAL DISPLACEMENT IN LITERATURE AND USING PROAES_NL

Node	W [33] (m)	W [34] (m)	W [35] (m)	W (PROAES_NL) (m)
11	1.710	1.701	1.716	1.743

In Table 2.14 are shown the comparison of results for the vertical displacement, W.

TABLE 2.14. COMPARISON OF RESULTS IN LITERATURE AND PROAES_NL

Node	Error W PROAES_NL VS [33] %	Error W PROAES_NL VS [34] %	Error W PROAES_NL VS [35] %
11	1.930	2.470	1.573

The graphic representation of the obtained results, in modulus, is shown in Figure 2.19 and Figure 2.20.

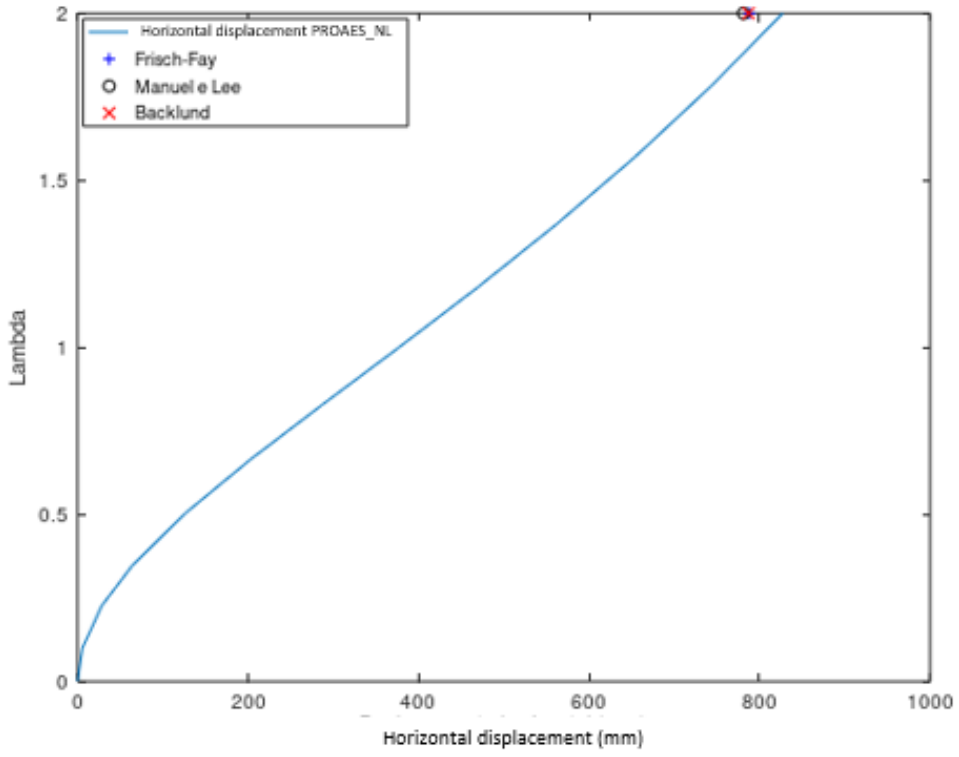

FIGURE 2.19. OBTAINED RESULTS FOR THE HORIZONTAL DISPLACEMENT AND COMPARISON WITH LITERATURE

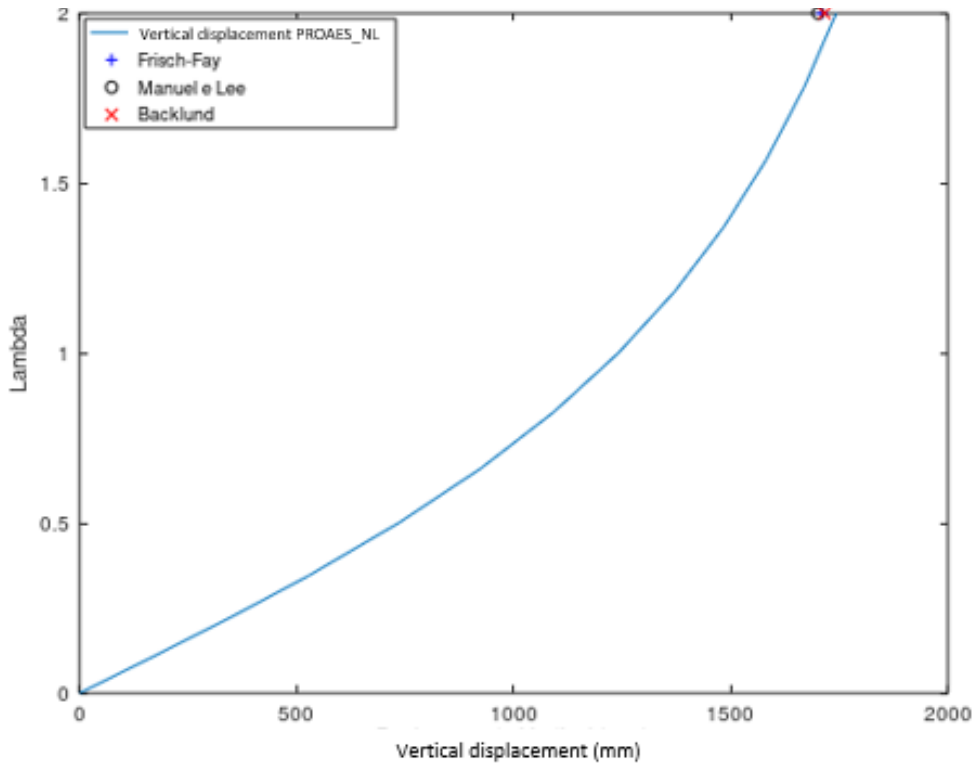

FIGURE 2.20. OBTAINED RESULTS FOR THE VERTICAL DISPLACEMENT AND COMPARISON WITH LITERATURE

2.2.3.2 COMPARISON OF THE RESULTS WITH *ANSYS*

A comparison was made between the results obtained using PROAES_NL and the results obtained through a nonlinear analysis using *ANSYS* for the final vertical and horizontal displacement of node 11. The modulus of the results is shown in Table 2.15.

TABLE 2.15. COMPARISON OF RESULTS BETWEEN PROAES_NL AND ANSYS

	PROAES_NL (m)	ANSYS (m)	Relative error (%)
U	0.82711	0.82869	0.191
W	1.74295	1.74420	0.072

2.2.4 EXAMPLE 4

The last example is a cantilever beam subjected to a concentrated force in its free end. The analytical form of this problem was studied by Bisshopp and Drucker[36]. The numerical analysis was made by several authors such as Hsiao and Hou [31], Horrigmoe and Bergan [37], Tada and Lee [38], and Urthaler and Reddy [32]. Urthaler e Reddy [32] present their results in the form of millimetric graphics, making it possible to extract with satisfactory approximation the results obtained. Therefore, the displacements obtained using PROAES_NL were compared with the results presented in [32] and [38].

The free end of the cantilever beam is subjected to a concentrated vertical load with a value of 100 N pointing in the negative direction of the vertical axis. The beam has a uniform rectangular cross-section of area A, a moment of inertia I, and Young modulus E. The values of these geometric and material properties are not provided in the literature and therefore the same values used in example 2 were applied. The values for the geometric and material properties can be consulted in Table 2.16.

For the numerical solution, 11 nodes and 10 beam finite elements with 3 DOF per node were defined. For better understanding, the reader is asked to consult Figure 2.21.

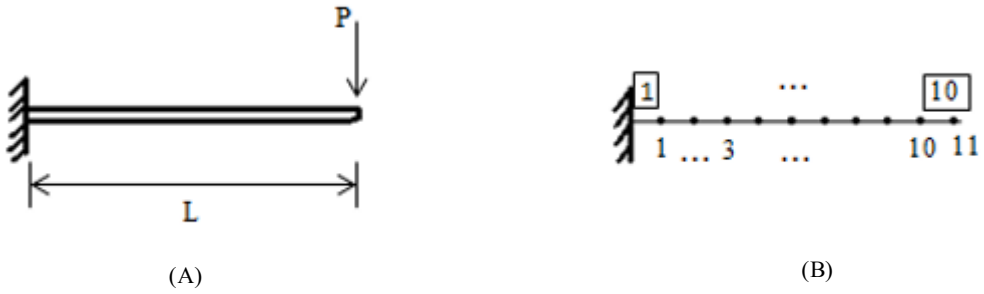

(A) (B)

FIGURE 2.21. CANTILEVER BEAM WITH A CONCENTRATED FORCE IN ITS FREE END A) SCHEMATICS B) FINITE ELEMENT MODEL

TABLE 2.16. GEOMETRIC AND MATERIAL PROPERTIES

Property	L (m)	A(m^2)	I (m^4)	E (N/m^2)
Value	10	0.1	$8.3(3)*10^{-5}$	$1.2*10^{8}$

2.2.4.1 NUMERICAL SOLUTION AND COMPARISON OF THE RESULTS WITH OTHER AUTHORS

The values for the horizontal and vertical displacement of the structure were measured in node 11.

The final configuration for $\frac{PL^2}{EI} = 5$ is displayed in Figure 2.22.

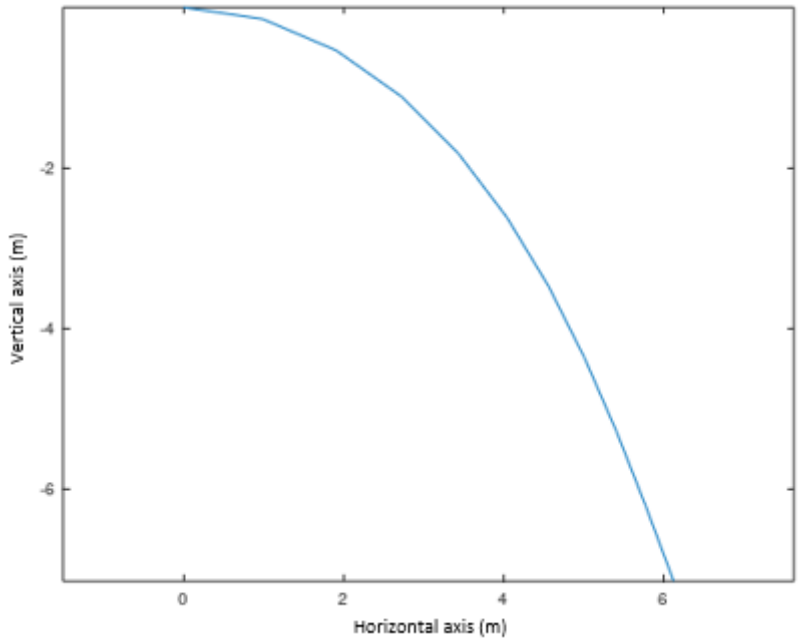

FIGURE 2.22. DEFORMED CONFIGURATION OF THE STRUCTURE

Both authors [32] and [38] present the vertical displacement in a normalized form.

The comparison between the results provided in the literature and the results obtained using PROAES_NL for the normalized vertical displacement is presented in Table 2.17.

TABLE 2.17. COMPARISON OF RESULTS BETWEEN LITERATURE AND PROAES_NL FOR THE NORMALIZED VERTICAL DISPLACEMENT

$\frac{PL^2}{EI}$	W/L (Tada e Lee)	W/L (Urthaler e Reddy)	W/L (PROAES_NL)	Relative error Tada e Lee vs PROAES_NL (%)	Relative error Urthaler e Reddy vs PROAES_NL (%)
1.0	0.303	0.305	0.302	0.330	0.984
2.0	0.495	0.490	0.494	0.202	0.816
3.0	0.604	0.600	0.604	0.000	0.667
4.0	0.671	0.660	0.671	0.000	1.667
5.0	0.712	0.720	0.715	0.421	0.694

The graphic comparison of the results for the vertical displacement is shown in Figure 2.23.

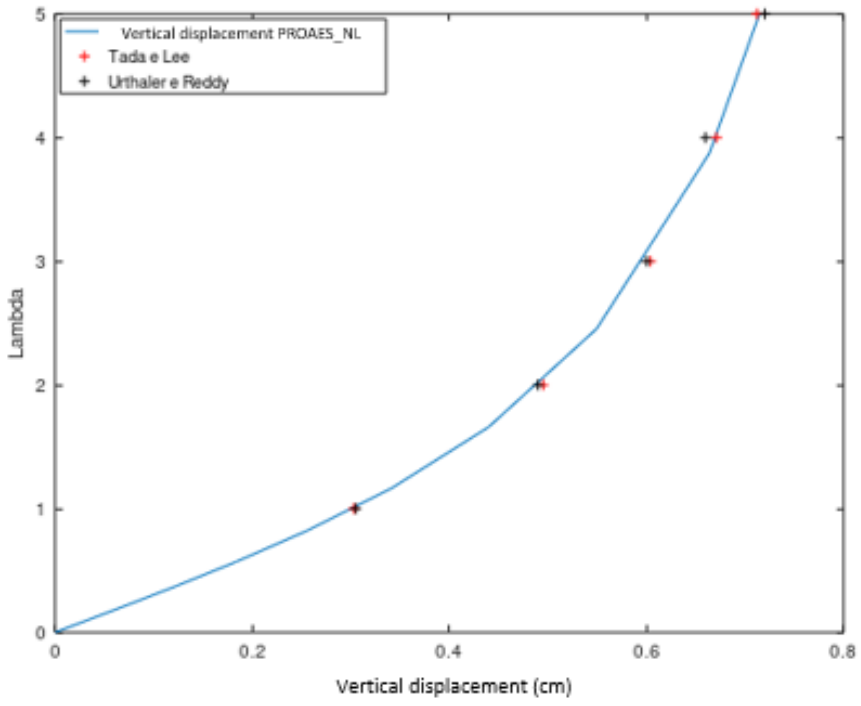

FIGURE 2.23. GRAPHIC COMPARISON OF THE RESULTS OBTAINED FOR THE VERTICAL DISPLACEMENT

The results for the horizontal displacement are presented in both [32] and [38] in a normalized way.

In Table 2.18 is shown the comparison of results for the horizontal displacement between PROAES_NL and [32] and [38].

TABLE 2.18. COMPARISON OF RESULTS BETWEEN LITERATURE AND PROAES_NL FOR THE NORMALIZED HORIZONTAL DISPLACEMENT

$\frac{PL^2}{EI}$	1-U/L (Tada e Lee)	1-U/L (Urthaler e Reddy)	1-U/L (PROAES_NL)	Relative error Tada e Lee vs PROAES_NL(%)	Relative error Urthaler e Reddy vs PROAES_NL (%)
1.0	0.836	0.945	0.944	12.92	0.106
2.0	0.726	0.842	0.840	15.70	0.238
3.0	0.655	0.740	0.746	13.89	0.811
4.0	0.641	0.670	0.671	4.680	0.150
5.0	0.568	0.610	0.613	7.923	0.492

The graphic comparison of the results obtained for the horizontal displacement is shown in Figure 2.24.

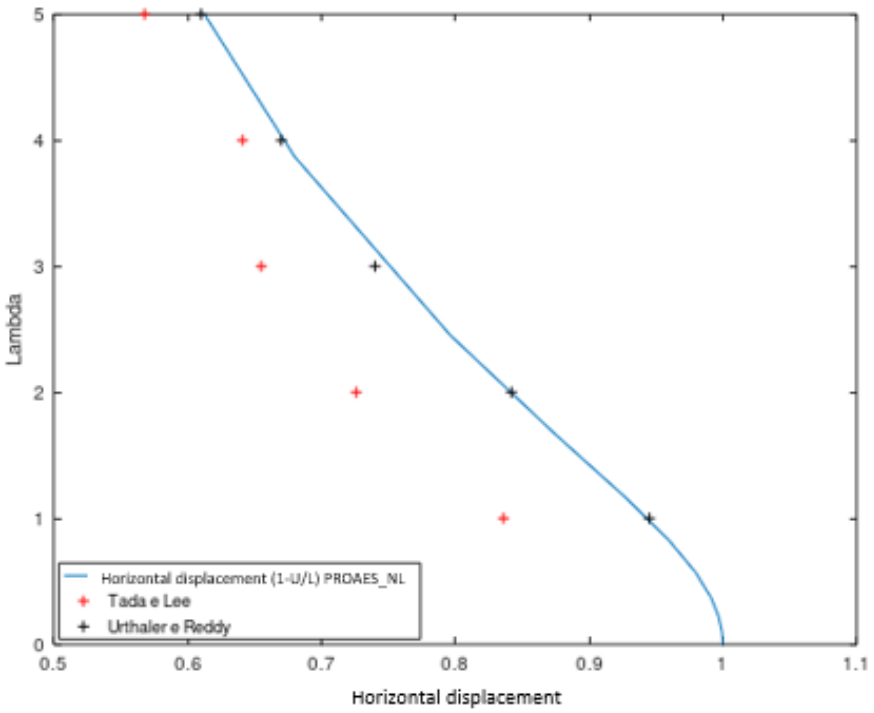

FIGURE 2.24. GRAPHIC COMPARISON OF RESULTS FOR THE HORIZONTAL DISPLACEMENT

Through the analysis of the results obtained, one can conclude that a close agreement exists for the vertical displacement between both articles and PROAES_NL with relative error well below 2%.

However, for the horizontal displacement, a slight discrepancy can be observed between the values presented by Tada and Lee and the values provided by Urthaler and Reddy. The values obtained using PROAES_NL are in close accordance with the results provided by Urthaler and Reddy with a relative error below 1%.

2.2.4.1 COMPARISON OF RESULTS WITH *ANSYS*

A comparison was made between the results obtained using PROAES_NL and the results obtained through a nonlinear analysis using *ANSYS* for the vertical and horizontal displacement of node 11.

The modulus of the results obtained and the comparison between *ANSYS* and PROAES_NL are shown in Table 2.19.

TABLE 2.19. COMPARISON OF RESULTS OBTAINED USING ANSYS AND PROAES_NL

	PROAES_NL (m)	ANSYS (m)	Relative error (%)
U	3.875	3.883	0.210
W	7.146	7.151	0.070

Both the values obtained for the horizontal and vertical displacement are in close accordance with the values obtained using *ANSYS* with a relative error below 0.3%. Therefore, an assumption can be made that there is the possibility of a mistake in the results presented by Tada and Lee for the horizontal displacement given the fact that the values shown by Urthaler and Reddy are in accordance with the values obtained using *ANSYS*.

2.2.5 FINAL REMARKS

To test the code developed in program PROAES_NL, four examples from literature were taken into consideration. The comparison between the results obtained using PROAES_NL and the results presented in the articles and the results obtained using *ANSYS* allows one to verify the high quality and coherence of PROAES_NL. Therefore, the methodology implemented in PROAES_NL for the analysis of structures with geometrically nonlinear behavior is validated. Moving forward, the program

PROAES_NL will be used in the development of this thesis for topology optimization, given the fact that it can perform accurate analysis for a structure with nonlinear behavior.

CHAPTER 3

SIZING DESIGN SENSITIVITY

3.1 THEORY DESCRIPTION

The theory of design differentiability of nonlinear structural response has been fully developed by Santos [1] and was the base for the development of this thesis. A more extensive analysis on the subject can be found in [1] and some essential parts on the two articles published by Santos and Choi [39] and [17]. For the purpose of this work, the impact of a variation of displacement vs. the resulting variation in the cross-section area of the elements is going to be considered. The theory used for the development of this thesis is now summarized and presented as a way of providing context for the work that follows.

Using the principle of virtual work, it is possible to write the static equilibrium equation of an elastic system in the configuration at time $t + \Delta t$ in its variational form as:

$$a_u({}^{t+\Delta t}z, \bar{z}) = l_u(\bar{z}), \quad \text{for all } \bar{z} \in Z \tag{3.1}$$

Where Z is the space of cinematically admissible displacements. Being $\bar{z}(x)$ an arbitrary function that satisfies the boundary conditions also known in classical mechanics as virtual displacements. The subscript u denotes dependence of the quantities on the design u. It's not possible to solve this equation directly since the configuration of the structure at time $t + \Delta t$ is unknown. It's possible to obtain a solution by referring all variables to a known calculated equilibrium. In this thesis, having used the corotational formulation in the development of the nonlinear analysis program the variables are referred to the initial equilibrium configuration of the structure at time $t = 0$.

To find the variations of structural performances due to the variations in the design, u, the first derivative of equation 3.1 with respect to the design must be calculated.

Considering the configuration at time $t + \Delta t$ for a perturbed design $u + \tau\delta u$ with the reference configuration at time 0, equation 3.1 can be rewritten as:

$$a_{u+\tau\delta u}\left({}^{t+\Delta t}_{0}z, {}_{0}\bar{z}\right) = l_{u+\tau\delta u}(\bar{z}), \quad \text{for all } \bar{z} \in z \tag{3.2}$$

Where the subscript $u + \tau\delta u$ is used to indicate that the equilibrium equation corresponds to design $u + \tau\delta u$, ${}_{0}\bar{z}$ is the cartesian component of the virtual displacement vector referred to configuration time 0 and ${}^{t+\Delta t}_{0}z$ is the cartesian component of displacement in configuration time $t + \Delta t$ referred to configuration time 0.

The first variation of the energy form in equation 3.2 with respect to the design, u, is:

$$a'_{\delta u}({}^{t}_{0}z, {}_{0}\bar{z}) = \frac{d}{d\tau} a_{u+\tau\delta u}({}^{t}_{0}\tilde{z}, {}_{0}\bar{z})|_{\tau=0} \tag{3.3}$$

Where ${}^{t}_{0}\tilde{z}$ denotes the state ${}^{t}_{0}z$ with dependence on τ suppressed and ${}_{0}\bar{z}$ is independent of τ.

The first variation of the load form in equation 3.2 with respect to the design, u, is:

$$l'_{\delta u}({}_{0}\bar{z}) = \frac{d}{d\tau} l_{u+\tau\delta u}({}_{0}\bar{z})|_{\tau=0} \tag{3.4}$$

Considering that the variation of the solution of equation 3.2 with respect to the design, u, is:

$${}_{0}z' = \frac{d}{d\tau} {}^{t+\Delta t}_{0}z(u+\tau\delta u)|_{\tau=0} \tag{3.5}$$

Using the chain rule of differentiation and equation 3.3 and equation 3.5, it is possible to write:

$$\frac{d}{d\tau}\left[a_{u+\tau\delta u}\left({}^{t+\Delta t}_{0}z(u+\tau\delta u), {}_{0}\bar{z}\right)\right]|_{\tau=0} = a'_{\delta u}({}^{t}_{0}z, {}_{0}\bar{z}) + a^{*}_{u}({}^{t}_{0}z; {}_{0}z', {}_{0}\bar{z}) \tag{3.6}$$

By inserting equations 3.4 and 3.6 in equation 3.3, it is possible to obtain:

$$a^{*}_{u}({}^{t}_{0}z; {}_{0}z', {}_{0}\bar{z}) = l'_{\delta u}({}_{0}\bar{z}) - a'_{\delta u}({}^{t}_{0}z, {}_{0}\bar{z}) \tag{3.7}$$

3.1.1. ADJOINT VARIABLE METHOD FOR DESIGN SENSITIVITY ANALYSIS

It's now necessary to determine the expressions of a general functional, ψ, for sizing design sensitivity analysis.

A measure of structural performance in integral form can be written as

$${}^{t+\Delta t}_{0}\psi_{\tau} = \int_{{}^{0}V} g\left({}^{t+\Delta t}_{0}z, {}_{0}\nabla^{t+\Delta t}z, u+\tau\delta u\right)^{0} dV \tag{3.8}$$

The variation of the functional in equation 3.8 with respect to the design, u, can be written as:

$$ {}_0^t\psi' = \frac{d}{d\tau}\left[\int_{0_V} g\left({}^{t+\Delta t}_{0}z(u+\tau\delta u),\ {}_0\nabla^{t+\Delta t}z(u+\tau\delta u), u+\tau\delta u\right)^0 dV\right]|_{\tau=0} \tag{3.9} $$

$$ = \int_{0_V} \left(g_{{}^t_0z\ 0}z' + g_{{}_0\nabla^t z\ 0}\nabla z' + g_u\delta u\right)^0 dV $$

By replacing ${}_0z'$ in equation 3.9 with a virtual displacement ${}_0\bar{\lambda}$ and equating the terms involving the virtual displacement into the energy bilinear form a_u^*, it's possible to create the adjoint equation for the adjoint variable ${}_0\bar{\lambda}$:

$$ a_u^*\left({}_0^tz;\ {}_0\lambda', {}_0\bar{\lambda}\right) = \int_{0_V}\left(g_{{}^t_0z\ 0}\bar{\lambda} + g_{{}_0\nabla^t z\ 0}\nabla\bar{\lambda}\right)^0 dV, \text{ for all } {}_0\bar{\lambda} \in {}_0z \tag{3.10} $$

Because ${}_0z' \in {}_0z$ by evaluating equation 3.10 at ${}_0\bar{\lambda} = {}_0z'$ one obtains:

$$ a_u^*({}_0^tz;\ {}_0\lambda\ ,\ {}_0z') = \int_{0_V}\left(g_{{}^t_0z\ 0}z' + g_{{}_0\nabla^t z\ 0}\nabla z'\right)^0 dV \tag{3.11} $$

Because ${}_0\bar{z}$ and ${}_0\lambda$ are in ${}_0z$ by evaluating equation 3.7 at ${}_0\bar{z} = {}_0\lambda$ one obtains:

$$ a_u^*({}_0^tz;\ {}_0z'\ ,\ {}_0\lambda) = l'_{\delta u}({}_0\lambda) - a'_{\delta u}({}_0^tz,\ {}_0\lambda) \tag{3.12} $$

By substituting equations 3.11 and 3.12 in equation 3.9, one obtains:

$$ {}_0^t\psi' = \int_{0_V}(g_u\delta u)^0 dV + l'_{\delta u}({}_0\lambda) - a'_{\delta u}({}_0^tz,\ {}_0\lambda) \tag{3.13} $$

In the focus of this dissertation, it will only be considered the functional that defines the value of the displacement at an isolated point $\hat{x}$ which can be written using the Dirac function.

$$ {}^{t}_{0}\psi' = \int_{0}^{{}^{0}l} \hat{\delta}({}^{0}x - {}^{0}\hat{x})\, {}_{0}z'({}^{0}x) d\,{}^{0}x \tag{3.14} $$

Therefore, the adjoint equation is now written as:

$$ a^{*}_{u}({}^{t}_{0}z; {}_{0}\lambda, {}_{0}\lambda) = \int_{0}^{{}^{0}l} \hat{\delta}({}^{0}x - {}^{0}\hat{x})\, {}_{0}\bar{\lambda} d\,{}^{0}x, \text{ for all } {}_{0}\bar{\lambda} \in {}_{0}z \tag{3.15} $$

Interpreting the Dirac measure as a unit load applied at the point ${}^{0}\hat{x}$ the physical interpretation of ${}_{0}\lambda$ can be of the displacement of the structure from the final equilibrium configuration due to a unit load applied at ${}^{0}\hat{x}$. The variation of the functional equation can then be rewritten as:

$$ {}^{t}_{0}\psi' = l'_{\delta u}({}_{0}\lambda) - a'_{\delta u}({}^{t}_{0}z, {}_{0}\lambda) \tag{3.16} $$

For the problems considered in this work the variation of the load form $l'_{\delta u}$ is zero. Therefore, the variation of the functional can be written as:

$$ {}^{t}_{0}\psi' = -a'_{\delta u}({}^{t}_{0}z, {}_{0}\lambda) \tag{3.17} $$

Using the undeformed configuration for reference, the energy form of a beam/truss component is

$$ \begin{aligned} a_{u}({}^{t}_{0}z, {}_{0}\bar{z}) = & \int_{0}^{{}^{0}l} \{ EA \left[{}^{t}_{0}z_{1,1} + \frac{1}{2}\sum_{i=1}^{3} ({}^{t}_{0}z_{i,1})^{2} \right] [{}_{0}\bar{z}_{1,1} + {}^{t}_{0}z_{i,1}\, {}_{0}\bar{z}_{i,1}] \}\, d\,{}^{0}x \\ & + \int_{0}^{{}^{0}l} [EI^{2}\, {}^{t}_{0}z_{2,11}\, {}_{0}\bar{z}_{2,11} + EI^{3}\, {}^{t}_{0}z_{3,11}\, {}_{0}\bar{z}_{3,11}]\, d\,{}^{0}x \end{aligned} \tag{3.18} $$

Where E is the young's modulus, A is the cross-sectional area of the beam, I^{i} is the moment of inertia, ${}^{t}z_{1}$, ${}^{t}z_{2}$ and ${}^{t}z_{3}$ are the axial displacement and the two orthogonal lateral displacements corresponding to the configuration at time t referred to the configuration at time 0, respectively and ${}_{0}\bar{z}_{i}$ are the cartesian components of the virtual displacement vector referred to the configuration at time 0. It is of the utmost importance to remember that the vector ${}^{t}z = [{}^{t}z_{1}, {}^{t}z_{2}, {}^{t}z_{3}]$ only contains the components of the displacement due to the deformation of the element.

In the specific case of considering the cross-section area as the design variable, the variation of the energy form with respect to a variation of the area δA is:

$$a'_{\delta A}({}^{t}_{0}z,\ {}_{0}\bar{z}) = \int_{0}^{0_l} \{E\left[{}^{t}_{0}z_{1,1} + \frac{1}{2}\sum_{i=1}^{3}({}^{t}_{0}z_{i,1})^2\right][{}_{0}\bar{z}_{1,1} + {}^{t}_{0}z_{i,1}\,{}_{0}\bar{z}_{i,1}]\}\delta A\, d^0x + \int_{0}^{0_l} [EI^2_{,A}\,{}^{t}_{0}z_{2,11}\,{}_{0}\bar{z}_{2,11} + EI^3_{,A}\,{}^{t}_{0}z_{3,11}\,{}_{0}\bar{z}_{3,11}]\delta A\, d^0x \tag{3.19}$$

The calculation of the former integral requires the substitution of the virtual displacement vector for an adjoint variable vector.

For the purpose of this dissertation, only bidimensional problems will be considered. Therefore, the components that refer to displacements along the third axis will be removed from equation 3.19.

Considering z_1 the first component of the incremental displacement vector as u, z_2 the second component of the incremental displacement vector as v, $\bar{z}_1$ the first component of the adjoint variable vector as λ_u and $\bar{z}_2$ the second component of the adjoint variable vector as λ_v.

Equation 3.19 can thus be rewritten as:

$$a'_{\delta A}({}^{t}_{0}z,\ {}_{0}\bar{z}) = \int_{0}^{0_l} \{E\left[{}^{t}_{0}\left(\frac{\partial u}{\partial x}\right) + \frac{1}{2}\,{}^{t}_{0}\left(\frac{\partial u}{\partial x}\right)^2 + \frac{1}{2}\,{}^{t}_{0}\left(\frac{\partial v}{\partial x}\right)^2\right][{}^{t}_{0}\left(\frac{\partial \lambda_u}{\partial x}\right) + \frac{\partial u}{\partial x}\frac{\partial \lambda_u}{\partial x} + \frac{\partial v}{\partial x}\frac{\partial \lambda_v}{\partial x}]\}\,\delta A d^0x + \int_{0}^{0_l} [E\frac{\partial I_z}{\partial A}\frac{\partial^2 v}{\partial x^2}\frac{\partial^2 \lambda_v}{\partial x^2}]\,\delta A d^0x \tag{3.20}$$

In order to compute the derivatives in the first and second integral of equation 3.20, it is necessary to recall shape functions and Hermite polynomials for a beam element.

Using linear shape functions for the axial displacement in a beam element:

$$N_I = 1 - \frac{x}{L} \tag{3.21}$$

$$N_{II} = \frac{x}{L} \tag{3.22}$$

Their first derivative being:

$$\frac{\partial N_I}{\partial x} = -\frac{1}{L} \tag{3.23}$$

$$\frac{\partial N_{II}}{\partial x} = \frac{1}{L} \tag{3.24}$$

The first derivative of $u, v, \lambda_u$and λ_v can be written as:

$$\frac{\partial u}{\partial x} = \frac{\partial N_I}{\partial x} u_I + \frac{\partial N_{II}}{\partial x} u_{II} = \{-\frac{1}{L} \quad \frac{1}{L}\} \begin{Bmatrix} u_I \\ u_{II} \end{Bmatrix} \tag{3.25}$$

$$\left(\frac{\partial u}{\partial x}\right)^2 = \{ u_I \quad u_{II}\} \begin{Bmatrix} -\frac{1}{L} \\ \frac{1}{L} \end{Bmatrix} \{-\frac{1}{L} \quad \frac{1}{L}\} \begin{Bmatrix} u_I \\ u_{II} \end{Bmatrix} = \{u_I \quad u_{II}\} \begin{bmatrix} \frac{1}{L^2} & -\frac{1}{L^2} \\ -\frac{1}{L^2} & \frac{1}{L^2} \end{bmatrix} \begin{Bmatrix} u_I \\ u_{II} \end{Bmatrix} \tag{3.26}$$

$$\frac{\partial v}{\partial x} = \frac{\partial N_I}{\partial x} v_I + \frac{\partial N_{II}}{\partial x} v_{II} = \{-\frac{1}{L} \quad \frac{1}{L}\} \begin{Bmatrix} v_I \\ v_{II} \end{Bmatrix} \tag{3.27}$$

$$\left(\frac{\partial v}{\partial x}\right)^2 = \{ v_I \quad v_{II}\} \begin{Bmatrix} -\frac{1}{L} \\ \frac{1}{L} \end{Bmatrix} \{-\frac{1}{L} \quad \frac{1}{L}\} \begin{Bmatrix} v_I \\ v_{II} \end{Bmatrix} = \{v_I \quad v_{II}\} \begin{bmatrix} \frac{1}{L^2} & -\frac{1}{L^2} \\ -\frac{1}{L^2} & \frac{1}{L^2} \end{bmatrix} \begin{Bmatrix} v_I \\ v_{II} \end{Bmatrix} \tag{3.28}$$

$$\frac{\partial \lambda_u}{\partial x} = \frac{\partial N_I}{\partial x} \lambda_{u_I} + \frac{\partial N_{II}}{\partial x} \lambda_{u_{II}} = \{-\frac{1}{L} \quad \frac{1}{L}\} \begin{Bmatrix} \lambda_{u_I} \\ \lambda_{u_{II}} \end{Bmatrix} \tag{3.29}$$

$$\frac{\partial \lambda_v}{\partial x} = \frac{\partial N_I}{\partial x} \lambda_{v_I} + \frac{\partial N_{II}}{\partial x} \lambda_{v_{II}} = \{-\frac{1}{L} \quad \frac{1}{L}\} \begin{Bmatrix} \lambda_{v_I} \\ \lambda_{v_{II}} \end{Bmatrix} \tag{3.30}$$

Using the Hermite polynomials:

$$N_I = 1 - \frac{3}{L^2} x_1^2 + \frac{2}{L^3} x_1^3 \tag{3.31}$$

$$N_{II} = x_1 - \frac{2}{L} x_1^2 + \frac{1}{L^2} x_1^3 \tag{3.32}$$

$$N_{III} = \frac{3}{L^2} x_1^2 - \frac{2}{L^3} x_1^3 \tag{3.33}$$

$$N_{IV} = -\frac{1}{L} x_1^2 + \frac{1}{L^2} x_1^3 \tag{3.34}$$

Their second derivative being:

$$\frac{\partial^2 N_I}{\partial x^2} = -\frac{6}{L^2} + \frac{12}{L^3} x_1 \tag{3.35}$$

$$\frac{\partial^2 N_{II}}{\partial x^2} = -\frac{4}{L} + \frac{6}{L^2} x_1 \tag{3.36}$$

$$\frac{\partial^2 N_{III}}{\partial x^2} = \frac{6}{L^2} - \frac{12}{L^3} x_1 \tag{3.37}$$

$$\frac{\partial^2 N_{IV}}{\partial x^2} = -\frac{2}{L} + \frac{6}{L^2} x_1 \tag{3.38}$$

The second derivative of v and λ_v can be written as:

$$\frac{\partial^2 v}{\partial x^2} = \frac{\partial^2 N_I}{\partial x^2} v_I + \frac{\partial^2 N_{II}}{\partial x^2} \theta_I + \frac{\partial^2 N_{III}}{\partial x^2} v_{II} + \frac{\partial^2 N_{IV}}{\partial x^2} \theta_{II} = \begin{Bmatrix} \frac{\partial^2 N_I}{\partial x^2} & \frac{\partial^2 N_{II}}{\partial x^2} & \frac{\partial^2 N_{III}}{\partial x^2} & \frac{\partial^2 N_{IV}}{\partial x^2} \end{Bmatrix} \begin{Bmatrix} v_I \\ \theta_I \\ v_{II} \\ \theta_{II} \end{Bmatrix} \tag{3.39}$$

$$\frac{\partial^2 \lambda_v}{\partial x^2} = \frac{\partial^2 N_I}{\partial x^2} \lambda_{v_I} + \frac{\partial^2 N_{II}}{\partial x^2} \lambda_{\theta_I} + \frac{\partial^2 N_{III}}{\partial x^2} \lambda_{v_{II}} + \frac{\partial^2 N_{IV}}{\partial x^2} \lambda_{\theta_{II}} = \begin{Bmatrix} \frac{\partial^2 N_I}{\partial x^2} & \frac{\partial^2 N_{II}}{\partial x^2} & \frac{\partial^2 N_{III}}{\partial x^2} & \frac{\partial^2 N_{IV}}{\partial x^2} \end{Bmatrix} \begin{Bmatrix} \lambda_{v_I} \\ \lambda_{\theta_I} \\ \lambda_{v_{II}} \\ \lambda_{\theta_{II}} \end{Bmatrix} \tag{3.40}$$

The first derivative of the moment of inertia with respect to the z axis will depend on the existing relationship between the width and the height of the cross-section of the beam element. Consider A the cross-sectional area of the beam. It's then possible to write the moment of inertia of the cross-sectional area as

$$I_Z = \alpha A^2 \tag{3.41}$$

where α is a positive constant that depends on the shape of the cross section.

For better understanding consider a beam that has a height that is double of its width:

$$I_z = \frac{bh^3}{12} = \frac{8b^4}{12} = \frac{2(2b^2)^2}{12} = \frac{(2b^2)^2}{6} = \frac{A^2}{6} \tag{3.42}$$

In this case $\alpha = \frac{1}{6}$. The derivative of the moment of inertia becomes

$$\frac{\partial I_z}{\partial A} = \frac{A}{3} = 2 * \alpha * A \tag{3.43}$$

Given the dependence of α with the geometry of the cross section of the element this constant is an input value for the program and must be calculated by the user.

The first derivatives calculated above were inserted into the first integral of equation 3.20 and the second derivatives into the second integral of equation 3.20.

Considering that the Young's modulus remains constant throughout the process it can be taken out of the integral.

Taking into consideration that only small deformations occur the area of the element remains, similarly to the length, unchanged throughout the loading process. The integral can then be solved simply by multiplying the quantities in the equation by the value of the lenght. Additionally, because only small strains are being considered, one can assume that the initial length of the elements remains practically the same as the final length of the element. Therefore, the initial value of the length of the element can be used.

The resulting equation is simplified enough to be numerically implemented using post-processional data from the non-linear analysis:

$$a'_{\delta u}({}^{t}_{0}z,\ {}_{0}\vec{z}) = EL \times \tag{3.44}$$

$$\left[\begin{Bmatrix} -\frac{1}{L} & \frac{1}{L} \end{Bmatrix}\begin{Bmatrix} u_I \\ u_{II} \end{Bmatrix}\right.$$

$$+\frac{1}{2}\left[\begin{Bmatrix} u_I & u_{II} \end{Bmatrix}\begin{bmatrix} \frac{1}{L^2} & -\frac{1}{L^2} \\ -\frac{1}{L^2} & \frac{1}{L^2} \end{bmatrix}\begin{Bmatrix} u_I \\ u_{II} \end{Bmatrix} + \begin{Bmatrix} v_I & v_{II} \end{Bmatrix}\begin{bmatrix} \frac{1}{L^2} & -\frac{1}{L^2} \\ -\frac{1}{L^2} & \frac{1}{L^2} \end{bmatrix}\begin{Bmatrix} v_I \\ v_{II} \end{Bmatrix}\right] \times$$

$$\times \left[\begin{Bmatrix} -\frac{1}{L} & \frac{1}{L} \end{Bmatrix}\begin{Bmatrix} \lambda_{u_I} \\ \lambda_{u_{II}} \end{Bmatrix} + \begin{Bmatrix} -\frac{1}{L} & \frac{1}{L} \end{Bmatrix}\begin{Bmatrix} u_I \\ u_{II} \end{Bmatrix}\begin{Bmatrix} -\frac{1}{L} & \frac{1}{L} \end{Bmatrix}\begin{Bmatrix} \lambda_{u_I} \\ \lambda_{u_{II}} \end{Bmatrix} + \right.$$

$$\left. + \begin{Bmatrix} -\frac{1}{L} & \frac{1}{L} \end{Bmatrix}\begin{Bmatrix} v_I \\ v_{II} \end{Bmatrix}\begin{Bmatrix} -\frac{1}{L} & \frac{1}{L} \end{Bmatrix}\begin{Bmatrix} \lambda_{v_I} \\ \lambda_{v_{II}} \end{Bmatrix}\right]$$

$$+E2\alpha A\begin{Bmatrix} v_I & \theta_I & v_{II} & \theta_{II} \end{Bmatrix}\begin{bmatrix} \frac{12}{L^3} & \frac{6}{L^2} & -\frac{12}{L^3} & \frac{6}{L^3} \\ & \frac{4}{L} & -\frac{6}{L^2} & \frac{2}{L} \\ & & \frac{12}{L^3} & -\frac{6}{L^2} \\ SYM & & & \frac{4}{L} \end{bmatrix}\begin{Bmatrix} \lambda_{v_I} \\ \lambda_{\theta_I} \\ \lambda_{v_{II}} \\ \lambda_{\theta_{II}} \end{Bmatrix}$$

The flow chart for the computational implementation is presented in the next page, see Figure 3.1. The following space is left intentionally empty.

3.1.2 COMPUTATIONAL IMPLEMENTATION

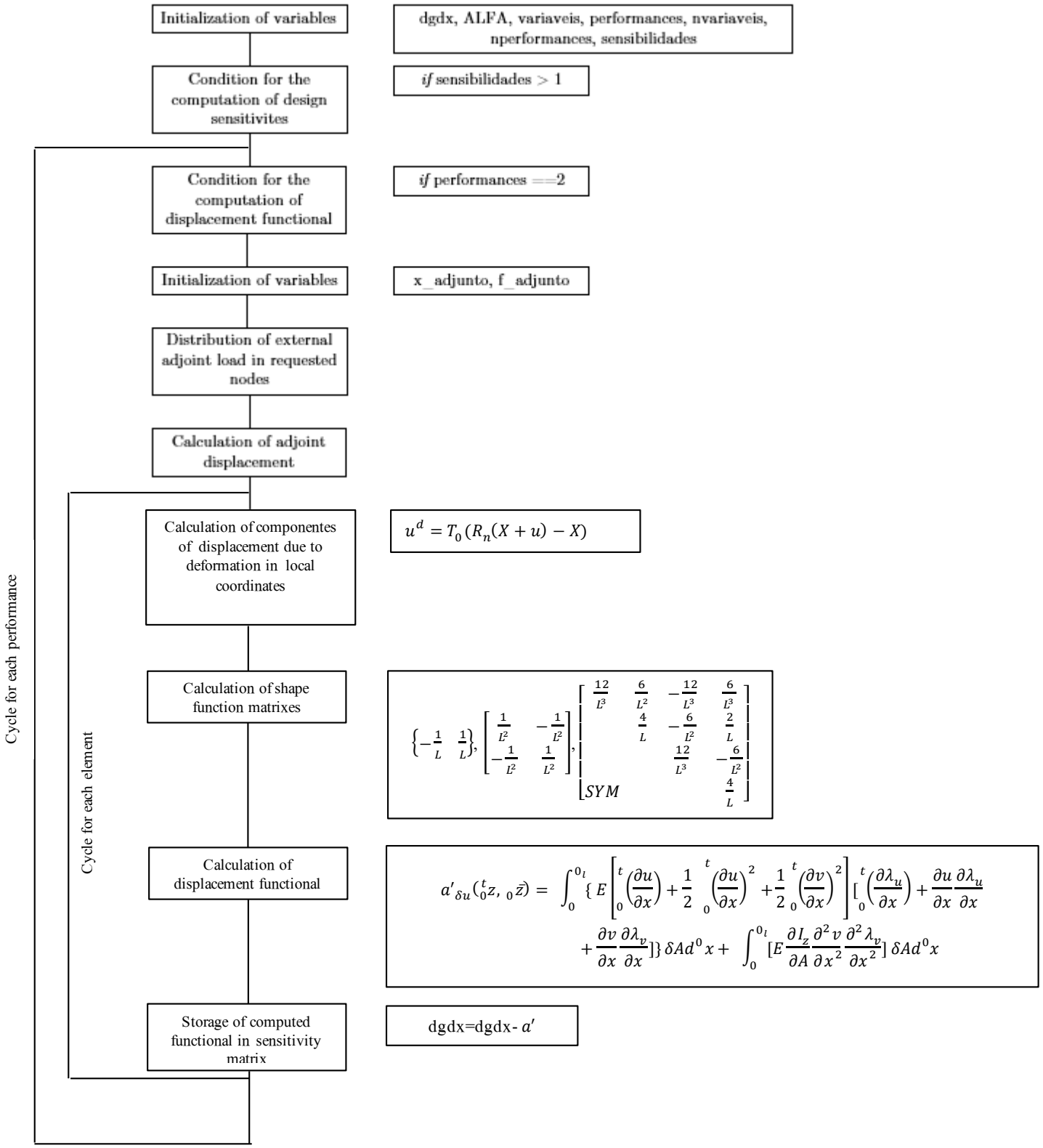

FIGURE 3.1. COMPUTATIONAL IMPLEMENTATION OF SENSITIVITIES CALCULATION

3.2 EXAMPLES

In the following examples, the 2D beam finite element with 6 degrees of freedom is used.

The accuracy of the design sensitivity analysis is checked by comparison of the results against the values obtained using the finite difference method. In the examples that follow consider Ψ_p^1 and Ψ_p^2 the values of the performance functional evaluated for a design variation of $u - u * \delta u$ and $u + u * \delta u$, respectively. Where $\delta u = 0.01$ and central finite differences calculated using the following expression 3.45.

$$\Delta\Psi_p = \frac{\Psi_p^2 - \Psi_p^1}{\Delta u} \tag{3.45}$$

3.2.1 CANTILEVER BEAM WITH CONCENTRATED MOMENT AND FORCES IN ITS FREE END

The first example is the 60 inches cantilever beam shown in Figure 3.2. This example is presented in the article "Sizing design sensitivity analysis of non-linear structural systems. Part II: Numerical method" by José L.T. Santos and Kyung K. Choi [17]. Both performance functional values and design sensitivity predictions are compared with the results presented in the article before mentioned. The beam was modelled with 21 nodal points and 20 finite elements. The geometric and material properties can be found in Table 3.1.

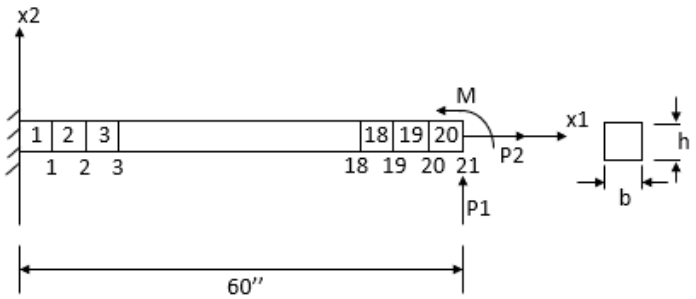

FIGURE 3.2. CANTILVER BEAM FINITE ELEMENT MODEL

TABLE 3.1. GEOMETRIC AND MATERIAL PROPERTIES

Width, b (in)	Height, h (in)	Young's modulus (psi)	Poison's ratio
0.25	0.5	$30.0 * 10^6$	0.3

The design parameter vector is

$$p = [b_1, h_1, b_2, h_2, \ldots, b_{20}, h_{20}]^T$$

where b_i and h_i are the width and height of the ith element.

The beam is subjected to two concentrated loads and one concentrated moment with the values presented in Table 3.2.

TABLE 3.2. LOADS APPLIED TO THE STRUCTURE

Axial load P_2 (lb)	Transverse load P_1 (lb)	Moment M $(lb - in)$
100	100	100

As all the design parameters are affected by the same variation δp, this is equivalent to consider just one design variable, the cross-section area, A, from which the moment of inertia depends upon, Eq. (3.41).

Considering a design variation of $p - p * \delta p$ for the cross-sectional measures b and h, Ψ_p^1 is obtained with the following values for area and moment of inertia in PROAES_NL:

$$A^1 = 0.24750 * 0.495 = 0.12251$$

$$I^1 = \frac{0.24750 * 0.495^3}{12} = 0.0025016$$

Considering a design variation of $p + p * \delta p$ for the cross-sectional measures b and h, Ψ_p^2 is obtained with the following values for area and moment of inertia in PROAES_NL:

$$A^2 = 0.2525 * 0.505 = 0.1275125$$

$$I^2 = \frac{0.2525 * 0.505^3}{12} = 0.0027099063$$

The total variation in the design variable, A, can be obtained by subtracting the cross-sectional areas calculated above:

$$\Delta u = A^2 - A^1 = 0.1275125 - 0.12251 = 0.0050025$$

The expression for the moment of inertia of the beam with dependence to the value of the area of the cross-section is:

$$I = \frac{bh^3}{12} = \frac{8b^4}{12} = \frac{2(2b^2)^2}{12} = \frac{(2b^2)^2}{6} = \frac{A^2}{6}$$

Therefore, the input value for the derivative of the moment of inertia with respect to the area of the beam is $\frac{A}{3}$.

The performance functional was defined as the vertical displacement and the design sensitivity values were calculated for six different nodal points: 2, 5, 9, 13, 17, and 21. The results obtained using PROAES_NL are shown in Table 3.3.

TABLE 3.3. PERFORMANCE AND DESIGN SENSITIVITY VALUES OBTAINED USING PROAES_NL

Node	Ψ_p^1	Ψ_p^2	$\Delta\Psi_p$	Ψ'_p
2	0.1429	0.1371	-1.1414	-1.1399
5	2.0157	1.9442	-14.2929	-14.2675
9	6.8435	6.6369	-41.2934	-41.1880
13	13.2132	12.8682	-68.9655	-68.7428
17	20.4076	19.9339	-94.6927	-94.3097
21	28.0158	27.4176	-119.580	-119.076

The comparison between design sensitivity predictions and central finite differences is shown in Table 3.4 using the following expression:

$$Relative\ error = \left|\frac{design\ sensitivity\ prediction - central\ finite\ differences}{design\ sensitivity\ prediction}\right| \quad (3.46)$$

TABLE 3.4. COMPARISON BETWEEN DESIGN SENSITIVITY PREDICTIONS AND CENTRAL FINITE DIFFERENCES

Node	Relative error (%)
2	0.132
5	0.178
9	0.256
13	0.324
17	0.406
21	0.423

The results presented in [17] for performance functionals and design sensitivity predictions are shown in Table 3.5.

TABLE 3.5. RESULTS PRESENTED IN THE REFERENCED ARTICLE FOR PERFORMANCE AND DESIGN SENSITIVITY PREDICTIONS

Node	Ψ_p^1	Ψ_p^2	$\Delta\Psi_p$	Ψ'_p
2	0.1428	0.1371	-1.1394	-1.1394
5	2.0157	1.9441	-14.3128	-14.3128
9	6.8435	6.6369	-41.2993	-41.3193
13	13.2131	12.8681	-68.9655	-69.0055
17	20.4075	19.9338	-94.6927	-94.7526
21	28.0157	27.4173	-119.620	-119.700

The comparison between the before mentioned and PROAES_NL is shown in Table 3.6 using the following expression:

$$Relative\ error = \left|\frac{Santos\ [1] - PROAES\_NL}{Santos\ [1]}\right| \tag{3.47}$$

TABLE 3.6. COMPARISON BETWEEN REFERENCED ARTICLE AND PROAES_NL

Node	Relative error (%)
2	0.044
5	0.316
9	0.318
13	0.381
17	0.467
21	0.521

It is observed that using PROAES_NL, the results obtained for design sensitivity agree with the values obtained through the finite difference method with relative errors below 0.5 percent. Moreover, the results obtained for design sensitivity using PROAES_NL agree with the values presented in [17] with a relative error below 1 percent. The comparison between PROAES_NL and the referenced article shows that both the non-linear analysis method and the design sensitivity analysis method implemented in PROAES_NL are showing excelent results.

3.2.2 CANTILEVER BEAM WITH END FORCE

Consider the cantilever beam with a vertical end force represented in Figure 3.3. Design sensitivity predictions are compared with the values obtained using the finite difference method. The beam is modelled with 11 nodal points and 10 finite elements.

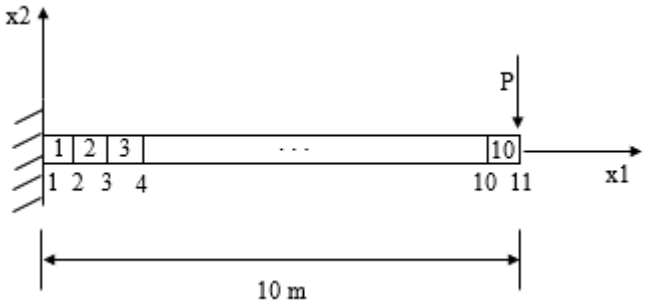

FIGURE 3.3. CANTILEVER BEAM WITH END FORCE FINITE ELEMENT MODEL

The beam has a rectangular cross-section with $width = 1m$ and $height = 0.1m$.

The geometric and material properties can be found in Table 3.7.

TABLE 3.7. GEOMETRIC AND MATERIAL PROPERTIES

Area (m^2)	Moment of inertia (m^4)	Young's modulus (N/m^2)
0.1	$8.3(3) * 10^{-5}$	$1.2 * 10^8$

For this example, the design variable is the cross-sectional area, A.

The structure is subjected to one concentrated vertical force, P, with a value of 100 N.

The expression for the moment of inertia of the beam with dependence to the value of the area of the cross-section is:

$$I = \frac{bh^3}{12} = \frac{10h^4}{12} = \frac{A^2}{120}$$

Therefore, the input value for the derivative of the moment of inertia with respect to the area of the beam is $\frac{A}{60}$.

Considering a design variation of $u - u * \delta u$ for the cross-sectional area, Ψ_p^1 is obtained with the insertion of the following values for area and moment of inertia in PROAES_NL:

$$A^1 = 0.1 - 0.01 * 0.1 = 0.099\, m^2$$

$$I^1 = \frac{0.099^2}{120} = 8.1675 * 10^{-5}\, m^4$$

Considering a design variation of $u + u * \delta u$ for the cross-sectional area, Ψ_p^2 is obtained with the insertion of the following values for area and moment of inertia in PROAES_NL:

$$A^2 = 0.1 + 0.01 * 0.1 = 0.101\ m^2$$

$$I^2 = \frac{0.101^2}{120} = 8.5008333 * 10^{-5}\ m^4$$

The total variation in the design variable can be obtained by subtracting the cross-sectional areas calculated above:

$$\Delta u = A^2 - A^1 = 0.101 - 0.099 = 0.002\ m^2$$

Performance functionals were considered to be vertical displacements and design sensitivity values were calculated for four different nodal points: 2, 5, 9, and 10. The results obtained using PROAES_NL are shown in Table 3.8.

TABLE 3.8. PERFORMANCE AND DESIGN SENSITIVITY PREDICTIONS USING PROAES_NL

Node	$\Psi_p^1(m)$	$\Psi_p^2(m)$	$\Delta\Psi_p$	Ψ'_p
2	-0.0818	-0.0794	1.2000	1.1914
5	-1.1226	-1.0924	15.100	14.995
9	-3.5846	-3.4991	42.750	42.415
10	-4.2847	-4.1848	49.950	49.535

The comparison between design sensitivity predictions and central finite differences is shown in Table 3.9 using expression 3.46.

TABLE 3.9. COMPARISON BETWEEN DESIGN SENSITIVITY PREDICTIONS AND FINITE DIFFERENCES

Node	Relative error (%)
2	0.722
5	0.700
9	0.790
10	0.838

The results obtained for the sensitivity of the design to a variation of the cross-sectional area are in close accordance with the results obtained using the finite difference method with all the nodal points with a relative error below 1 percent.

3.2.3 LEE'S FRAME

The structure shown in Figure 3.4 was already studied in chapter 2 to validate the non-linear analysis method implemented in PROAES_NL. Design sensitivity predictions are

compared with the values obtained using the finite difference method. The beam is modelled with 21 nodal points and 20 finite elements, as presented by [27], [28] and [29].

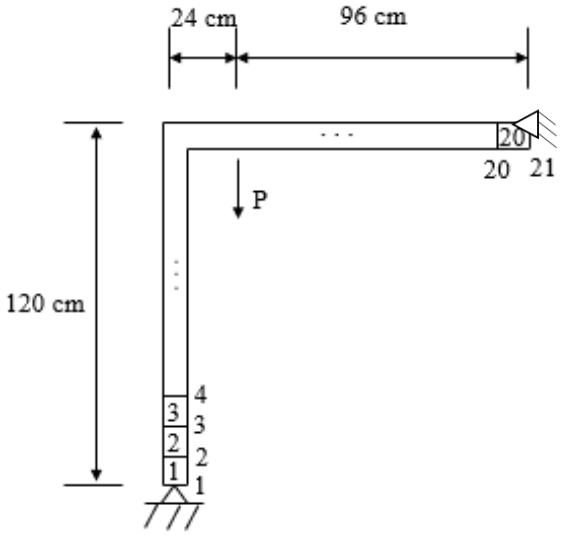

FIGURE 3.4. LEE'S FRAME FINITE ELEMENT MODEL

The beam has a rectangular cross-section with $width = 3\ cm$ and $height = 2\ cm$.

The geometric and material properties can be found in Table 2.1.

A single design variable is used, representing the cross-sectional area of all the elements.

The structure is subjected to one concentrated vertical force, P, with a value of 1000 Kgf.

The expression for the moment of inertia of the beam with dependence to the value of the area of the cross-section is:

$$I = \frac{bh^3}{12} = \frac{1.5h^4}{12} = \frac{A^2}{18}$$

Therefore, the input value for the derivative of the moment of inertia with respect to the area of the beam is $\frac{A}{9}$.

Considering a design variation of $u - u * \delta u$ for the cross-sectional area Ψ_p^1 is obtained with the following values for area and moment of inertia in PROAES_NL:

$$A^1 = 6 - 0.01 * 6 = 5.94\ cm^2$$

$$I^1 = \frac{5.94^2}{18} = 1.9602\ cm^4$$

Considering a design variation of $u + u * \delta u$ for the cross-sectional area Ψ_p^2 is obtained with the following values for area and moment of inertia in PROAES_NL:

$$A^2 = 6 + 0.01 * 6 = 6.06\ cm^2$$

$$I^2 = \frac{6.06^2}{18} = 2.0402\ cm^4$$

The total variation in the design variable can be obtained by subtracting the cross-sectional areas calculated above:

$$\Delta u = A^2 - A^1 = 6.06 - 5.94 = 0.12$$

Performance functional were considered to be the vertical displacement and design sensitivity values were calculated for six different nodal points: 2, 5, 9, 13, 17, and 20. The results obtained using PROAES_NL are shown in Table 3.10.

TABLE 3.10. PERFORMANCE AND DESIGN SENSITIVITY PREDICTIONS USING PROAES_NL

Node	$\Psi_p^1\ (cm)$	$\Psi_p^2 (cm)$	$\Delta\Psi_p$	Ψ'_p
2	-19.1380	-19.1337	0.03583	0.03470
5	-70.6415	-70.5989	0.35500	0.34838
9	-102.299	-102.147	1.26667	1.25623
13	-92.8424	-92.7513	0.75920	0.75613
17	-47.8443	-47.8275	0.14000	0.13927
20	-11.9265	-11.9191	0.06167	0.06152

The comparison between design sensitivity predictions and central finite differences is shown in Table 3.11 using expression 3.46.

TABLE 3.11. COMPARISON BETWEEN DESIGN SENSITIVITY PREDICTIONS AND FINITE DIFFERENCES

Node	Relative error (%)
2	3.256
5	1.900
9	0.831
13	0.406
17	0.524
20	0.244

The results obtained for the sensitivity of the design to a variation of the cross-sectional area are in close accordance with the results obtained using the finite difference method

with 4 of the nodal points with a relative error below 1 percent and 1 nodal point with a slightly larger error of 3 percent.

3.2.4 SIX-BAR TRUSS

Consider the six-bar truss structure shown in Figure 3.5. This example is featured in the work of Santos [1]. Once again, both performance functional values and design sensitivity predictions are compared with the results presented in [1]. The structure was modeled using five nodal points and six finite elements.

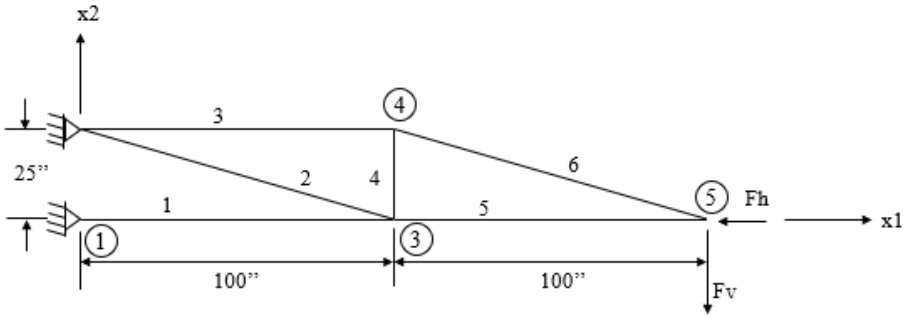

FIGURE 3.5. SIX-BAR TRUSS FINITE ELEMENT MODEL

The geometric and material properties can be found in Table 3.12.

TABLE 3.12. GEOMETRIC AND MATERIAL PROPERTIES

Area (in^2)	Young's modulus (psi)	Poison's ratio
0.1	$30.0 * 10$	0.3

The design variable is considered to be the cross-sectional area for all the finite elements, A.

The structure is subjected to two concentrated loads. The values of the vertical and horizontal loads are presented in Table 3.13.

TABLE 3.13. VALUES FOR HORIZONTAL AND VERTICAL FORCES

Load case	
Horizontal load F_H (lb)	Vertical load F_V (lb)
5000	5000

Considering a design variation of $u - \delta u$ for the cross-sectional area Ψ_p^1 is obtained with the insertion of the following values for area and moment of inertia in PROAES_NL:

$$A^1 = 0.1 - 0.01 * 0.1 = 0.099\ in^2$$

Considering a design variation of $u + \delta u$ for the cross-sectional area Ψ_p^2 is obtained with the insertion of the following values for area and moment of inertia in PROAES_NL:

$$A^2 = 0.1 + 0.01 * 0.1 = 0.101\ in^2$$

The total variation in the design variable can be obtained by subtracting the cross-sectional areas calculated above:

$$\Delta u = A^2 - A^1 = 0.101 - 0.099 = 0.002$$

Performance functional and design sensitivity values were calculated for three different nodal points: 3,4, and 5. The results obtained using PROAES_NL are shown in Table 3.14. The comparison between design sensitivity predictions and central finite differences is shown in Table 3.15 using expression 3.46.

TABLE 3.14. PERFORMANCE AND DESIGN SENSITIVITY PREDICTIONS USING PROAES_NL

Node	$\Psi_p^1\ (in)$	$\Psi_p^2\ (in)$	$\Delta\Psi_p$	Ψ'_p
3	-9.93471	-9.71802	108.345	104.858
4	-10.1168	-9.89326	111.770	108.245
5	-26.8087	-26.2237	292.500	285.146

TABLE 3.15. COMPARISON BETWEEN DESIGN SENSITIVITY PREDICTIONS AND FINITE DIFFERENCES

Node	Relative error (%)
3	3.214
4	3.150
5	2.510

The results presented have a small error when compared with finite differences. In Table 3.16 are shown the results presented in [1] for design sensitivity predictions.

TABLE 3.16. RESULTS FOR DESIGN SENSITIVITY PREDICTIONS PRESENTED IN [1]

Node	Ψ'_p
3	108.332
4	111.786
5	292.461

A slight discrepancy is noted in this example when comparing the results obtained using PROAES_NL to the results presented in [1] because, in [1], a bar element is used.

Whereas in the design sensitivity method implemented in PROAES_NL, a beam element is considered.

3.2.5 TWO-STORY FRAME

Consider the two-story structure shown in Figure 3.6. Design sensitivity predictions are compared with the values obtained using the finite difference method. The structure was modeled using 9 nodal points with 10 finite elements. The beam considered was a HEB 100.

This example is not based in any existing literature and was created to assess if a difference would arise between the displacements obtained using PROAES, that performs linear analysis, and PROAES_NL, that performs nonlinear analysis. This would determine if the nonlinear effects are, or not, significant.

The geometric and material properties can be found in Table 3.17.

TABLE 3.17. GEOMETRIC AND MATERIAL PROPERTIES

Area (mm^2)	Young's modulus (N/mm^2)	Moment of inertia (mm^4)
2480	200000	4322667,002

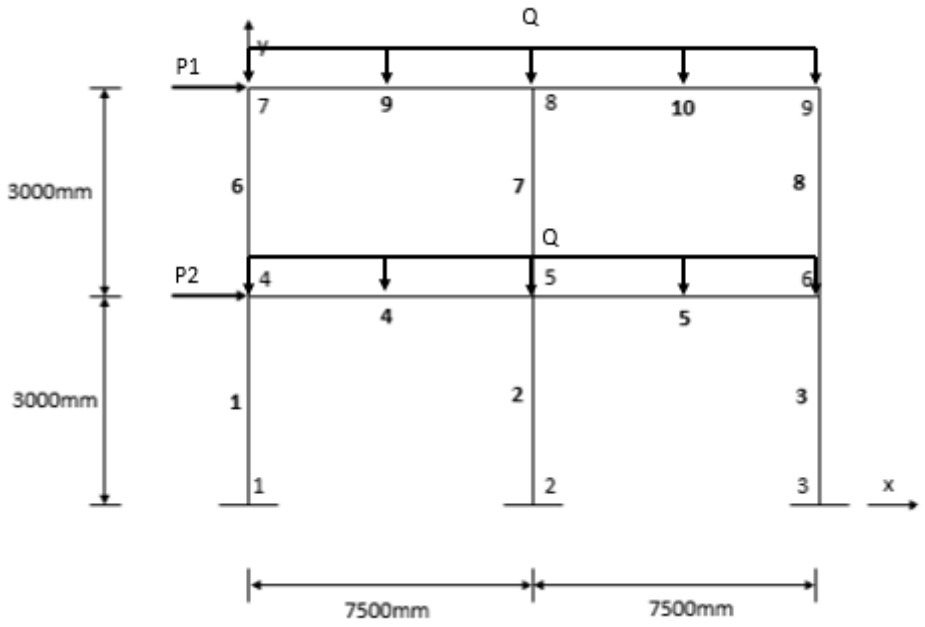

FIGURE 3.6. TWO-STORY FRAME FINITE ELEMENT MODEL

The structure is subjected to two concentrated horizontal loads, P1 and P2 and two distributed loads, Q, with equal intensity. The values of P1, P2, and Q are shown in Table 3.18.

TABLE 3.18. LOADS APPLIED TO THE STRUCTURE

P1 (N)	P2 (N)	Q (N/mm)
13500	9000	4

Knowing that the measures of the cross-section of the beam can be written in terms of measure B, see Figure 3.7, as,

$$H = B$$

$$t = \frac{B}{100}$$

$$e = \frac{6B}{100}$$

It is now possible to determine the expression of the area with respect to the value of measure B, see Figure 3.7.

$$A = HB - (H - 2t)(B - e) = 0{,}248B^2$$

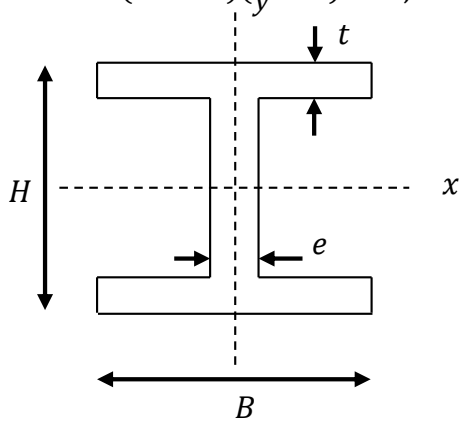

FIGURE 3.7. HEB 100 BEAM CROSS SECTION

The expression for the moment of inertia of the beam with dependence to the value of the area of the cross-section is:

$$I = \frac{BH^3}{12} - \frac{(B - e)(H - 2t)^3}{12} \Leftrightarrow$$

$$\Leftrightarrow I = 0{,}702826971A^2$$

Therefore, the input value for the derivative of the moment of inertia with respect to the area of the beam is

$$I'_A = 1{,}405653942A$$

Assuming a single design variable, A, representing the cross-section area of all the finite elements and considering a design variation of $u - u * \delta u$, Ψ_p^1 is obtained with the following values for area and moment of inertia:

$$A^1 = 2480 - 2480 * 0{,}01 = 2455{,}2\ mm^2$$

$$I^1 = 0{,}702826971 * 2455{,}2^2 = 4236645{,}929\ mm^4$$

Considering a design variation of $u + u * \delta u$ for the cross-sectional area Ψ_p^2 is obtained with the following values for area and moment of inertia:

$$A^2 = 2480 + 2480 * 0{,}01 = 2504{,}8\ mm^2$$

$$I^2 = 0{,}702826971 * 2504{,}8^2 = 4409552{,}609\ mm^4$$

The total variation in the design variable can be obtained by subtracting the cross-sectional areas calculated above:

$$\Delta u = A^2 - A^1 = 2504{,}8 - 2455{,}2 = 49{,}6$$

Performance functional and design sensitivity values for horizontal displacement were calculated for six different nodal points: 4, 5, 6, 7, 8, and 9. The results obtained using PROAES_NL are shown in Table 3.19.

TABLE 3.19. PERFORMANCE AND DESIGN SENSITIVITY VALUES OBTAINED USING PROAES_NL

Node	$\Psi_p^1\ (mm)$	$\Psi_p^2\ (mm)$	$\Delta\Psi_p$	Ψ'_p
4	43.88294	42.06707	-0.036610	-0.036850
5	43.88768	42.07165	-0.036614	-0.036855
6	43.91987	42.10318	-0.036627	-0.036869
7	94.64112	90.73307	-0.078791	-0.079406
8	94.35768	90.45527	-0.078678	-0.079291
9	94.17882	90.27991	-0.078607	-0.079220

The comparison between design sensitivity predictions and central finite differences is shown in Table 3.20 using expression 3.46.

TABLE 3.20. COMPARISON BETWEEN DESIGN SENSITIVITY ANALYSIS AND FINITE DIFFERENCE

Node	Relative error (%)
4	0.6556
5	0.6582
6	0.6564
7	0.7745
8	0.7731
9	0.7738

The results provided for the design sensitivity are in close accordance with the results obtained using the finite difference method with a relative error below 0.8%.

The values for vertical and horizontal displacement on the nodes of the structure obtained performing a nonlinear analysis using PROAES_NL are shown in Table 3.21.

TABLE 3.21. VERTICAL AND HORIZONTAL DISPLACEMENT VALUES OBTAINED USING PROAES_NL

Node	$Dx\,(mm)$	$Dy\,(mm)$
4	42.960	-0.4541
5	42.965	-0.5048
6	42.997	-0.5070
7	92.656	-0.9410
8	92.375	-1.0130
9	92.198	-1.0050

The values obtained using the linear code PROAES are shown in Table 3.22.

TABLE 3.22. VERTICAL AND HORIZONTAL DISPLACEMENT VALUES OBTAINED USING PROAES

Node	Dx	Dy
4	40.663	-0.1482
5	40.667	-0.1979
6	40.698	-0.1983
7	87.763	-0.2235
8	87.482	-0.2998
9	87.304	-0.2932

Comparing the results obtained using both programs, a relative difference can be computed using the following formula.

$$Relative\ difference = \frac{|PROAES - PROAES\_NL|}{PROAES} * 100 \tag{3.47}$$

The results for the relative difference are shown in Table 3.23.

TABLE 3.23. COMPARISON OF VERTICAL AND HORIZONTAL DISPLACEMENT VALUES OBTAINED USING PROAES_NL AND PROAES

Node	Relative error Dx (%)	Relative error Dy (%)
4	5.649	206.41
5	5.651	155.08
6	5.649	155.67
7	5.575	321.03
8	5.593	237.89
9	5.606	242.77

One can conclude that there is a significant difference between performing a linear and nonlinear analysis. In this example, an average relative difference of 5.6 % is found in the horizontal displacement, and a much higher average difference of 219.8% is found in the vertical displacement. In accordance, the design sensitivity prediction using a nonlinear analysis, PROAES_NL, see Table 3.19, is significantly different than the design sensitivity prediction using a linear analysis, PROAES, see Table 3.24.

TABLE 3.24. DESIGN SENSITIVITY PREDICTIONS USING PROAES

Node	Ψ'_p
4	6.8612e-07
5	3.2976e-07
6	-2.8289e-06
7	-2.65083-05
8	1.29453-06
9	1.8972e-05

CHAPTER 4

TOPOLOGY OPTIMIZATION

A minimum compliance optimization with a volume constraint was performed using Octave SQP algorithm. It was considered a problem with the following formulation:

Minimizing $f(X)$

Subjected to: $g_i(X) \leq 0 \quad 1 = 1, \dots, p$

$$h_m(X) = 0, \quad m = 1, \dots, k$$

$$^{l}X_j \leq X_j \leq {}^{u}X_j, \quad j = 1, \dots, n$$

Where:

- X is the vector with the design variables, in this case, the cross-sectional area of the elements.
- $f(X)$ is the objective function, in this case, the objective function is the displacement of the node where the external load is applied, as minimizing the compliance for a single load applied results in minimizing the displacement.
- $g_i(X)$ and $h_m(X)$ are the p inequality constraints and the k equality constraints, respectively. In this case, one inequality constraint was used for the admissible volume and no equality constraints were used.

The lower and upper bound limits for the cross-sectional area of the elements are $^{l}X_j$ and $^{u}X_j$, respectively.

In order to compare the optimum designs obtained using the nonlinear code, PROAES_NL, and the linear code, PROAES, the work of Kang and Luo [11] was used. In [11] density based topology optimization is used and the designs obtained using both linear and nonlinear analysis codes are presented.

4.1 EXAMPLES

The initial admissible volume considered was of 0.1% of the total volume of the structure when all the bars have their maximum area value. This value was then updated according to the example. A uniform circular cross-section was considered.

The vector x is initialized with the areas considered to be at their upper bound.

The tolerance considered for the SQP optimization tool was 10^{-12}.

4.1.2 FIXED-FREE 38 BAR TRUSS

The design domain and loading conditions for this example are illustrated in Figure 4.1. This example is based on the example presented in the master thesis of André Teixeira [40] where two-dimensional bar elements were used. The rectangular ground structure, with a geometrical dimension of 16m x 6m, is fixed at the nodes of the left extremity and free in the opposed nodes. A concentrated vertical force is applied at the mid-point node of the right extremity. The model was created using 15 nodes and 38 two-dimensional beam elements.

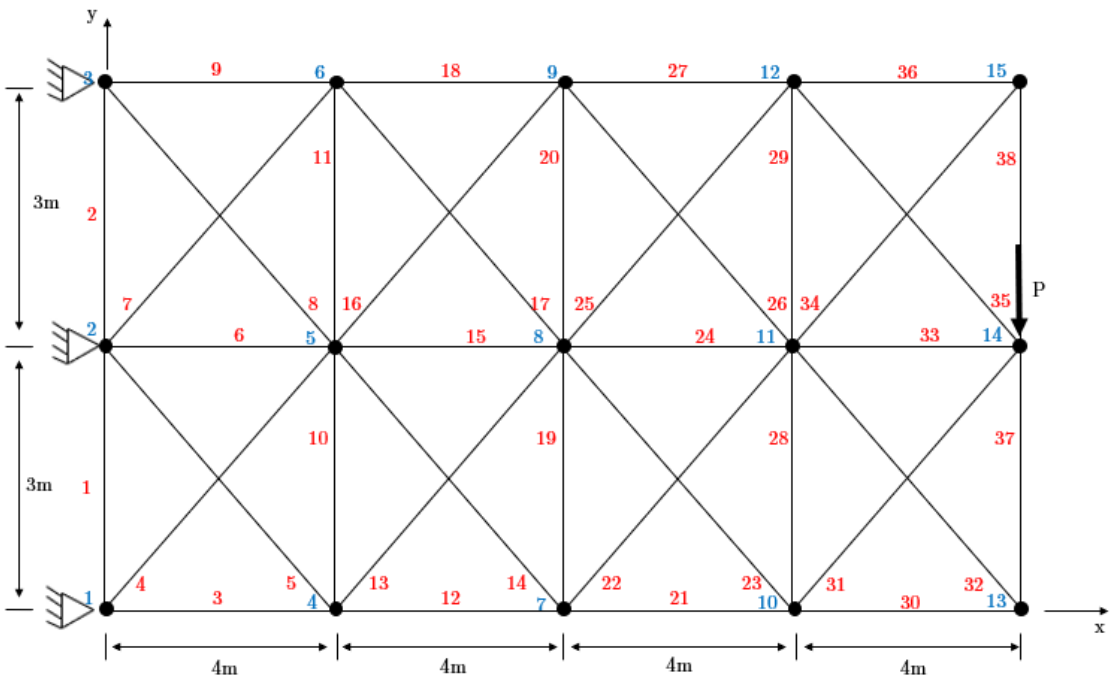

FIGURE 4.1. INITIAL GROUND STRUCTURE FOR THE FIXED-FREE 38 BAR TRUSS EXAMPLE

4.1.2.1 OPTIMIZATION USING PROAES

The structure was first optimized with the PROAES linear code.

The variations allowed for the value of the area of the elements are presented on Table 4.1.

TABLE 4.1. LOWER AND UPPER BOUND FOR THE LINEAR OPTIMIZATION OF THE FIXED-FREE 38 BAR TRUSS EXAMPLE

Lower bound	Higher bound
1e-8 m^2	3.142e-4 m^2

The maximum volume of the structure is 4.9637e-2 m^3. The admissible volume of 0.00452m^3, approximately 0.1% of the maximum volume, was considered. Using two-dimensional bar finite elements in PROAES it was possible to obtain a final design in accordance with the one presented in [40]. Neglecting the bars with an area below 2.1e-

05, in the final solution, it is possible to obtain the optimum design presented in Figure 4.2.

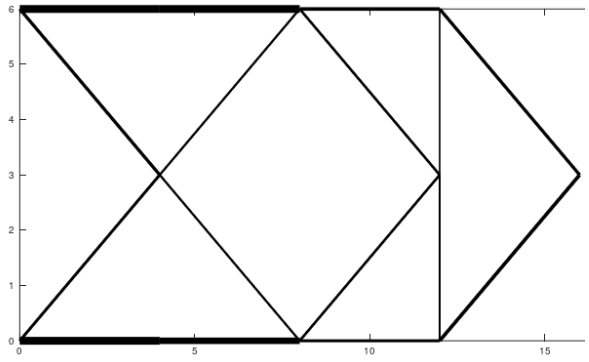

FIGURE 4.2. OPTIMUM LINEAR DESIGN USING 2D BAR ELEMENTS

Changing the type of finite element used from bar to beam but maintaining the same admissible volume as used for the optimization with bar element led to an inconclusive optimum configuration, as can be seen in Figure 4.3 (a). Although a structure similar to the one in Figure 4.2 is seen, the area of the element 25, that doesn't belong to the previous solution is superior to the area of the element 29 that does belong to the solution. The maximum admissible volume was then increased until a configuration was visible. The evolution of the final designs with the increase of the admissible volume can be seen in Figure 4.3. Elements with an area below 1.5e-5 were not considered in the representation.

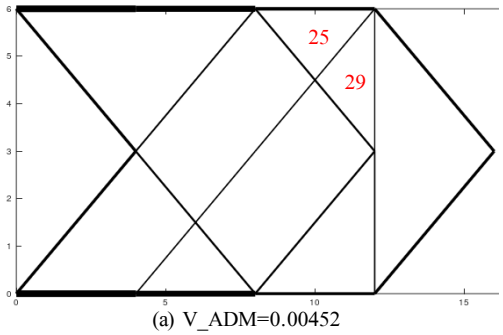

(a) V_ADM=0.00452

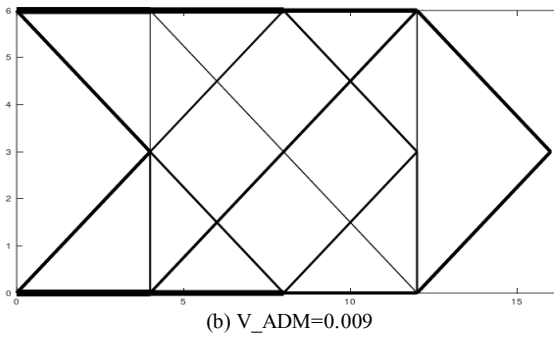

(b) V_ADM=0.009

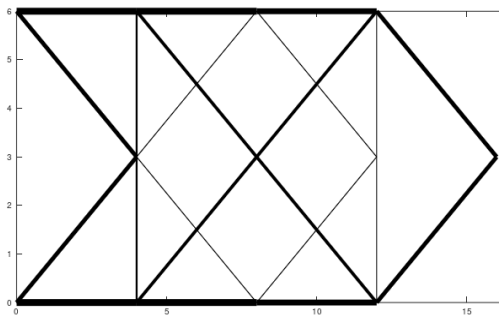

(c) V_ADM=0.015

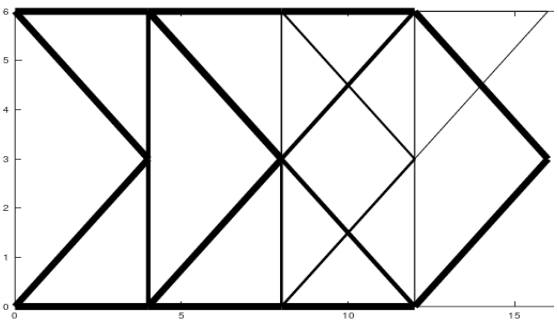

(d) V_ADM=0.02

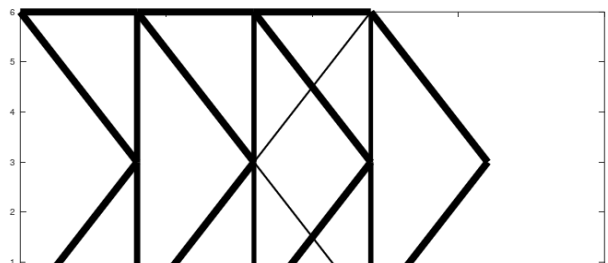

FIGURE 4.3. EVOLUTION OF THE LINEAR OPTIMIZATION USING 2D BEAM ELEMENTS

The final optimum design with the admissible volume of 0.025 is different from the design obtained using bar elements. In the beam configuration there wasn't any element overlapping. The configuration (e) in Figure 4.3 shows great similarities to the one presented in the article by Kang and Luo [11], although in the article the studied structure is subjected to both an horizontal and vertical force. Neglecting the elements with an area below 8.3e-5 in configuration (e) the comparison between both designs can be made through Figure 4.4.

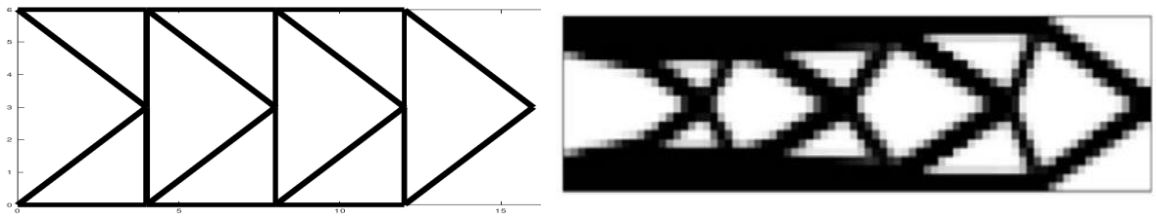

(A) (B)

FIGURE 4.4. COMPARISON OF STRUCTURES: (A) PROAES (B) SOURCE [10]

The visible difference resides in the vertical bars of the PROAES optimum design when in the article they have an inclination. This is due to the fact that in the article density-based optimization is used allowing the bars to take a free disposition in the admissible space. Whereas in PROAES the disposition of the elements depends on the initial ground structure that was created by the user.

For the design (e) in Figure 4.3 the final value for the objective function, final external load magnitude, ending code, duration of the optimization process and the number of iterations performed are listed in Table 4.2.

TABLE 4.2. FINAL PARAMETERS OF THE OPTIMIZATION

Ending code (SQP)	104
Time	281.494s
Iterations made	264
P (N)	100
Objective function	0.00012496

The optimized structure presents the 20 elements listed in Table 4.3.

TABLE 4.3. AREA AND VOLUME FOR THE ELEMENTS IN THE FINAL DESIGN

Number of the element	Area (m^2)	Percentage of the total volume
3	3.142000e-04	5.027
4	3.142000e-04	6.284
8	3.142000e-04	6.284
9	3.142000e-04	5.027
10	2.571579e-04	3.086
11	2.532505e-04	3.039
12	3.142000e-04	5.027
13	3.142000e-04	6.284
17	3.142000e-04	6.284
18	3.142000e-04	5.027
19	2.053484e-04	2.464
20	2.090345e-04	2.508
21	3.142000e-04	5.027
22	3.142000e-04	6.284
26	3.142000e-04	6.284
27	3.142000e-04	5.027
28	2.174483e-04	2.609
29	1.860135e-04	2.232
31	3.142000e-04	6.284
35	3.142000e-04	6.284

The 20 elements make up to 96.4% of the volume of the structure.

4.1.2.2 OPTIMIZATION USING PROAES_NL

The same optimization formulation was then used with the PROAES_NL nonlinear code.

The variations allowed for the value of the area of the elements are presented on Table 4.4.

TABLE 4.4. LOWER AND UPPER BOUND FOR THE NONLINEAR OPTIMIZATION OF THE FIXED-FREE 38 BAR TRUSS EXAMPLE

Lower bound	Higher bound
3e-6 m^2	3.142e-4 m^2

The usage of nonlinear analysis has inherent challenges, for example, it's not possible to use lower bounds as low as the ones used for linear analysis or considerable high external loads.

The lower bound was then raised from 1e-8 to 3e-6 in order to avoid convergence errors. The value of 3e-6 was found through trial and error.

Considering a circular cross-section, the input value for alfa, α, in PROAES_NL was the same as in the previous example.

Using the same maximum admissible volume as used in configuration (e) of Figure 4.3, 0.025, and neglecting the bars with an area below 7.7e-6, the resulting configuration is presented in Figure 4.5.

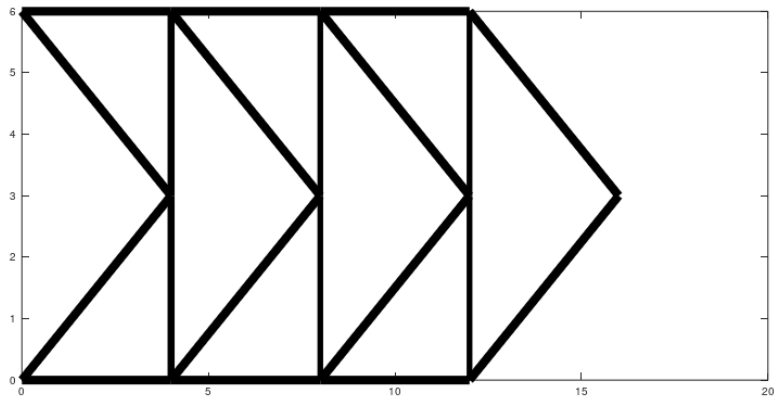

FIGURE 4.5. OPTIMUM DESIGN USING NONLINEAR ANALYSIS AND 2D BEAM ELEMENTS

This configuration is equal to the one found using the linear code PROAES, seen in Figure 4.4 a).

The final value for the objective function, final external load magnitude, ending code, duration of the optimization process and the number of iterations performed are listed in Table 4.5.

TABLE 4.5. FINAL PARAMETERS OF THE OPTIMIZATION

Ending code (SQP)	104
Time	373.596s

Iterations made	57
P (N)	100
Objective function	0.00012500

The optimized structure presents the 20 elements listed in Table 4.6.

TABLE 4.6. AREA AND VOLUMES OF THE ELEMENTS IN THE FINAL CONFIGURATION

Number of the element	Area (m^2)	Percentage of the total volume
3	3.142000e-04	5.027
4	3.142000e-04	6.284
8	3.142000e-04	6.284
9	3.142000e-04	5.027
10	2.526828e-04	3.032
11	2.526812e-04	3.032
12	3.142000e-04	5.027
13	3.142000e-04	6.284
17	3.142000e-04	6.284
18	3.142000e-04	5.027
19	2.054922e-04	2.466
20	2.054903e-04	2.466
21	3.142000e-04	5.027
22	3.142000e-04	6.284
26	3.142000e-04	6.284
27	3.142000e-04	5.027
28	2.051298e-04	2.462
29	2.051180e-04	2.461
31	3.142000e-04	6.284
35	3.142000e-04	6.284

The 20 elements make up to 96.4% of the volume of the structure.

When trying to modify the admissible volume and lower bound to see if a different design would arise convergence errors occurred. Therefore, in this example it was only possible to reach with the nonlinear code, PROAES_NL, an optimum design equal to the one obtained using the linear analysis, PROAES.

4.1.2.3 ANALYSIS AND COMPARISON OF RESULTS

In this example the optimum design obtained using PROAES with bar finite elements is in accordance with the design presented in the reference [11]. The design obtained using PROAES is shown in Figure 4.6 (a) and the design presented in [11] is shown in Figure 4.6 (b).

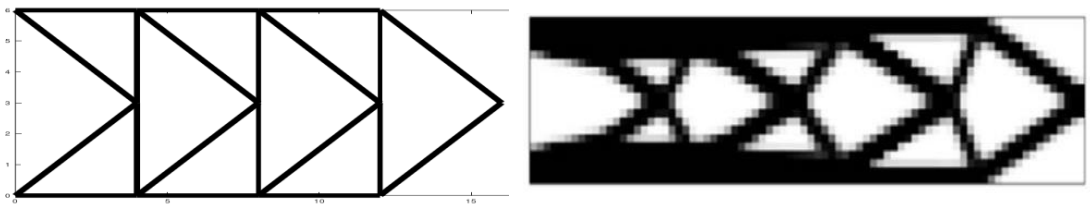

(a) (b)

FIGURE 4.6. COMPARISON OF STRUCTURES: (A) PROAES (B) SOURCE [10]

The design obtained using PROAES_NL was equal to the one obtained using PROAES. Is this example, due to convergence errors it was not possible to try different combinations of maximum admissible volume and lower bound. When analyzing the nonlinear solution presented in [11], the reader is referred to Figure 4.7, it's possible to conclude that the difference between the linear and the nonlinear design is mainly in the localization of the nodes. Consequently, the length of the elements is altered. In addition, an extra node appears in the nonlinear solution.

FIGURE 4.7. NONLINEAR OPTIMUM DESIGN PRESENTED IN [10]

This would not be possible to achieve using the initial ground structure with PROAES_NL since the coordinates of the nodes are not a variable of the problem and it's not implemented in PROAES_NL the possibility of removing or introducing new nodes and elements.

Therefore, the final configuration obtained using linear and non-linear analysis is presented in Figure 4.8.

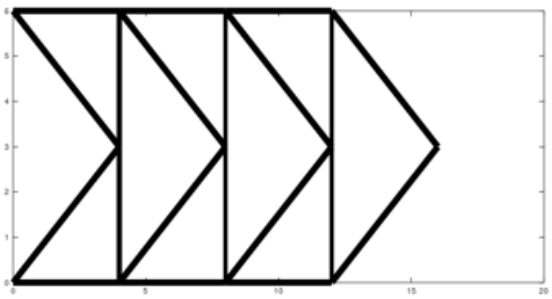

FIGURE 4.8. OPTIMUM DESIGN OBTAINED USING LINEAR AND NON-LINEAR ANALYSIS

4.1.3 TWO POINT SUPPORTED 46 BAR TRUSS

The design domain and loading conditions of this example are illustrated in Figure 4.9. This example is based on the example presented in the article by Kang and Luo [11], considering some modifications. The rectangular ground structure, with a geometrical dimension of 16m x 4m, is fixed at the mid-points of both ends. The width, w, and height, h, of the structure is in accordance to the proportion used in [11] of w/h=4. A concentrated force P is applied at the center of the structure.

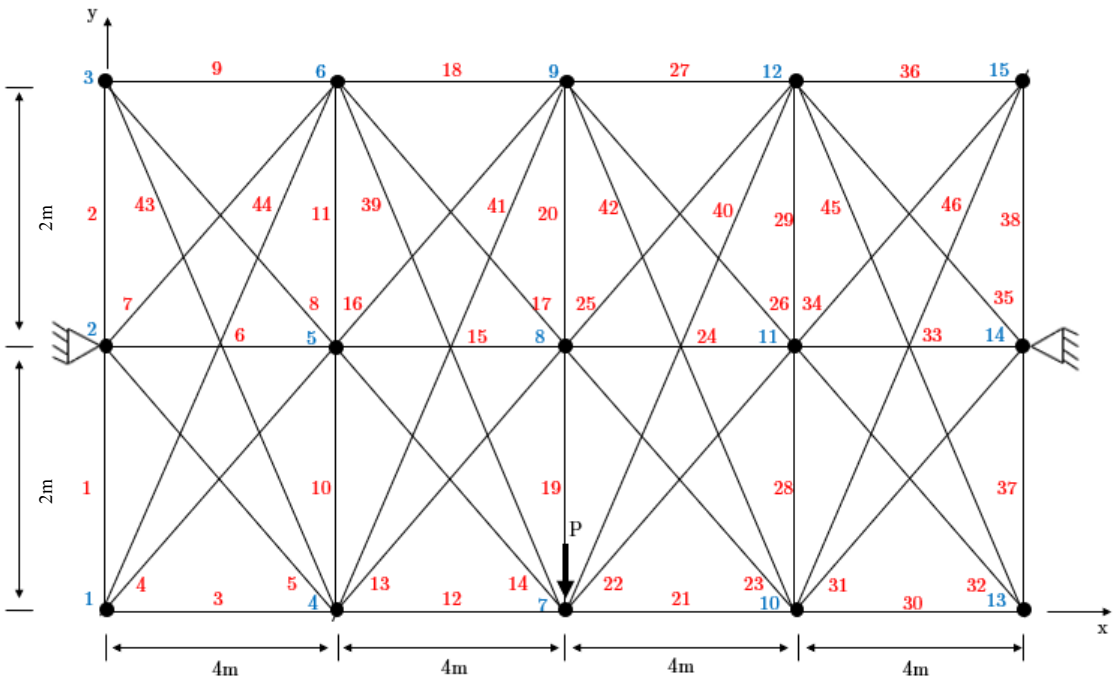

FIGURE 4.9. INITIAL GROUND STRUCTURE FOR THE TWO-POINT SUPPORTED 46 BAR TRUSS

4.1.3.1 OPTIMIZATION USING PROAES

The variations allowed for the value of the area of the elements are presented on Table 4.7.

TABLE 4.7. LOWER AND UPPER BOUND FOR THE LINEAR OPTIMIZATION OF THE 46 BAR TRUSS EXAMPLE

Lower bound	Higher bound
1e-8 m^2	3.12e-2 m^2

The maximum volume of the structure, with the area of the elements at the upper bound is $5.766m^3$. Considering the admissible volume of $0.6\ m^3$, approximately 0.1% of the maximum volume, the optimal topology obtained using the linear code PROAES is presented in Figure 4.10.

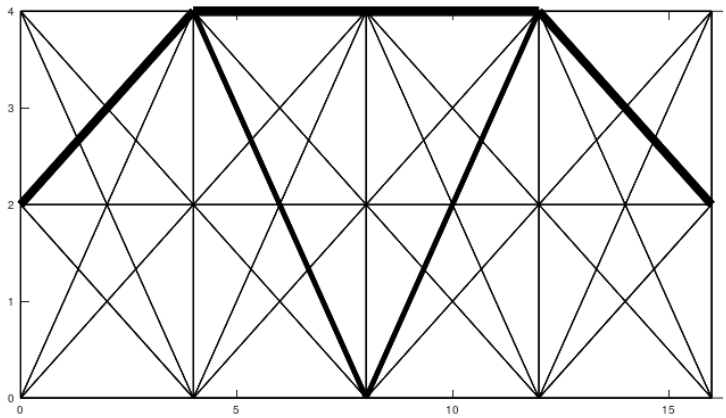

FIGURE 4.10. OPTIMUM TOPOLOGY WITH LINEAR ANALYSIS

Neglecting the bars with an area below 6.0e-4 because of their proximity with the lower bound it is possible to obtain the optimum design presented in Figure 4.11. This result is in accordance with the results presented by [11] which can be seen in Figure 4.12.

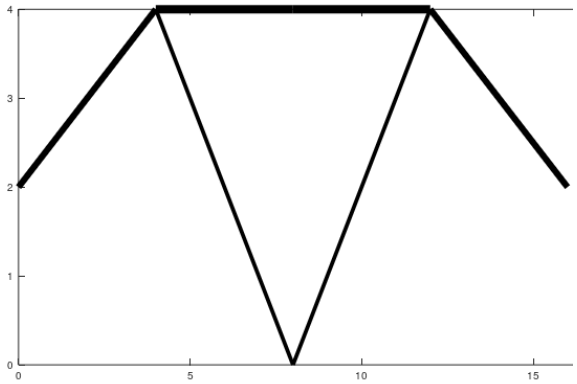

FIGURE 4.11. FINAL OPTIMUM LINEAR DESIGN USING PROAES

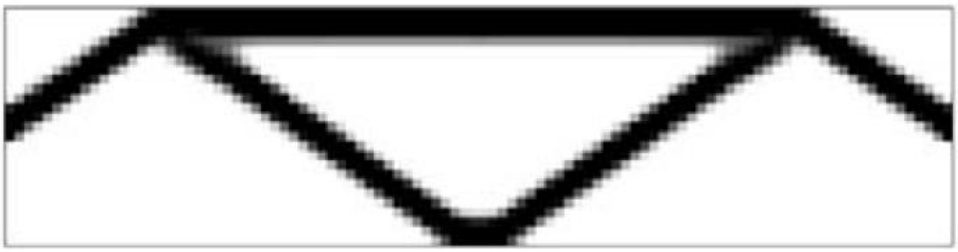

FIGURE 4.12. OPTIMUM LINEAR DESIGN PRESENTED IN [11]

The final value for the objective function, final external load magnitude, ending code, duration of the optimization process and the number of iterations performed are listed in Table 4.8.

TABLE 4.8. FINAL PARAMETERS OF THE OPTIMIZATION

Ending code (SQP)	104
Time	89.799 s
Iterations made	69
P (N)	200
Objective function	2.9562e-4

The optimized structure presents the 6 elements listed in Table 4.9.

TABLE 4.9. AREA AND VOLUME OF THE ELEMENTS IN THE FINAL LINEAR CONFIGURATION

Number of the element	Area (m^2)	Percentage of the total volume
7	2.203345e-02	16.423
18	2.977477e-02	19.850
27	2.977471e-02	19.850
35	2.203345e-02	16.423
39	1.387695e-02	13.083
40	1.387695e-02	13.083

The 6 elements make up to 98.7% of the volume of the structure. The optimum design is symmetric along a vertical axis with the outer elements taking the biggest percentage of the total volume. One can observe this in Figure 4.12 through the analysis of the thickness of the elements and through the analysis of Table 4.9.

4.1.3.2 OPTIMIZATION USING PROAES_NL

The variations allowed for the value of the area of the elements are presented on Table 4.10.

TABLE 4.10. LOWER AND UPPER BOUND FOR THE NONLINEAR OPTIMIZATION OF THE 46 BAR TRUSS EXAMPLE

Lower bound	Higher bound
3.12e-4 m^2	3.12e-2 m^2

The lower bound was raised to 3.12e-4 m^2 because it is a value known to the author that guaranties the proper functioning of PROAES_NL without convergence errors.

Considering a circular cross-section, the expression for the moment of inertia of the beam with dependence to the value of the area of the cross-section is:

$$I = \frac{1}{4\pi} A^2$$

Therefore, the input value for alfa, α, in PROAES_NL is:

$$\alpha = \frac{1}{4\pi}$$

Considering the maximum admissible volume of 0.6 m^3, same as used in the linear optimization, the optimal topology obtained using PROAES_NL is presented in Figure 4.13.

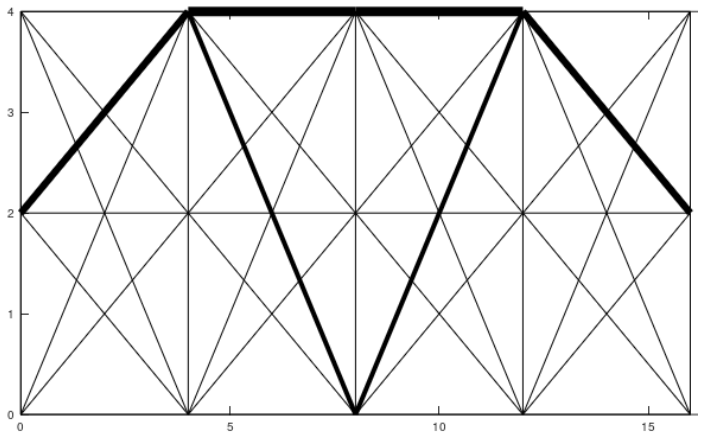

FIGURE 4.13. NONLINEAR DESIGN USING THE SAME PARAMETERS FROM THE LINEAR OPTIMIZATION

The final value for the objective function, final external load magnitude, ending code, duration of the optimization process and the number of iterations performed are listed in Table 4.11.

TABLE 4.11. FINAL PARAMETERS OF THE OPTIMIZATION

Ending code (SQP)	104
Time	405.078 s
Iterations made	42
P (N)	200
Objective function	3.1434e-4

The optimized structure presents the 6 elements listed in Table 4.12.

TABLE 4.12. AREA AND VOLUME OF THE ELEMENTS IN THE NONLINEAR CONFIGURATION

Number of the element	Area (m^2)	Percentage of the total volume
7	2.013490e-02	15.008
18	2.754749e-02	18.365
27	2.754749e-02	18.365
35	2.013490e-02	15.008
39	1.276395e-02	12.034
40	1.276395e-02	12.034

The optimum design in Figure 4.13 was obtained using the same parameters that were used in the linear optimization with exception of the lower bound of the area that needed to be raised to assure the proper functioning of PROAES_NL. The resulting structure is similar to the one obtained using linear optimization. Therefore, the author proceeded to vary the external load, the maximum admissible volume and the lower bound of the area in order to verify if it would be possible to obtain a final design different from the linear response and similar with the nonlinear result presented in [11].

The nonlinear design presented in [11] is displayed in Figure 4.14.

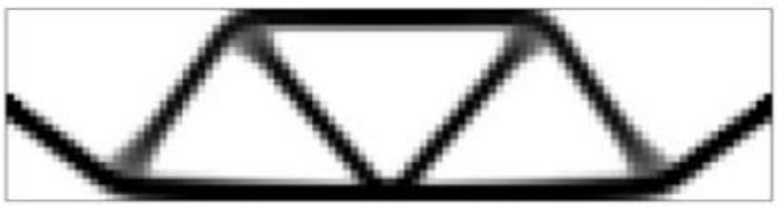

FIGURE 4.14. NONLINEAR DESIGN PRESENTED IN [11]

The solution presented in [11] had a considerable higher number of elements, implying a higher total volume of the structure, when compared with the linear solution. Therefore, the admissible volume had to be raised. Otherwise, the algorithm would never be able to achieve this solution.

The admissible volume was raised until a visible difference from the linear response appeared. The historic of optimization is displayed in Figure 4.15.

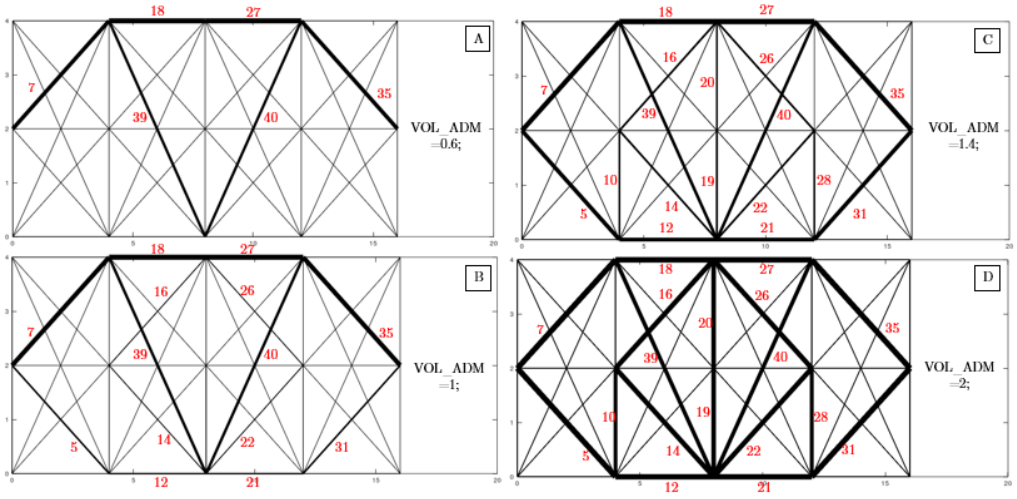

FIGURE 4.15. HISTORIC OF OPTIMIZATION WHILE INCREASING THE MAXIMUM ADMISSIBLE VOLUME

The admissible volume used in each optimization is displayed to the right of each image under the variable name "VOL_ADM".

Image A is the design presented in Figure 4.15 and obtained using the same parameters as the ones used for the linear optimization. In image B it's possible to see that elements 5, 12, 21, 31, 14, 16, 22 and 26 have a slightly increased area. In image C the elements mentioned before present now an even higher area and two new elements appear with an increased area: elements 19 and 20. In the final image, D, all the elements mentioned before now appear to have a higher contribution in area comparing to the elements 39 and 40 that belong to the linear optimum design. Therefore, the maximum admissible volume of 2 was chosen as the starting point for the lower bound and external load variations.

The final value for the objective function, final external load magnitude, ending code, duration of the optimization process and the number of iterations performed for the chosen configuration D are listed in Table 4.13.

TABLE 4.13. FINAL PARAMETERS OF THE OPTIMIZATION

Ending code (SQP)	104
Time	559.046 s
Iterations made	76
P (N)	200
Objective function	1.0211e-4

The optimized structure presents the 18 elements listed in Table 4.14.

TABLE 4.14. AREA AND VOLUME OF THE ELEMENTS IN CONFIGURATION D

Number of the element	Area (m^2)	Percentage of the total volume
5	3.120000e-02	6.977

7	3.120000e-02	6.977
10	1.971213e-02	1.971
12	3.120000e-02	6.240
14	2.902176e-02	6.489
16	2.875974e-02	6.431
18	3.120000e-02	6.240
19	2.606190e-02	2.606
20	2.601425e-02	2.601
21	3.120000e-02	6.240
22	2.902176e-02	6.489
26	2.875974e-02	6.431
27	3.120000e-02	6.240
28	1.971213e-02	1.971
31	3.120000e-02	6.977
35	3.120000e-02	6.977
39	1.623804e-02	4.593
40	1.623804e-02	4.593

Having determined the maximum admissible volume the lower bound of the area was decreased to evaluate what happened to the optimized structure. Figure 4.16 describes the evolution of the area of the 18 elements present in Figure 4.15, configuration D, as the lower bound decreases.

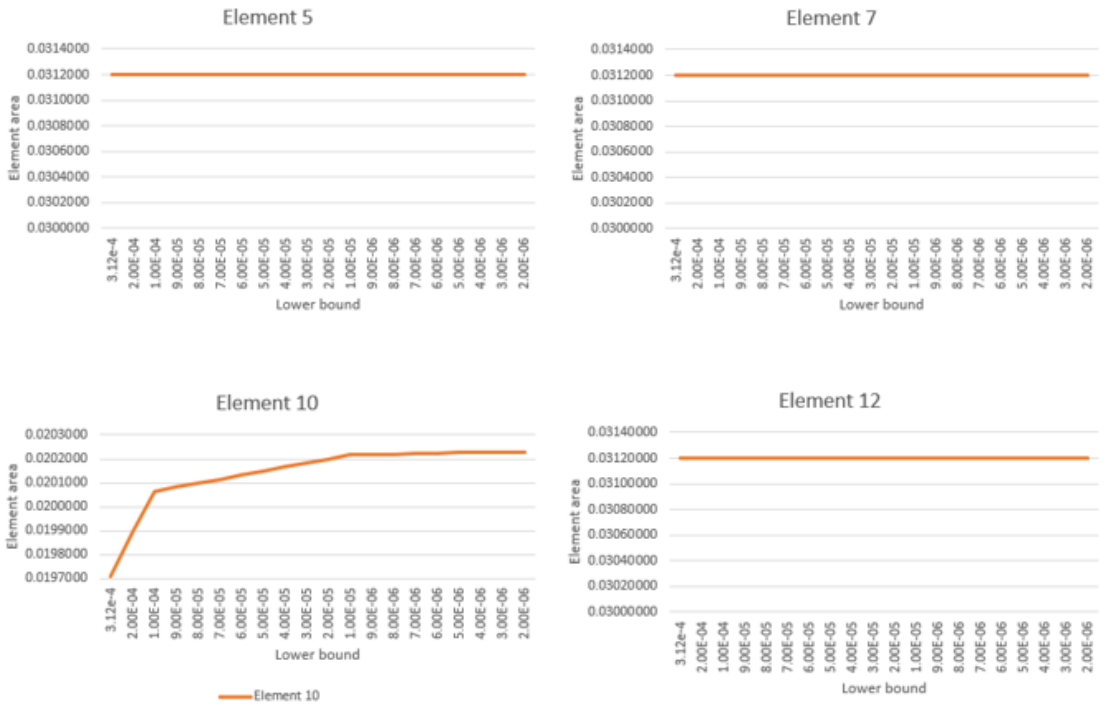

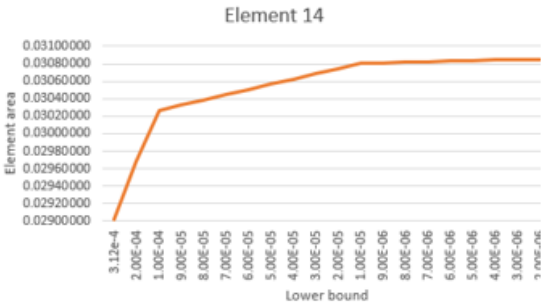
Element 14
Element area
Lower bound

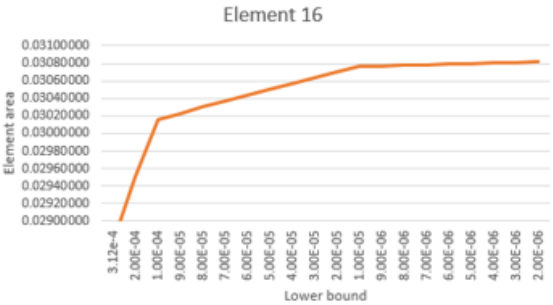
Element 16
Element area
Lower bound

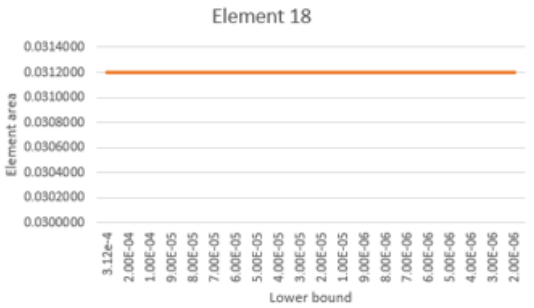
Element 18
Element area
Lower bound

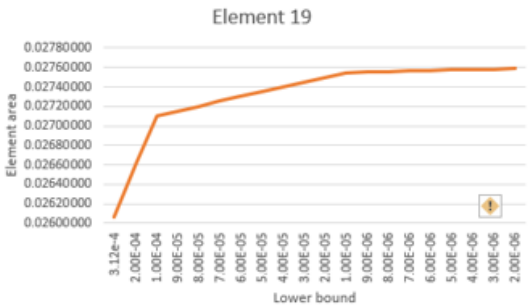
Element 19
Element area
Lower bound

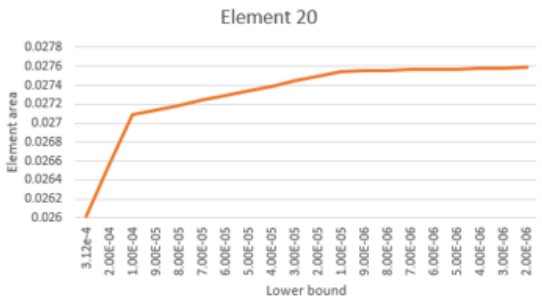
Element 20
Element area
Lower bound

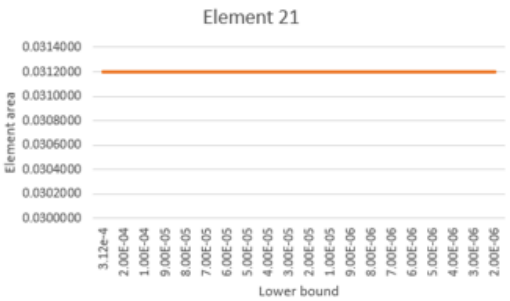
Element 21
Element area
Lower bound

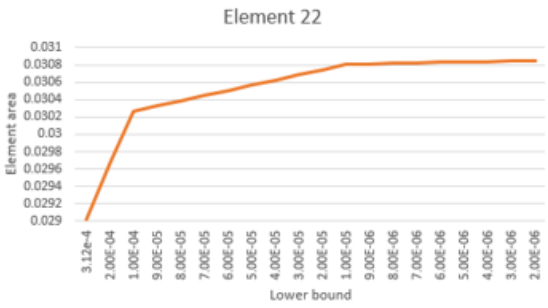
Element 22
Element area
Lower bound

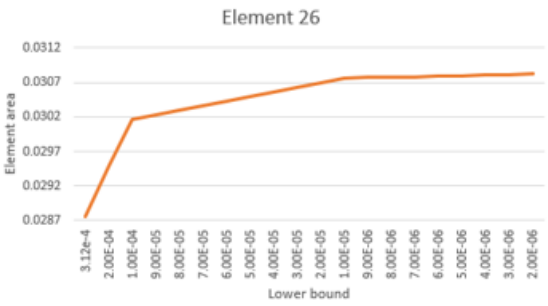
Element 26
Element area
Lower bound

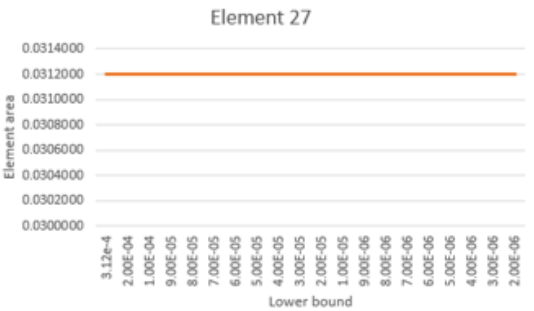
Element 27
Element area
Lower bound

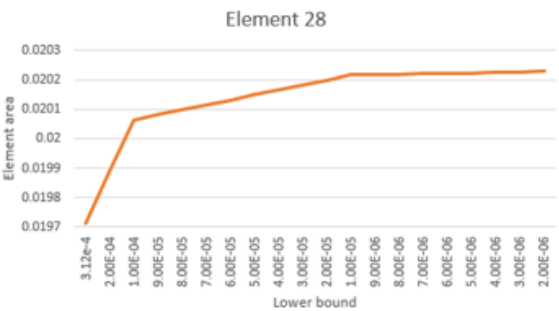
Element 28
Element area
Lower bound

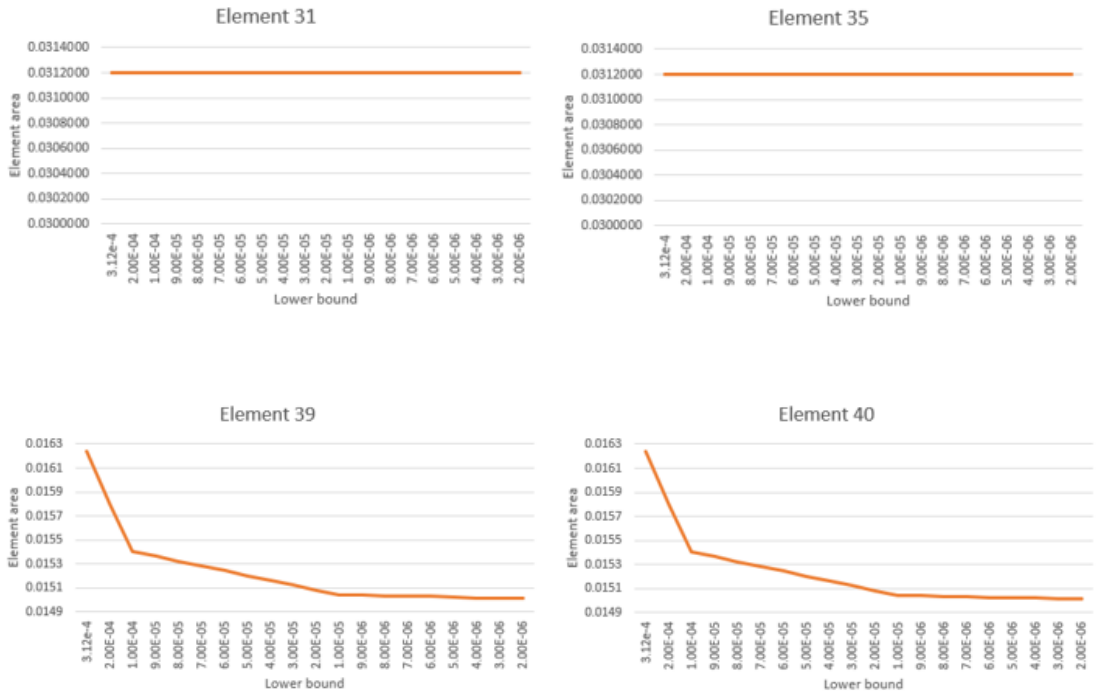

FIGURE 4.16. EVOLUTION OF THE AREA OF THE ELEMENTS IN CONFIGURATION D AS THE LOWER BOUND DECREASES

Through the analysis of the graphics in Figure 4.16 one can conclude that the area of the bars that belong to the linear results, elements 39 and 40, is steadily decreasing whereas the area of the other 16 elements listed in Table 4.14 is steadily increasing. Elements 5, 7, 12, 18, 21, 27, 31 and 35 already had their areas at the upper bound which remain equal throughout the several optimizations.

The analysis couldn't be made further past a lower bound of 2e-6 because of the limitation of the program when calculating $\delta\lambda$ using the quadratic equation. When the external load increased significantly or when the lower bound was lowered to try to approximate the lower bound used in linear optimization an error occurred, and the program failed to compute the value of $\delta\lambda$. This error will be called "D parameter" error throughout this work. However, it's expectable that if given the opportunity to extend the optimization to lower levels of lower bound the area of the elements 39 and 40 would continue to decrease.

It was possible to conclude that the variation of the lower bound had a significant impact in the variation of the cross-sectional area with cases where the area varied up to 8 percent.

Using the lower bound of 2e-6 m^2 and considering only the elements with an area above the area of elements 39 and 40, which from the 18 elements presented in Table 4.14 are the ones with the lowest cross-sectional area, the obtained optimum design is presented in Figure 4.17.

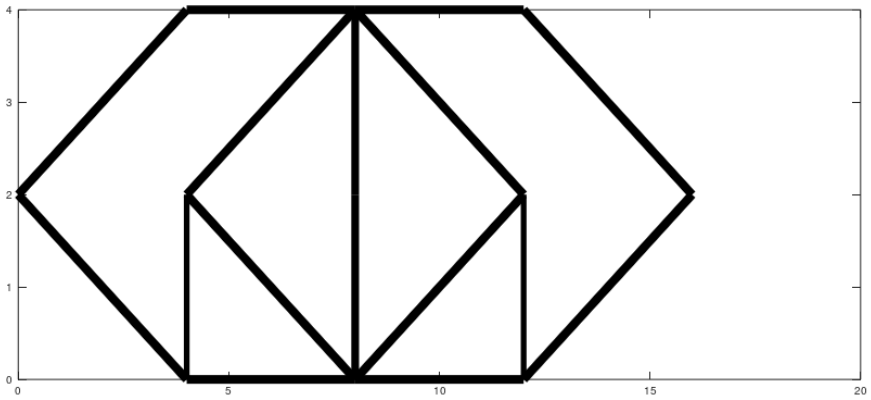

FIGURE 4.17. FINAL NONLINEAR OPTIMUM DESIGN USING PROAES_NL

The final value for the objective function, final external load magnitude, ending code, duration of the optimization process and the number of iterations performed for the optimum design are listed in Table 4.15.

TABLE 4.15. FINAL PARAMETERS OF THE OPTIMIZATION

Ending code (SQP)	104
Time	921.723s
Iterations made	123
P (N)	200
Objective function	1.0152e-4

The optimized structure presents the 16 elements listed in Table 4.16.

TABLE 4.16. AREA AND VOLUME OF THE ELEMENTS IN THE FINAL NONLINEAR CONFIGURATION

Number of the element	Area (m^2)	Percentage of the total volume
5	3.120000e-02	6.977
7	3.120000e-02	6.977
10	2.022934e-02	2.023
12	3.120000e-02	6.240
14	3.085140e-02	6.899
16	3.081829e-02	6.891
18	3.120000e-02	6.240

19	2.758859e-02	2.759
20	2.758986e-02	2.759
21	3.120000e-02	6.240
22	3.085297e-02	6.899
26	3.081985e-02	6.892
27	3.120000e-02	6.240
28	2.022928e-02	2.023
31	3.120000e-02	6.977
35	3.120000e-02	6.977

Using as a starting point the values used for the optimization D in Figure 4.15 but changing the lower bound to 2e-6 m^2, the external load was raised to see what effect it would have in the cross-sectional area. However, raising the external load to as little as 210N triggered the error of the D parameter. Consequentially, to study the effect of the external load in the cross-sectional area of the elements it was necessary to use a higher value for the lower bound. The value chosen was the first initial value used for the study of the maximum admissible volume, 3.12e-4 m^2.

The results are shown in Figure 4.18.

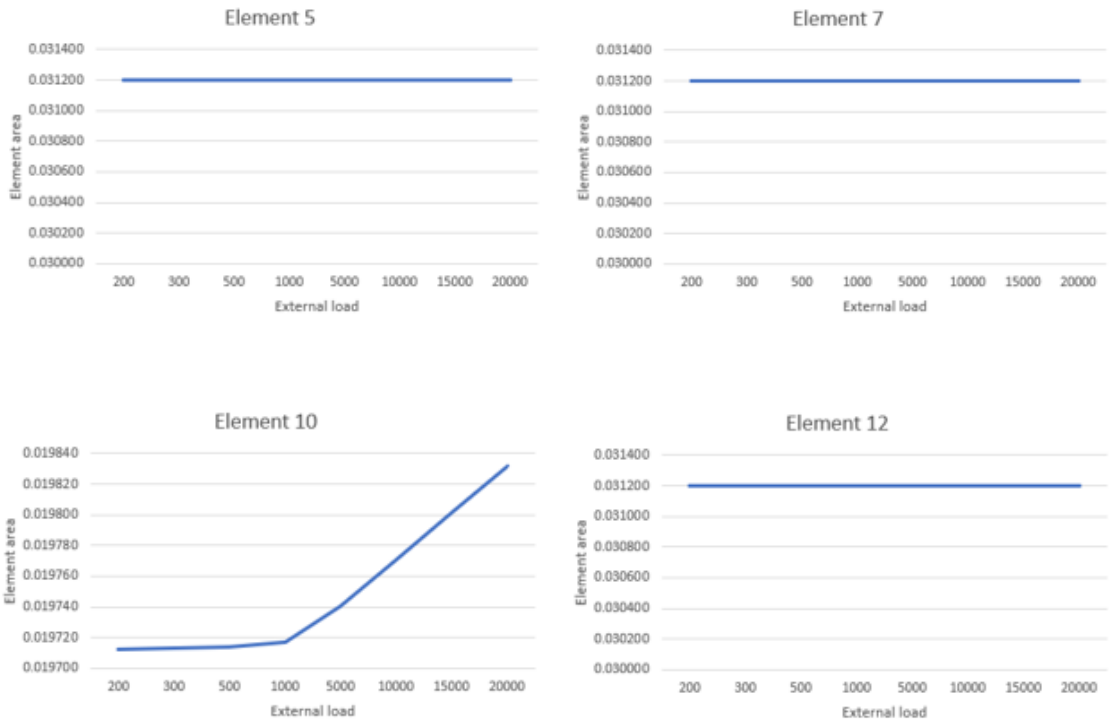

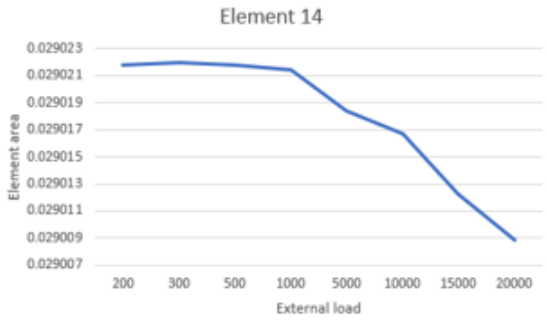
Element 14
Element area
0.029023
0.029021
0.029019
0.029017
0.029015
0.029013
0.029011
0.029009
0.029007
200 300 500 1000 5000 10000 15000 20000
External load

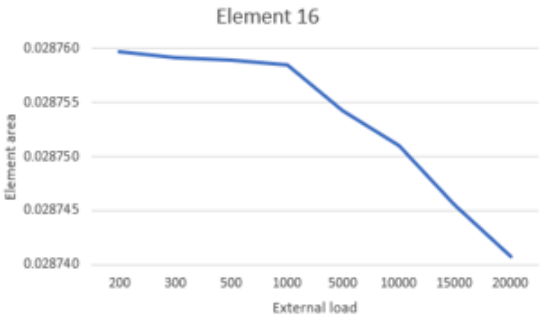
Element 16
Element area
0.028760
0.028755
0.028750
0.028745
0.028740
200 300 500 1000 5000 10000 15000 20000
External load

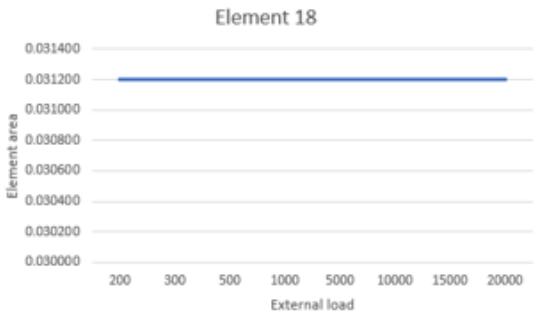
Element 18
Element area
0.031400
0.031200
0.031000
0.030800
0.030600
0.030400
0.030200
0.030000
200 300 500 1000 5000 10000 15000 20000
External load

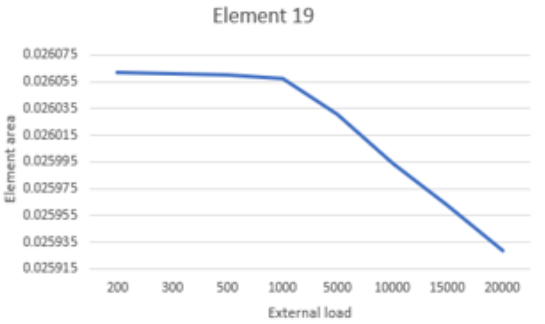
Element 19
Element area
0.026075
0.026055
0.026035
0.026015
0.025995
0.025975
0.025955
0.025935
0.025915
200 300 500 1000 5000 10000 15000 20000
External load

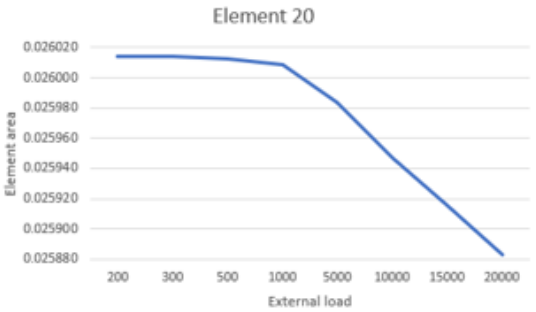
Element 20
Element area
0.026020
0.026000
0.025980
0.025960
0.025940
0.025920
0.025900
0.025880
200 300 500 1000 5000 10000 15000 20000
External load

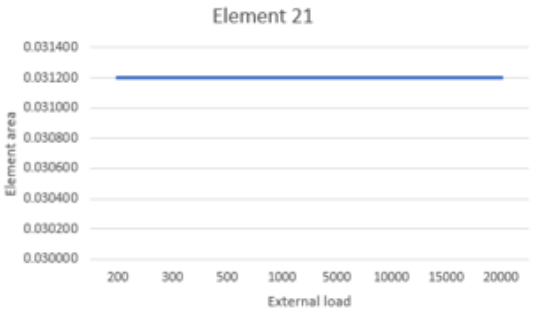
Element 21
Element area
0.031400
0.031200
0.031000
0.030800
0.030600
0.030400
0.030200
0.030000
200 300 500 1000 5000 10000 15000 20000
External load

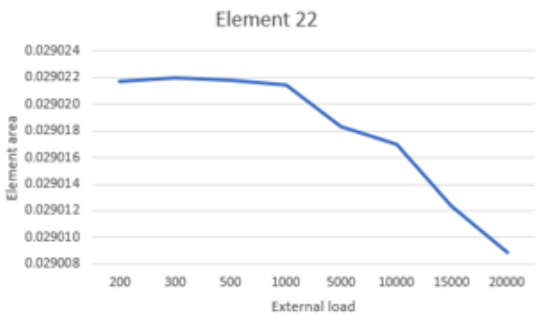
Element 22
Element area
0.029024
0.029022
0.029020
0.029018
0.029016
0.029014
0.029012
0.029010
0.029008
200 300 500 1000 5000 10000 15000 20000
External load

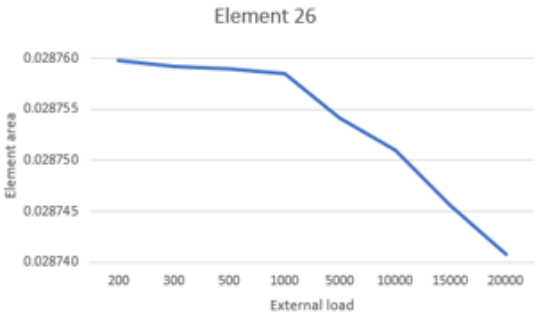
Element 26
Element area
0.028760
0.028755
0.028750
0.028745
0.028740
200 300 500 1000 5000 10000 15000 20000
External load

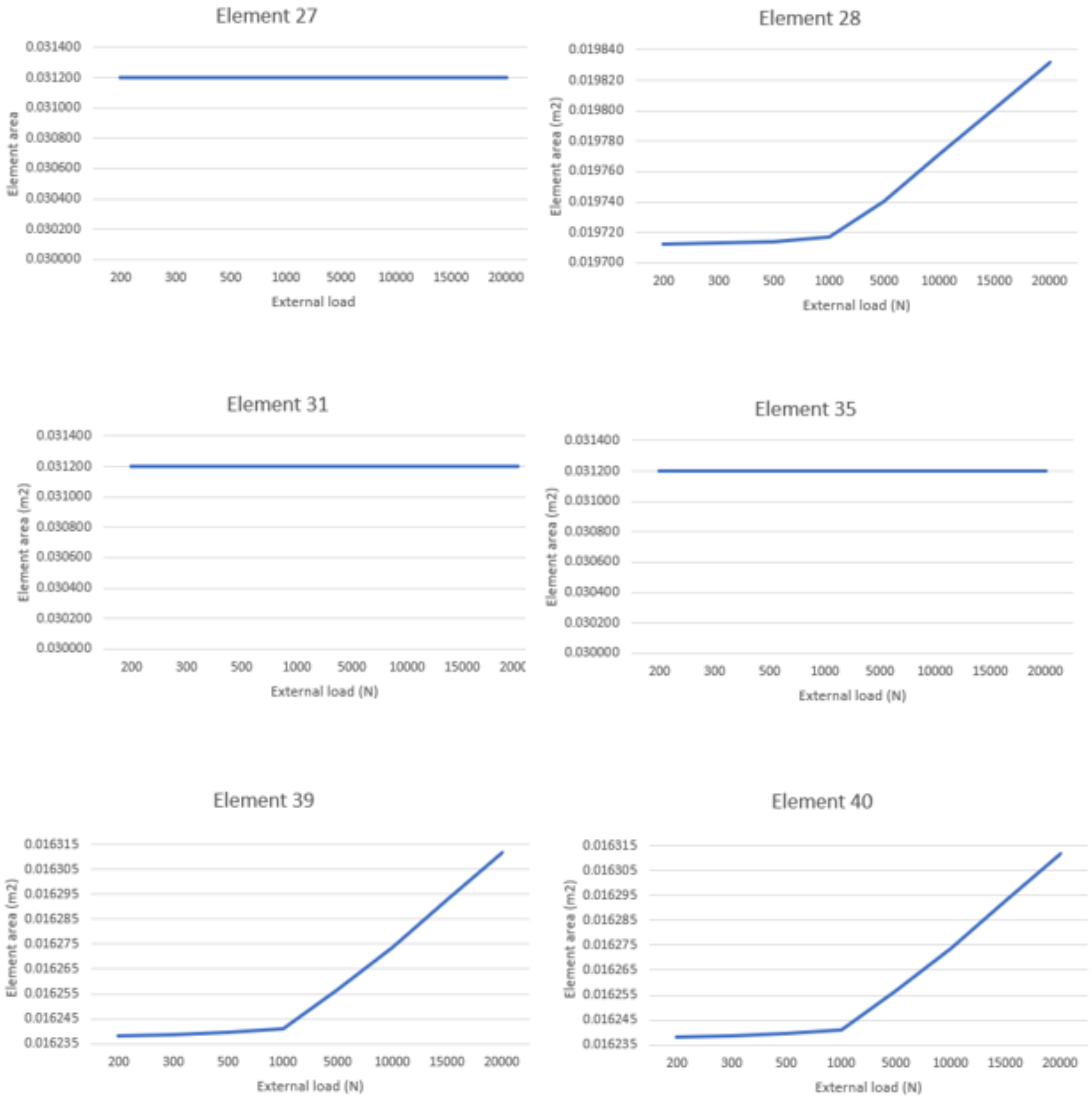

FIGURE 4.18. EVOLUTION OF THE AREA OF THE ELEMENTS IN CONDIGURATION D AS THE EXTERNAL LOAD INCREASES

When analyzing the graphics in Figure 4.18 it was possible to conclude that the area of the elements that make up the linear solution, elements 39 and 40, raised whereas in the previous case with the lower bound reduction they decreased. Some of the elements that had appeared in case D, Figure 4.15, had their areas reduced, elements 14, 16, 19, 20, 22 and 26 while others had their areas risen which is the case of elements 10 and 28.

The computational time necessary to perform each optimization increased greatly with the increasing of the external load. With an external load of 200N it took 581 seconds to perform the optimization while with the external load of 20000N it took 29008 seconds.

One can conclude that the variation of the external load did not have a great influence in the variation of the cross-sectional area of the elements. Although through the analysis of the graphics in Figure 4.18 one can see an increase or decrease in the value of the area, it represents as little as 0.4 percent of variation of the initial area.

Therefore, the results obtained with the variation of the lower bound are the ones that will be used to compare with the results obtained using the linear finite element analysis program.

4.1.3.3 ANALYSIS AND COMPARISON OF RESULTS

Using PROAES the linear optimum design obtained was in close accordance with the ones presented in [11]. Both designs can be seen in Figure 4.19.

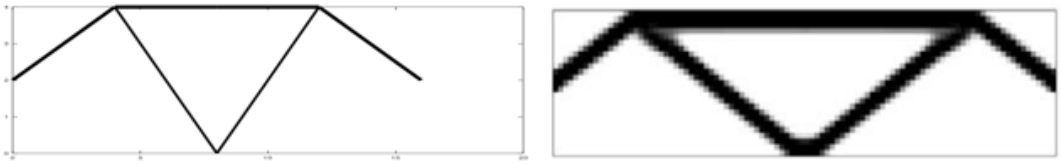

(A) (B)

FIGURE 4.19. FINAL LINEAR OPTIMUM DESIGN: (A) PROAES (B) SOURCE [10]

Using PROAES_NL and maintaining the same specifications as the ones used in Figure 4.19 (a), except for the lower bound that had to be raised, the obtained design was the same as the one obtained using PROAES.

In order to obtain a design that better approached the nonlinear design presented in [11] the maximum admissible volume, lower bound and external load were varied. After raising the maximum admissible volume and lowering the lower bound it was possible to obtain a final optimum design that better resembled the nonlinear results in the bibliography. The comparison of both designs can be made in Figure 4.20.

(A) (B)

FIGURE 4.20. FINAL NONLINEAR CONFIGURATION: (A) PROAES_NL (B) SOURCE [10]

The results presented in the bibliography were obtained using density-based optimization whereas in this work the optimization is made using an initial ground structure. Additionally, PROAES_NL doesn't have as a variable the coordinates of the nodes, it can only increase or decrease the area of the bars that are created initially and that are connected to the nodes that are defined by the user. For this reason, it will converge to a solution that is available using the available elements.

Therefore, the final nonlinear design is presented in Figure 4.21 (A) and the final linear design is presented in Figure 4.21 (B).

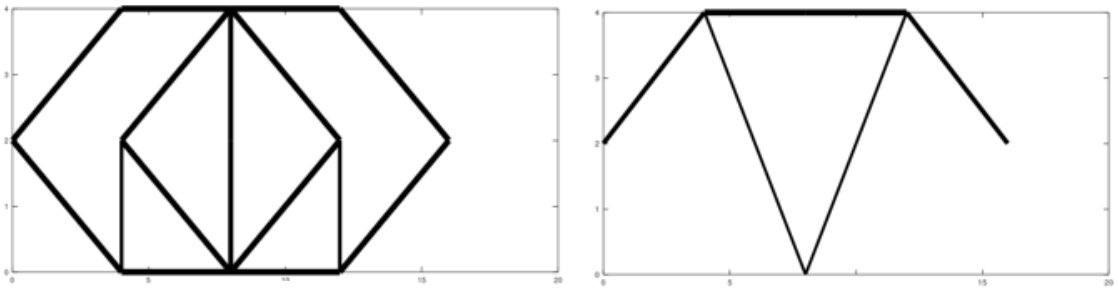

(A) (B)

FIGURE 4.21. FINAL OPTIMUM DESIGNS: (A) NONLINEAR (B) LINEAR

CHAPTER 5
CONCLUSION AND RECOMMENDATIONS

5.1 CONCLUSION

The first goal of this work was to validate the nonlinear finite element analysis program developed by Cardoso, PROAES_NL. This program was created using a corotational formulation for the cinematic of the elements and using the incremental-iterative Newton-Raphson method allied with the cylindrical arc length formulation for load control in order to obtain the equilibrium path of the structure. The displacements obtained using PROAES_NL were compared with the results presented in several published articles and with the values obtained using ANSYS. The results were very satisfactory with errors way below 7%. The program also demonstrated excellent accuracy in surpassing critical points such as snap-through having been able to construct the entire deformation path correctly, see Lee's frame example. Besides, the reading of the input file in PROAES_NL was modified to accommodate the way input information was given to PROAES, a linear finite element analysis program. This way the same input file can be read by both programs. However, the user must bear in mind that PROAES_NL up to this point is only able to perform calculations for bidimensional problems and using beam finite elements.

José L. T. Santos developed as the subject of his Ph.D. thesis the theory for sizing design sensitivity analysis for structures considering nonlinear behaviour. The conclusions drawn in the study were that software implementation of nonlinear design sensitivity analysis with established finite element programs was a possibility by using only postprocessing data outside of the finite element code. In addition, the theory developed allowed for a more efficient sensitivity analysis when compared with finite difference design sensitivity analysis methods which carry a high computational cost. The main purpose of this work was thus to implement the design sensitivity analysis theory inside PROAES_NL for the analysis of structures with geometric nonlinearities.

The translation of the integral equations for design sensitivity analysis from the mathematical domain into the physical domain was possible by using shape functions and Hermite polynomials for beam elements. It is highlighted that the displacement vectors in these integral equations refer to the components of the displacement due to the deformation of the element. The matrix of design sensitivities is constructed using two *for* cycles. A first cycle that goes through every requested performance and a second cycle inside the first one that goes through every element and evaluates the contribution of each element for the derivative of the performance with relation to the variable chosen. For the development of this thesis, only one variable was considered: the area of the elements. In the same manner, only two performances types were considered: the volume and the nodal displacement.

The results obtained for design sensitivity analysis with the software implemented were compared with the values obtained using finite difference methods and the values

presented by several authors in published articles. The conclusions drawn were that these results were in close accordance with the values obtained with both finite difference methods and published articles with an average error below 3%. The implementation was then assumed as validated with very satisfactory results. Therefore, PROAES_NL can now be used as a starting point for students and researchers for the study of nonlinear structural phenomena.

For the final part of this thesis, topology optimization was performed using the sensitivities implemented before and the ground structure approach. The goal was to test if any difference would arise between the optimum designs obtained using linear and nonlinear design sensitivity and finite element analysis. In most of the published studies, authors agree that for common structures no significant difference is verified and only in specific cases such as the design of space antennae's and MicroElectroMechanical systems a considerable difference is confirmed.

Two structures were studied: a 38-bar truss with three fixed supports in the left side and free on the right side and a two-point supported 46-bar truss. In the articles used for comparison a visible difference existed in both examples between linear and nonlinear analysis. The differences occurred in the location of the nodes and the resulting interconnecting bars. Using PROAES_NL only for the 46-bar truss example a nonlinear design that resembled the one presented in the articles was reached. The conclusions drawn were that in both cases the nonlinear analysis provided optimum designs similar to the designs obtained using linear analysis. Using the ground structure technique, it would be very difficult to achieve the results presented in the articles used for comparison since in those studies a density-based optimization methodology was used. This is due to the fact that the traditional ground structure method doesn't account for the addition or removal of nodes or elements and the coordinates of the nodes were not implemented as a variable. In addition, a limitation to the nonlinear analysis program was discovered. For the calculation of $\delta\lambda$ using the quadratic equation when the external load increased significantly or when the lower bound was lowered to try to approximate the lower bound used in linear optimization an error occurred, and the program failed to compute the value of $\delta\lambda$. This limited the nonlinear analysis by not allowing the run of nonlinear optimization with the exact same presets like the ones used for linear optimization.

5.2 RECOMMENDATIONS

Because nonlinear phenomena, such as buckling, can exist in a multitude of structures the development of a program capable of assisting technicians and engineers in the verification of the occurrence of this critical state would be necessary during both the design and work-life stages of a structure.

Overall, the author concluded that a difference can exist between performing a linear and nonlinear topology optimization. However, it was not possible to corroborate this

affirmation due to convergence errors that are inherent to nonlinear structural analysis. As a consequence, it was not possible to use the same values for external load, maximum admissible volume, and area lower bound for both linear and nonlinear optimization. Although, one must bear in mind that, in some cases, the maximum admissible volume may have to be adjusted to reach a nonlinear design since it may encompass a higher number of elements and, therefore, a higher total volume.

Regarding the optimization method, it should be considered a change from the classical ground structure method to a growing ground structure method in order to allow for the removal and insertion of nodes and elements. Also, in the articles studied where a visible difference between linear and nonlinear optimum designs was presented, the location of the nodes varied between both designs. Therefore, the coordinates of the nodes should be introduced as a variable for optimization.

REFERENCES

[1] Santos, L. T. J., 1987, *Design sensitivity analysis of nonlinear structural systems and numerical implementation with established finite element codes*, ph.D thesis, The University of Iowa

[2] Coelho, P., 2018, *Tópicos avançados em mecânica estrutural,* Apontamentos da disciplina, FCT/UNL.

[3] Zegard, T. and Paulino, G. H., 2016, Bridging topology optimization and additive manufacturing, *Struct. Multidiscip. Optim.* **53:** 175-192

[4] Dorn, W., Gomory, R. and Greenberg, H., 1964, Automatic design of optimal structures, *J. Mec,* 25:52

[5] Hajela, P. and Lee, E., 1995, Genetic algorithms in truss topological optimization, *Int. J. Solids Struct,* **32**: 3341-3357

[6] Hagishita, T. and Ohsaki, M., 2009, Topology optimization of trusses by growing ground structure method, *Struct. Multidiscip. Optim,* **37**: 377-393

[7] Zhang, X., Ramos, A. S. and Paulino, G. H., 2017, Material nonlinear topology optimization using the ground structure method with a discrete filtering scheme, *Struct. Multidiscip. Optim,* **55:** 2045-2072

[8] Bruns, T. E. and Tortorelli, D. A., 1998, Topology optimization of geometrically nonlinear structures and compliant mechanisms 1874-1882

[9] Gea, H. C. and Luo, J., 2001, Topology optimization of structures with geometrical nonlinearities, *Comput. Struct,* **79:** 1977-1985

[10] Buhl, T., Pedersen, C. B. W. and Sigmund, O., 2000, Stiffness design of geometrically nonlinear structures using topology optimization, *Struct. Multidiscip. Optim.,* **19:** 93-104

[11] Kang, Z. and Luo, Y., 2009, Non-probabilistic reliability-based topology optimization of geometrically nonlinear structures using convex models, *Comput. Methods Appl. Mech. Eng.,* **198:** 3228-3238

[12] Changizi, N. and Jalalpour, M., 2018, Topology optimization of steel frame structures with constraints on overall and individual member instabilities, *Finite Elem. Anal. Des.,* **141:** 119-134

[13] Ryu, Y ., Haririan, M. Wu. C . and Arora, J. S., 1985, Structural design sensitivity analysis nonlinear response *Comput. Struct.,* **21:** 245-255

[14] Park, J. S. and Choi ,K. K., 1990, Design sensitivity analysis of critical load factor for nonlinear structural systems, *Comput. Struct.,* **36:** 823-838

[15] Cardoso, J., 2019, *Métodos computacionais em engenharia mecânica*, Apontamentos da disciplina, FCT/UNL

[16] Tortorelli, D. A., Habert, R. B. and Luj, S. C., 1991, Adjoint Sensitivity Analysis for

Nonlinear Dynamic Thermoelastic Systems, *AIAA J.,* **29:** 253-263

[17] Santos, J. L. T. and Choi, K. K., 1988 ,Sizing Design Sensitivity Analysis of Non-Linear Structural Systems. Part II: Numerical Method, *Int. J. Numer. Methods Enginnering,* **26:** 2097-2114

[18] Bergan, P., Horrigmoe, G., Krakeland, B. and Soreide, T., 1978, Solution techniques for non-linear finite element problems, *Int. J. Numer. Methods Enginnering,* **12:** 1677-1696

[19] Wempner, G., 1969, Finite elements, finite rotations and small strains of flexible shells, *Int. J. Solids Struct.,* **5:** 117-153

[20] Belytschko, T. and Hsieh, B., 1973, Non-linear transient finite element analysis with convected co-ordinates, *Int. J. Numer. Methods Enginnering,* **7**: 255-271

[21] Brogan, F. A. and Rankin, C., 1986, An Element Independent Corotational Procedure for the Treatment of Large Rotations, *J. Press. Vessel Technol.,* **108:** 165-174

[22] ANSYS, 2013, *ANSYS Mechanical APDL Theory Reference,* vol 15

[23] Menin, R., 2006, *Aplicação da descrição cinemática co-rotacional na análise não linear geométrica de estruturas discretizadas por elementos finitos de treliças, vigas e cascas,* Tese de doutoramento, Universidade de Brasília

[24] Riks, I., 1978, An incremental approach to the solution of snapping and buckling problems, *Int. J. Solids Struct.,* **15:** 529-551

[25] Crisfield, M., 1981, A fast incremental/iterative solution procedure that handles "snap-through", *Comput. Struct.,* **13:** 55-62

[26] Crisfield, M., *Non-linear Finite Element Analyis of Solids and Structures,* vol 1

[27] Cichon, C., 1984, Large in-Plane Analysis of Elastic-Plastic Frames, *Comput. Struct.,* **19:** 737-745

[28] Lee, S.L., Manuel, F. and Rossow, E.C., 1968, Large deflections and stability of elastic frames", *J. Eng. Mech. Div.,* **94:** 521-548

[29] Cescotto, S., 1978, *Etude par elements finis des grands deplacements et grandes deformations*

[30] Lewis, G. and Monasa, F., 1982, Large deflections of cantilever beams of non-linear materials of the ludwick type subjected to an end moment, *Int. J. Non-linear Mech.,* **17**: 1-6

[31] Hsiao, K. M. and Hou, F. Y., 1987, Nonlinear finite element analysis of elastic frames, *Comput. Struct.,* **26:** 693-701

[32] Urthaler, Y. and Reddy, J. N., 2005, A corotational finite element formulation for the analysis of planar beams, *Commun. Numer. Methods Eng.,* **21:** 553-570

[33] Frisch-Fay, R., 1961, A new approach to the analysis of the deflection of thin

cantilevers, *J. Appl. Mech.,* 87-90

[34] Manuel, F. and Lee, S., 1968, Flexible bars subjected to arbitrary discrete loads and boundary conditions, *J. Franklin Inst.,* **285:** 452-474

[35] Backlund, J., 1976, Large deflection analysis of elasto-plastic beams and frames, *Int. J. Mech. Sci.,* **18:** 269-277

[36] Bisshopp, K. E., Drucker, D. C., 1945, Large deflection of cantilever beams, **3**

[37] Horrigmoe, G. and Bergan, P. G., 1978, Nonlinear analysis of free-form shells by flat finite elements, *Comput. Methods Appl. Mech. Eng.,* **16:** 11-35

[38] Lee, G. C. and Yasuo, T., 1970, Finite Element Solution To an Elastica Problem of Beams, *Int. J. Numer. Methods Enginnering,* **2:** 229-241

[39] Santos, T. and Choi, K., 1987, Design sensitivity analysis of non-linear structural systems part I : Theory, *Int. J. Numer. Methods Enginnering,* **24:** 2039-2055

[40] Teixeira, A. F. A., 2017, *Otimização de topologia de treliças considerando incerteza,* Dissertação de mestrado, FCT/UNL